

## Proposal to upgrade the MIPP Experiment

M. Sadler

*Abilene Christian University<sup>†</sup>*

V. Singh

*Banaras Hindu University, Varanasi 221005, India<sup>†</sup>*

H. Kirk, R. B. Palmer

*Brookhaven National Laboratory, Upton, New York 11973 <sup>†</sup>*

M. R. Anantharaman, V. C. Kuriakose, M. Sabir, R. B. Thayyullathil

*Cochin University of Science and Technology, Kochi 682022, India <sup>†</sup>*

R. J. Peterson

*University of Colorado, Boulder*

B.C. Choudhury

*University of Delhi, Delhi 110007, India<sup>†</sup>*

W. Baker, B. Baldin, D. Carey, D. Christian, M. Demarteau, S. Hansen, D. Jensen,  
C. Johnstone, M. Larwill, R. Raja \*, A. Ronzhin, W. Wester, J.-Y. Wu, R. Zwaska

*Fermi National Accelerator Laboratory*

W. Briscoe, I. Strakovsky, R. Workman

*George Washington University, Washington D.C<sup>†</sup>*

H. Gutbrod, B. Kolb, K. Peters

*GSI, Darmstadt, Germany<sup>†</sup>*

G. Feldman

*Harvard University*

B. Bambah, R. Mohanta, E. Harikumar

---

\* contactperson

*University of Hyderabad, Andhra Pradesh 500046, India* †

A. K. Giri

*Inidan Institute of technology, Hyderabad, Andhra Pradesh 502205, India* †

Y. Torun

*Illinois Institute of Technology*

M.D. Messier, J. Paley

*Indiana University*

U. Akgun, G. Aydin, F. Duru, E. Gülmez, Y. Gunaydin, Y. Onel, A. Penzo

*University of Iowa*

V. Avdeichikov, P. Filip, J. Manjavidze, V. Nikitin, I. Rufanov, T. Topuria, A. Zinchenko

*Joint Institute of Nuclear Research, Dubna, Russia* †

D. M. Manley

*Kent State University* †

H. Löhner, J. Messchendorp

*KVI, Groningen, Netherlands* †

H. R. Gustafson, M. Longo, T. Nigmanov, D. Rajaram

*University of Michigan*

V. Bhatnagar, A. Kumar, S. Mahajan, S. Sahijpal, A. Singh

*Panjab University, Chandigarh 160014, India* †

S. P. Kruglov, I. V. Lopatin, N. G. Kozlenko, A. A. Kulbardis,

D. V. Nowinsky, A. K. Radkov, V. V. Sumachev

*Petersburg Nuclear Physics Institute, Gatchina, Russia* †

K.McDonald

---

† New MIPP Collaborating Institution

*Princeton University, Princeton, New Jersey* †

L. Gutay

*Purdue University*

D. Bergman, G. Thomson

*Rutgers University, New Jersey* †

S. R. Mishra, C. Rosenfeld

*University of South Carolina*

C. Dukes

*University of Virginia*

P. Desiati, F. Halzen, T. Montaruli

*University of Wisconsin, Madison* †

P. Sokolsky, W. Springer

*University of Utah* †

H. Meyer, N. Solomey

*Wichita State University, Kansas* †

(Dated: October 7, 2010)

## Abstract

The upgraded MIPP physics results are needed for the support of NuMI projects, atmospheric cosmic ray and neutrino programs worldwide and will permit a systematic study of non-perturbative QCD interactions. The MIPP TPC is the largest contributor to the MIPP event size by far. Its readout system and electronics were designed in the 1990's and limit it to a readout rate of 60 Hz in simple events and  $\approx 20$  Hz in complicated events. With the readout chips designed for the ALICE collaboration at the LHC, we propose a low cost scheme of upgrading the MIPP data acquisition speed to 3000 Hz. This will help us acquire particle production data on 30 nuclei at the rate of 5 million events per day and help significantly improve hadronic shower simulator programs such as GEANT4 and MARS. The upgrade will also help design and measure the LBNE target as well as the medium energy target to be used for the NO $\nu$ A/MINER $\nu$ A experiments. Measurements of nitrogen cross sections will permit a better understanding of cosmic ray shower systematics in the atmosphere. In addition, we explore the possibilities of providing tagged neutral beams using the MIPP spectrometer that may be crucial for validating the Particle Flow Algorithm proposed for calorimeters. Lastly, we outline the physics potential of such a detector in understanding non-perturbative QCD processes.

## Contents

<b>I. Current Status of the MIPP Experiment</b>	8
A. Experimental Setup	9
B. Some results from Acquired data	10
1. TPC performance	10
2. Time of flight system performance	11
3. MultiCell Cerenkov Performance	11
4. RICH system performance	12
5. Beam Cerenkov performance	13
6. Calorimeter Performance	15
7. NuMI target measurements	17
8. Target fragmentation multiplicities as a function of Atomic Number	19
<b>II. The proposal in a nutshell</b>	21
A. Beam Delivery rate assumed	21
B. Replacing the Jolly Green Giant Coils	21
C. TPC DAQ upgrade	21
D. Upgrade of the Rest of the DAQ	22
1. Triggering	23
2. Chamber electronics	24
3. Time of flight system and threshold Čerenkov detector	25
4. Calorimeter/Plastic Ball readout scheme	25
E. Upgrading the beamline to run at lower momenta	25
F. Other tasks	26
<b>III. Summary of the proposed physics for the Upgraded MIPP run</b>	27
A. Particle Production on neutrino targets in the NuMI beam	27
1. MINOS analysis	29
2. Measuring the $\text{NO}\nu\text{A}/\text{MINER}\nu\text{A}$ target	34
3. Design of the LBNE target	35
4. Benchmark test of Monte Carlos at the Hadronic Shower Simulation Workshop	35

B. Particle production on Nitrogen and the question of Cosmic Ray Showers in the Atmosphere	36
1. MIPP Measurement of $\pi/K$ ratios	40
C. Hadronic production on Nuclei and the Hadronic Shower Simulation Problem	41
D. Tagged Neutral beams and Calorimeter R&D	44
1. Observation of tagged neutron events in MIPP	45
<b>IV. Non-perturbative QCD physics</b>	46
A. Further testing of a Scaling Law of Hadronic Fragmentation	47
B. Antiproton Interactions in MIPP	48
C. High Multiplicity Events in MIPP and the question of bosonic condensation	49
D. Baryon Spectroscopy with the upgraded MIPP	50
E. Missing Cascades	52
<b>V. Hardware details of the MIPP Upgrade</b>	53
A. Jolly Green Giant repair	53
1. Former state of the JGG	54
2. New coil design	55
3. Coil replacement	57
4. Ziptracking the new magnetic field	57
B. The TPC Front End Electronics Upgrade	58
1. Brief Description of the MIPP TPC	58
2. ALICE ASICs	60
C. MIPP trigger system upgrades	66
1. Interaction Trigger	66
2. MIPP Trigger Electronics	68
D. MIPP Trigger Module	69
E. Upgrade for Chamber Readout Electronics	71
F. Time of Flight, T0, and threshold Čerenkov Readout	74
G. The Plastic Ball Recoil Detector	77
1. Transportation to Fermilab and Integration into MIPP	79
H. Plastic Ball Electronics [35]	80
I. EM Calorimeter Electronics	85

J. Upgrades to the Online Data Acquisition System	86
1. The VME systems	89
2. fPix readout	90
3. DAQ system Computer	90
4. Monitoring Computer	91
5. Data transfer to ENSTORE, Data storage in Feynman Computer center and Offline analysis needs	91
6. DAQ Task Summary	92
K. Cryogenic Target Upgrade	93
1. Modifications to the Cryo-target	93
2. Modifications to operate with cryogenic Nitrogen	94
3. Cryocooler	94
L. Gas System and Slow Control Upgrades	94
1. Ckov gas purification system	95
2. Methyral bath system	95
3. RICH Vessel Fill Automation	95
4. Other Gas Upgrade	96
5. Slow Controls Upgrades	96
M. Photomultiplier Tubes for RICH and Čerenkov detectors	96
N. Modifications to the beam line	97
O. Beam Veto upgrade	97
P. Rewinding the TPC	98
Q. Wire Chamber repairs	100
<b>VI. Cost and Schedule</b>	100
A. Cost estimate of the MIPP Upgrade	100
B. Schedule	102
<b>VII. Proposed Run Plan</b>	102
<b>VIII. Conclusions</b>	104
<b>References</b>	105

## I. CURRENT STATUS OF THE MIPP EXPERIMENT

We give a brief status report on the MIPP experiment and its performance to date. The Main Injector Particle Production Experiment (FNAL E-907, MIPP) [1] is situated in the Meson Center beamline at Fermilab. It received approval [2] in November 2001 and has installed and operated both the experiment and a newly designed secondary beamline in the interim. It received its first beams in March 2004, had an engineering run to commission the detector in 2004 and had its physics data-taking run in the period January 2005-March 2006.

MIPP is designed primarily as an experiment to measure and study in detail the dynamics associated with non-perturbative strong interactions. It has nearly 100% acceptance for charged particles and excellent momentum resolution. Using particle identification techniques that encompass  $dE/dx$ , time-of-flight [3], Multi-Cell Čerenkov [4] and a Ring Imaging Čerenkov (RICH) detector [5], MIPP is designed to identify charged particles at the  $3\sigma$  or better level in nearly all of its final state phase space. MIPP has acquired data of unparalleled quality and statistics for beam momenta ranging from 5 GeV/c to 90 GeV/c for 6 beam species ( $\pi^\pm$ ,  $K^\pm$  and  $p^\pm$ ) on a variety of targets as shown in Figure 1.

An important aspect of MIPP data-taking was the measurement of particle production off the NuMI [6] target in order to minimize the systematics in the near/far detector ratio in the MINOS [6] experiment. MIPP also made measurements with proton beams off various nuclei for the needs of proton radiography [2].

Another physics motivation behind MIPP is to restart the study of non-perturbative QCD interactions, which constitute over 99% of the strong interaction cross section. The available data are of poor quality, and sparsely populate the beam momentum,  $p_T$ , and atomic Weight phase space that makes comparisons between different experiments difficult. The Time Projection Chamber (TPC) [7] that is at the heart of the MIPP experiment represents the electronic equivalent of the bubble chamber with vastly superior data acquisition rates. It also digitizes the charged tracks in three dimensions, obviating the need for track matching across stereo views. Coupled with the particle identification capability of MIPP, the data from MIPP would add significantly to our knowledge base of non-perturbative QCD. This would help test inclusive scaling relations and also scaling nuclear reactions.

Data Summary 27 February 2006			Acquired Data by Target and Beam Energy Number of events, $\times 10^6$									
Target			E									Total
Z	Element	Trigger Mix	5	20	35	40	55	60	65	85	120	
0	Empty	Normal		0.10	0.14			0.52			0.25	1.01
	K Mass	No Int.				5.48	0.50	7.39	0.96			14.33
	Empty LH	Normal		0.30				0.61		0.31		7.08
1	LH	Normal	0.21	1.94				1.98		1.73		
4	Be	p only									1.08	1.75
		Normal			0.10			0.56				
6	C	Mixed						0.21				1.33
	C 2%	Mixed		0.39				0.26			0.47	
	NuMI	p only									1.78	1.78
13	Al	Normal			0.10							0.10
83	Bi	p only									1.05	2.83
		Normal			0.52			1.26				
92	U	Normal						1.18				1.18
<b>Total</b>			<b>0.21</b>	<b>2.73</b>	<b>0.86</b>	<b>5.48</b>	<b>0.50</b>	<b>13.97</b>	<b>0.96</b>	<b>2.04</b>	<b>4.63</b>	<b>31.38</b>

FIG. 1: The data taken during the first MIPP run as a function of nucleus. The numbers are in millions of events. During the last month of the run, the Jolly Green Giant magnet coils developed shorts. This time was used to acquire data without the TPC for exploring the feasibility of measuring the charged kaon mass using the RICH radii.

### A. Experimental Setup

We designed a secondary beam [8] specific to our needs. The 120 GeV/c primary protons are resonantly extracted in a slow spill from the Fermilab Main Injector and transported down the Meson Center line. They impinge on a 20 cm long copper target producing secondary beam particles. This target is imaged onto an adjustable momentum selection collimator which controls the momentum spread of the beam. This collimator is re-imaged on to our interaction target placed next to the TPC. The beam is tracked using three beam chambers and identified using two differential Čerenkovs [9] filled with gas, the composition and the pressure of which can be varied within limits depending on the beam momentum

and charge.

Figure 2 shows the layout of the apparatus. The TPC sits in a wide aperture magnet (the Jolly Green Giant) which has a peak field of 0.7 tesla. Downstream of the TPC are a 96 mirror multi-cell Čerenkov detector filled with  $C_4F_{10}$  gas, and a time of flight system. This is followed by a large aperture magnet (ROSIE) which runs in opposite polarity (at -0.6 tesla) to the Jolly Green Giant to bend the particles back into the Ring Imaging Čerenkov counter. The RICH has  $CO_2$  as the radiator and an array of phototubes of 32 rows and 89 columns [10]. Downstream of the RICH we have an electromagnetic calorimeter [11] and a hadron calorimeter [12] to measure forward-going photons and neutrons. The electromagnetic calorimeter provides a means of distinguishing forward neutrons from photons and will also serve as a device to measure the electron content of our beam at lower energies, which will be useful for measuring cross sections.

MIPP uses  $dE/dx$  in the TPC to separate pions, kaons and protons for momenta less than  $\approx 1$  GeV/c and the time of flight array of counters to do the particle identification for momenta less than 2 GeV/c. The multi-cell Čerenkov detector [4] contributes to particle identification in the momentum range  $\approx 2.5$  GeV/c-14 GeV/c and the RICH [5] for momenta higher than this. Tracking of the beam particles and secondary beam particles is accomplished by a set of drift chambers [13] and proportional chambers [14] each of which have 4 stereo layers.

## B. Some results from Acquired data

### 1. TPC performance

Figure 3 shows the pictures of reconstructed tracks in the TPC obtained during the data-taking run. The tracks are digitized and fitted as helices in three dimensions. Extrapolating three dimensional tracks to the other chambers makes the pattern recognition particularly easy.

Figure 4 shows the distribution of  $dE/dx$  of tracks measured in the TPC as a function of the track momentum for 120 GeV/c data. The TPC provides excellent identification of particles for lab momenta below 1 GeV/c.

# MIPP

## Main Injector Particle Production Experiment (FNAL-E907)

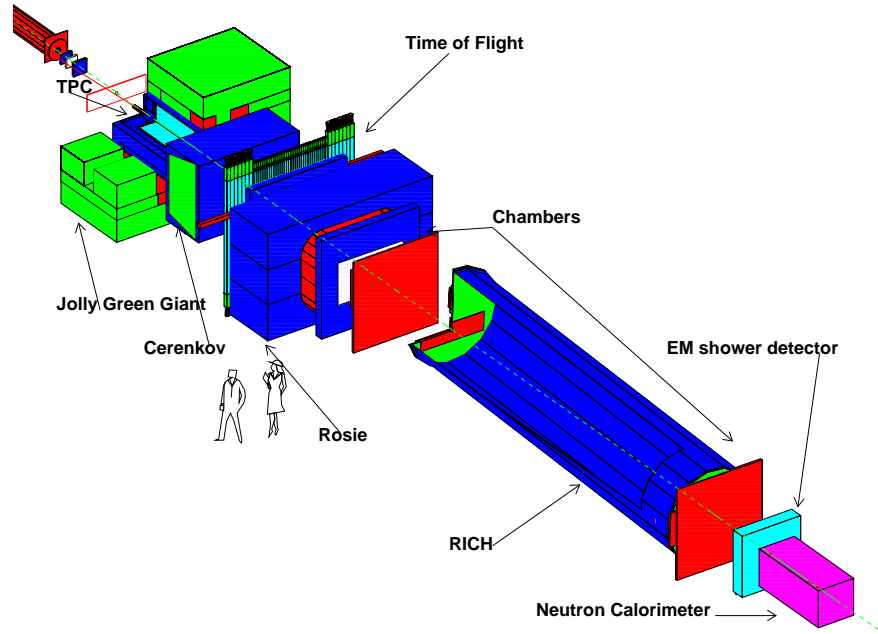


FIG. 2: The experimental setup. The picture is a rendition in Geant3, which is used to simulate the detector.

### 2. *Time of flight system performance*

Figure 5 shows the performance the MIPP time of flight system after calibrating for temperature and cross-talk induced systematics. Clear pion/electron, kaon and proton peaks are visible.

### 3. *MultiCell Cerenkov Performance*

Figure 6 shows the performance of the Multi-Cell Cerenkov counter and the ability of the MIPP Monte Carlo to simulate it.

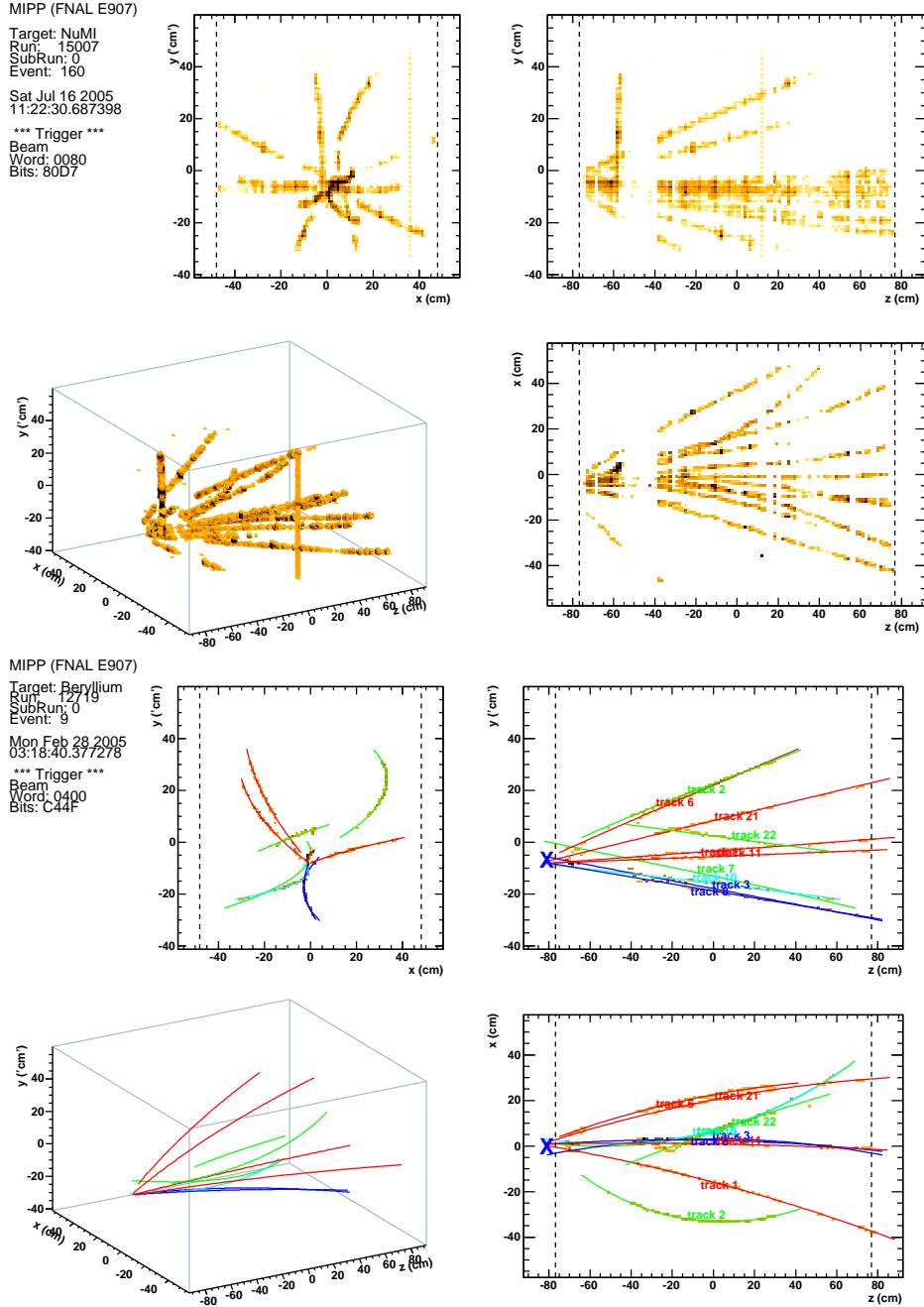


FIG. 3: RAW and Reconstructed TPC tracks from two different events.

#### 4. RICH system performance

Figure 7 shows events with rings in the RICH counter. Some are due to single beam tracks and others are due to tracks from interactions. Figure 8 shows the mass<sup>2</sup> variable deduced from the RICH radii compared with the fit to the global particle identification algorithm [18]. A finely binned version of the same plot on the right shows the electron and

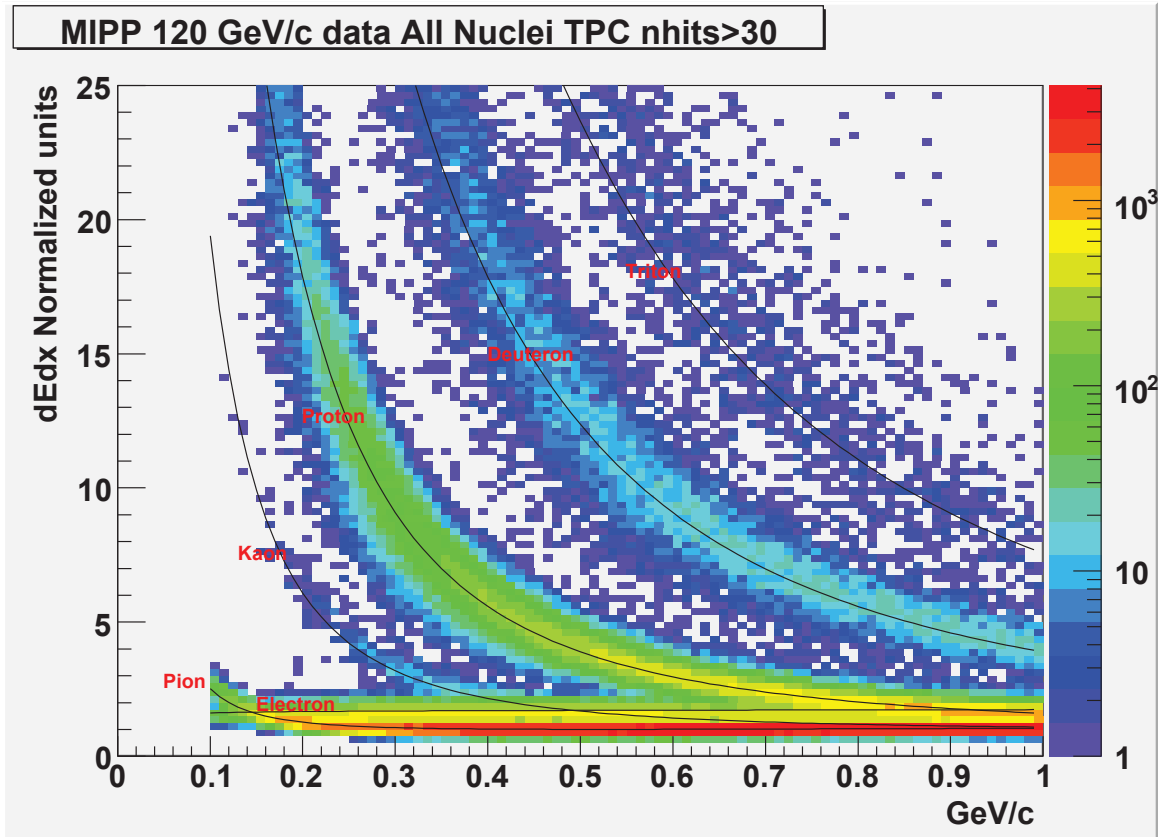


FIG. 4: TPC  $dE/dx$  distributions as a function of track momentum, normalized to minimum ionizing particle deposition being unity. The curves represent theoretical expectations for electrons, pions, kaons, protons, deuterons and tritons.

pion peaks clearly separated.

##### 5. Beam Čerenkov performance

Figure 9 shows the rich ring radii vs momentum of positive tracks originating from the NuMI target. Superimposed are the curves for known particles. This shows the excellent particle identification of the MIPP detector for forward going particles.

Figure 10 shows the histogram of ring radii for a +40 GeV secondary beam. There is clean separation between pions, kaons and protons and their relative abundances [15] match expectations. Applying the particle identification trigger from the beam Čerenkovs enables

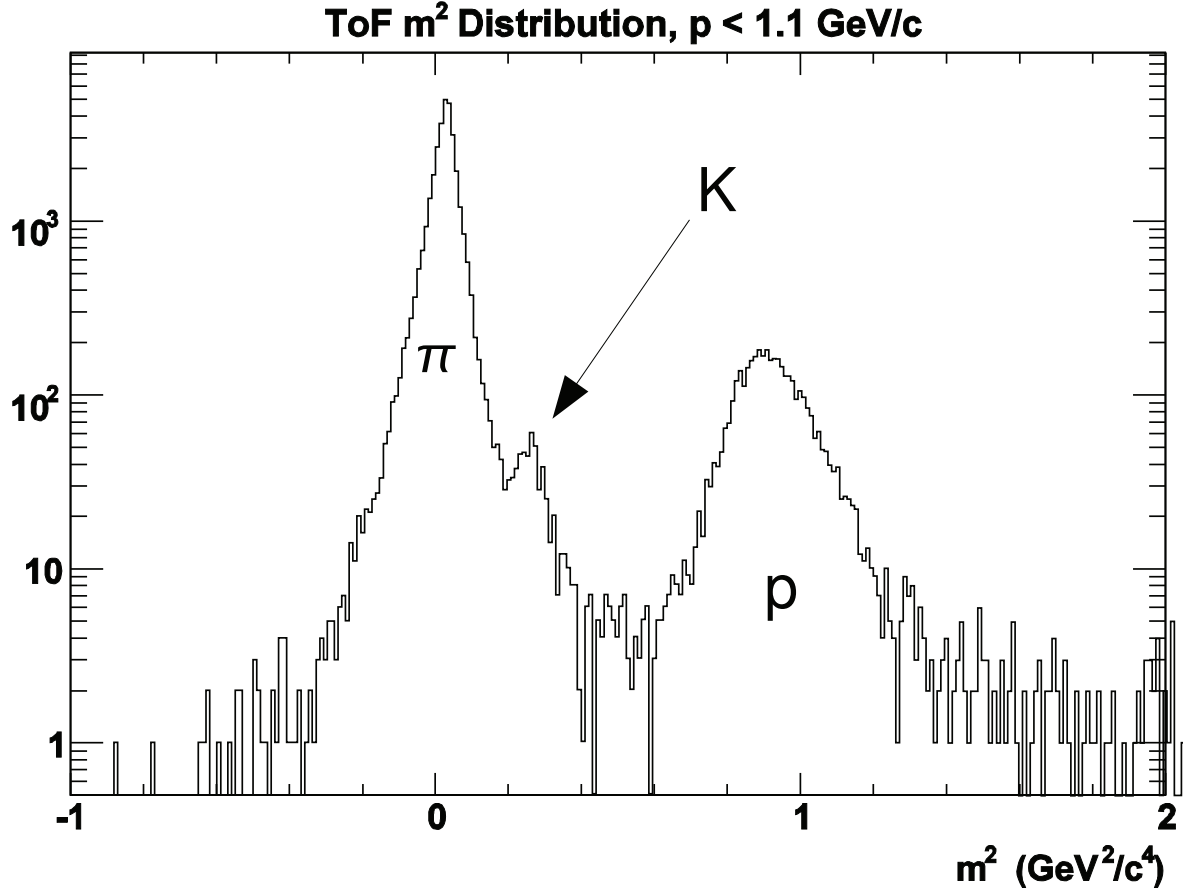


FIG. 5: The times of flight for particles below 1.1 GeV/c hitting the MIPP time of flight array translated into a mass<sup>2</sup> distribution. Peaks for pion (and electron), kaon and proton are visible.

us to separate the three particle species cleanly. The kaons which form 4% of the beam are cleanly picked out by the beam Čerenkov with very simple selection criteria. These can be made much more stringent with offline cuts to produce a very clean kaon beam.

The ring radius of the particle contains information on the mass of the particle. The pion and proton masses are very well known. The charged kaon mass, however, currently has measurement uncertainties of the order of 60 keV. Improving the precision of both charged kaon masses will pay dividends in rare charged kaon decay experiments where the matrix elements depend on the kaon mass raised to large powers. Towards the end of our physics run, when the Jolly Green Giant magnet coils failed, we switched off the TPC and acquired data at the rate of 300 Hz to investigate how well we can measure the charged kaon mass. These events, whose statistics are indicated in Figure 1, were analyzed and the results of

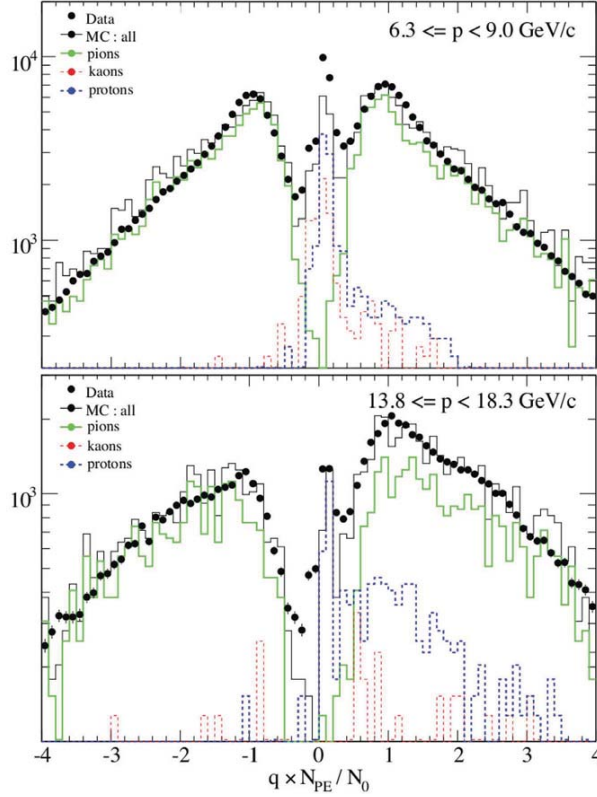


FIG. 6: Distribution of charge  $\times$  number of photoelectrons normalized  $N_{PE}$  to that expected from a  $\beta=1$  particle for data (solid circles) and Monte Carlo (solid line histogram) for two momentum ranges. Colored histograms are the contributions of various particles to the Monte Carlo total. The lower momentum range has only pions and electrons above threshold. The higher momentum range has the protons just going above threshold.

the analysis, which constitutes a new method to measure the charged kaon mass, have been published in a NIM article [17].

### 6. Calorimeter Performance

Both the Electromagnetic and hadronic calorimeters performed well and have been used to produce measurements of the forward neutron cross sections using proton beams as a function of nuclei [16]. Figure 11 shows the measurements of forward neutron cross sections for proton beams of 58 GeV/c and 120 GeV/c as a function of Atomic number. MIPP data disagrees significantly from the predictions of two Monte Carols Fluka and LAQGSM.

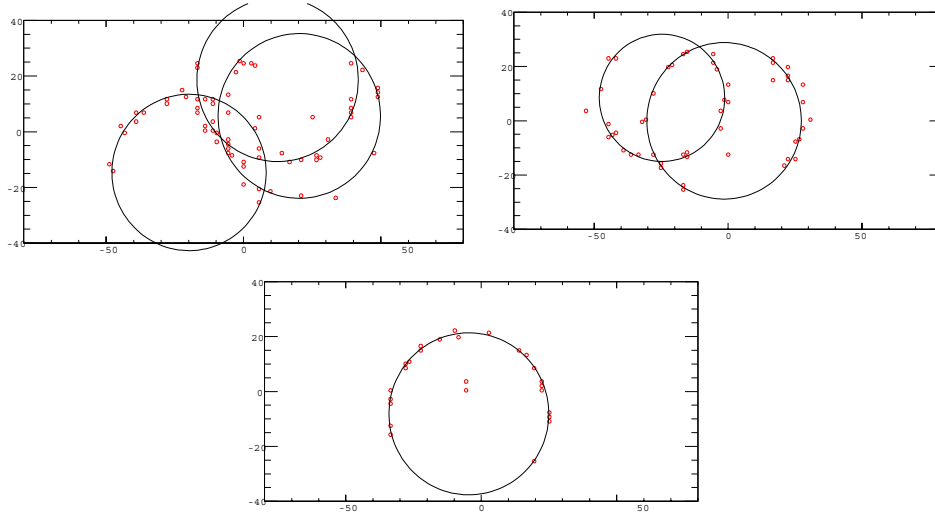


FIG. 7: Examples of events with rings in the RICH counter for a 40 GeV/c beam. The x and y axes are in cm.

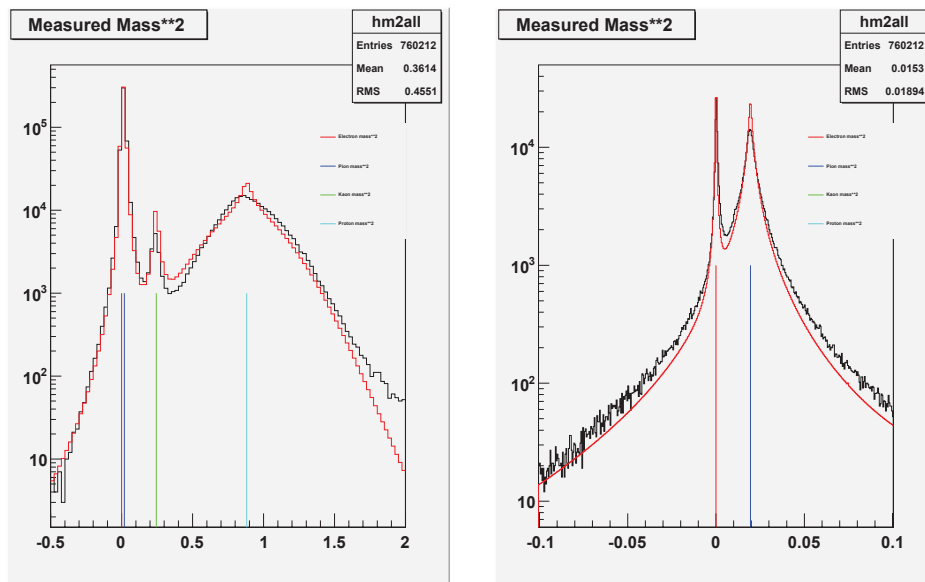


FIG. 8: RICH ring radii information converted to  $\text{mass}^2$ . Pion, Kaon and proton peaks are clearly visible. The curve is a fit to the RICH data by the global particle identification algorithm. The pion peak contains electrons as well. This can be better seen in the more finely binned plot on the right where the electron and pion peaks are clearly discriminated.

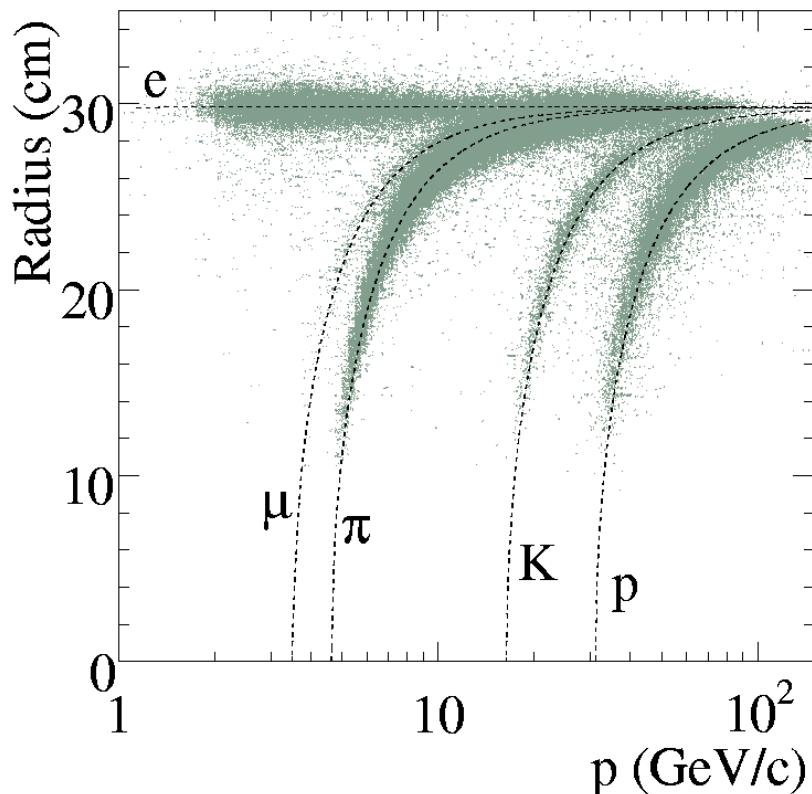


FIG. 9: RICH ring radii of positive tracks from the NuMI target vs momentum. Superimposed are the expected curves for  $e$ ,  $\mu$ ,  $K$  and  $p$  particles.

### 7. NuMI target measurements

MIPP took 1.75 million events using 120 GeV/c primary beam protons impinging on the NuMI (spare) target. These events will play a crucial role in the prediction of neutrino fluxes in the NuMI beamline and will enable the MINOS experiment to control the systematics in the near/far detector ratios as well as helping them understand the near detector performance. Figure 12 shows a radiograph of the MIPP measurements of the MINOS target. The graphite slabs and cooling tubes can be seen. These events were obtained during the commissioning phase of this target measurement where the beam was not yet fully focused and aligned on the target. The 1.75 Million events on the NuMI target were obtained after the beam was aligned and centered on the target.

Figure 13 shows the results of a preliminary analysis of NuMI target data in both energy spectrum of the tracks and track multiplicity and compares it to the FLUKA Monte Carlo.

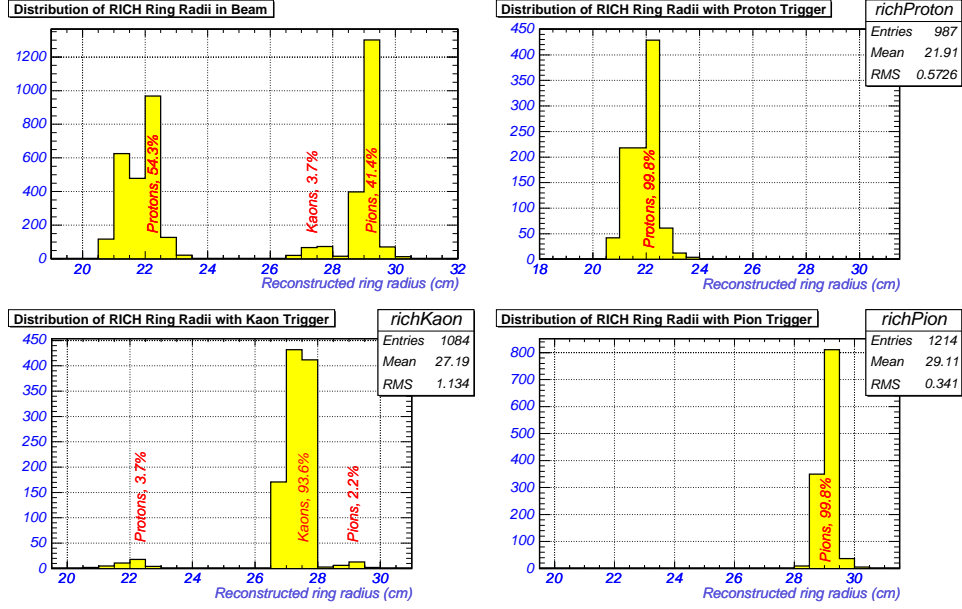


FIG. 10: An example of a 40 GeV/c primary beam (non-interacting) trigger. The RICH identifies protons, kaons and pions by the ring radii. The beam Čerenkov detectors can be used to do the same. When the beam Čerenkov identification is used, one gets a very clean separation of pions, kaons and protons in the RICH.

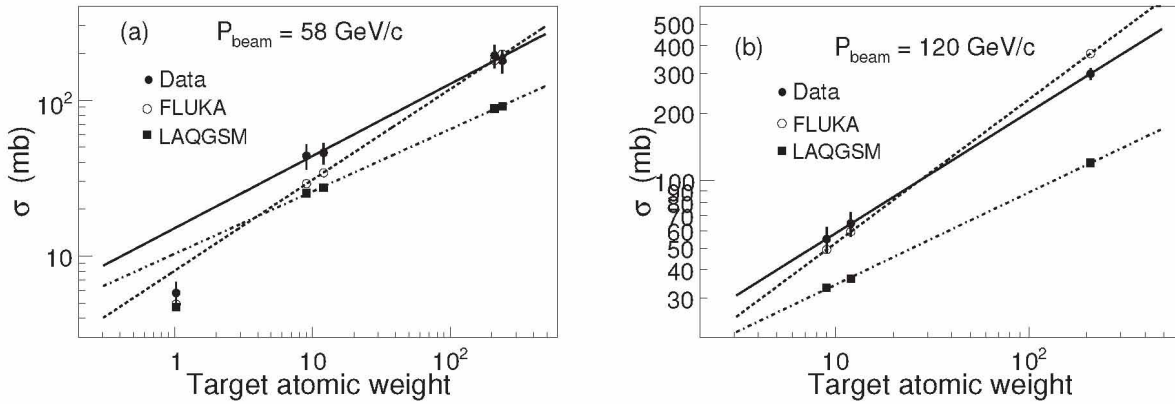


FIG. 11: Comparison of MIPP measurements of forward neutron cross sections vs atomic number for 58 GeV/c and 120 GeV/c proton beams with predictions of the Monte Carlos FLUKA and LAQGSM

We have performed a particle identification analysis on the NuMI target. Please see separate write-up on detailed results [18].

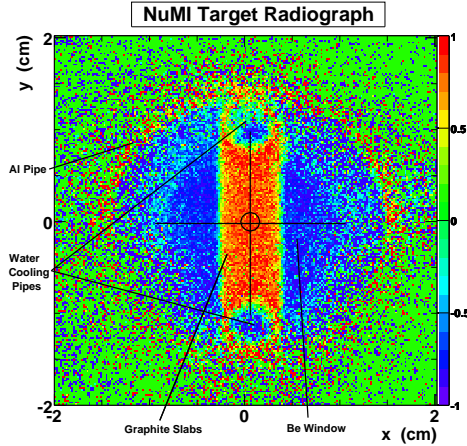


FIG. 12: Radiograph of the MINOS target. The beam direction is perpendicular to the paper.

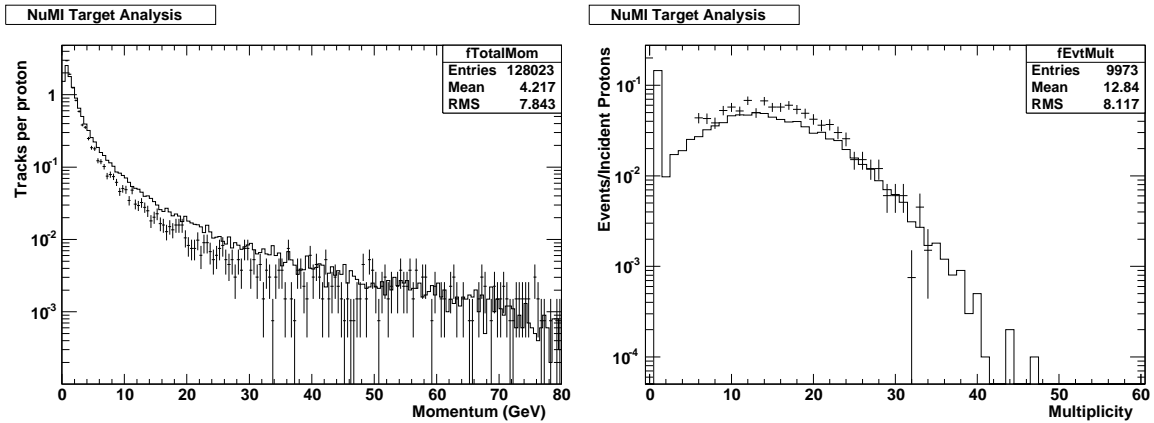


FIG. 13: Comparison (preliminary) of NuMI target data with predictions of the FLUKA Monte Carlo in charged particle momentum and multiplicity. Data have error bars

### 8. Target fragmentation multiplicities as a function of Atomic Number

We have analyzed the multiplicities in the TPC as a function of atomic number  $A$  of the target. Here we show (Figure 14) a preliminary analysis of the multiplicity of both positive and negative tracks in the momentum range  $0.1 \text{ GeV}/c$ - $1.0 \text{ GeV}/c$  for the nuclear targets  $H_2$ , Be, C, and Bi for 3 positive beam species  $\pi^+$ ,  $K^+$  and p at  $58 \text{ GeV}/c$  incident momentum. The data show a rise in target fragmentation multiplicity as a function of  $A$ . The positive multiplicities are higher, reflecting the charge of the target. The experiment has recently given a Wine and Cheese seminar on the status of it analysis. We currently have the following analysis at publication stage.

- A paper on forward neutron production cross sections on nuclei.

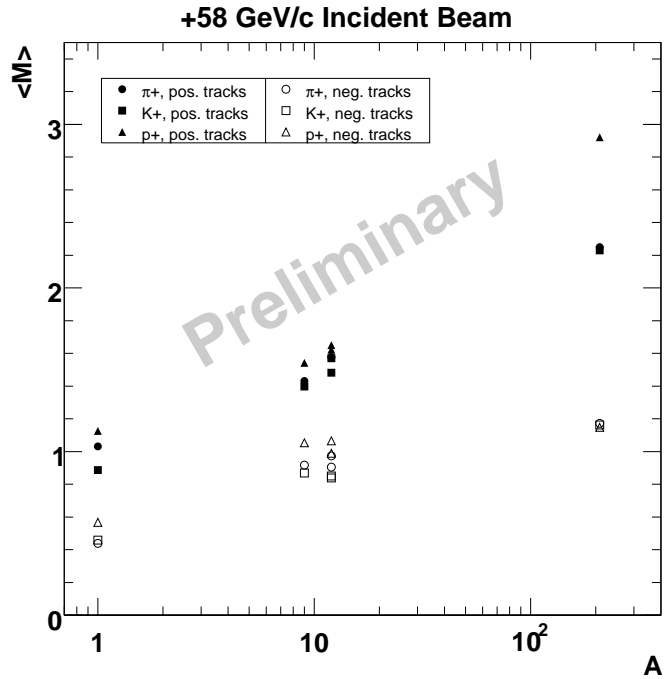


FIG. 14: Mean multiplicity  $\langle M \rangle$  of positive and negative tracks in the momentum range 0.1 GeV/c- 1.0 GeV/c (target fragmentation region) as a function of atomic number  $A$  of the target ( $H_2$ , Be, C and Bi) at 58 GeV/c beam momentum for the positive beam species  $\pi^+$ ,  $K^+$  and  $p$ .

- A paper on particle production on the NuMI target.
- A NIM paper describing the experimental apparatus.

In addition analyses are proceeding on particle production cross sections (with final state particle identification) on nuclei such as carbon and hydrogen as well as production of  $K_S^0$  particles from carbon and NuMI targets. The latter channel will help pin down sources of electron neutrinos from  $K_L^0$  decays.

MIPP has published two NIM articles on the performance of its calorimeter [16] and also on a new technique to measure the charged kaon mass using RICH radii [17].

## II. THE PROPOSAL IN A NUTSHELL

### A. Beam Delivery rate assumed

In what follows, we will assume that the Main Injector delivers one 4 second slow spill every two minutes to MIPP in the upgraded mode, with a machine downtime of 42%, and that the MIPP DAQ has been upgraded to run at 3 kHz. These are conservative estimates of machine delivery rate and downtime. At this rate, we are capable of acquiring 5 Million events per day.

### B. Replacing the Jolly Green Giant Coils

One month before the end of our run in March 2006, the Jolly Green Giant magnet failed. Two of its 4 coils became inoperative due to shorts. The Jolly Green Giant coils were fabricated in the 1960's and have seen a lot of power cycles. Even if we fix the broken coils, there is no guarantee as to how long the remaining coils will last. We have decided to replace all four coils with two aluminum coils with the same field strength as before. The aluminum conductor is cheaper than copper. In the process, we have made the coils longer along the beam direction by  $\pm 9$  inches so as to provide a more uniform field for the electron drift in the TPC.

### C. TPC DAQ upgrade

The MIPP sub-detector with the largest data output is our TPC. It is also the slowest in outputting this data, since its data acquisition electronics were designed and built [19] in the early 1990's. The TPC runs at  $\approx 60$  Hz for very simple events (single beam tracks). For complicated events this rate currently falls to  $\approx 20$  Hz. With modern electronics, it is possible to increase the DAQ rate to 3000 Hz, resulting in an over-all increase of 150 in our data acquisition capability. We have acquired the necessary 1100 ALTRO/PASA chips designed and tested for the ALICE collaboration at the LHC [20] for a cost of  $\approx$  \$90,000. This technology is also being used for the STAR, BONUS and TOTEM experiments. We have designed and fabricated new front end electronics cards for the TPC using these chips. With one 4-second slow spill every two minutes and allowing for a machine down-time of

42%, we can accumulate 5 Million events per day.

#### D. Upgrade of the Rest of the DAQ

We propose to improve the way MIPP is triggered, the DAQ electronics of the drift and wire chambers, the time of flight and threshold Čerenkov counters and the calorimeters. The only system that remains mostly unaltered is the RICH for which we built front end electronics for the first run. The only change here to add more buffer memory to store the larger number of events. The design of the buffer board would not affect the overall cost. The specification to run at 3 kHz trigger rate for the upgraded MIPP DAQ system requires all MIPP sub-systems to buffer events collected during the spill in a buffer memory for a subsequent readout between spills. All new electronics developed for the MIPP Upgrade complies with this requirement. The readout of the sub-system data will be executed by the MIPP Readout Controller module. The design of the module is under development. The module will interface with the MIPP Trigger module and will have eight serial channels for connecting to the sub-system electronics. The block diagram of the MIPP DAQ readout is shown in Figure 15. Each front-end is fitted with two RJ-45 connectors, each of which

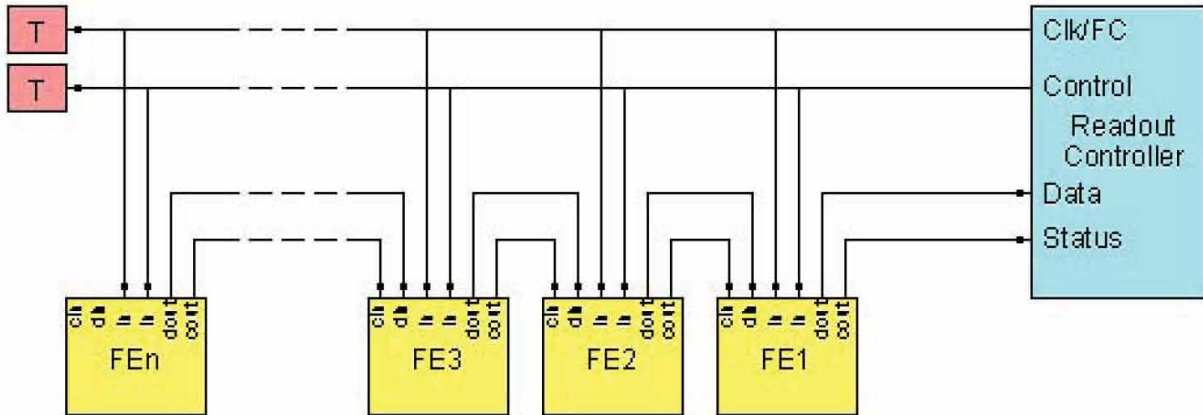


FIG. 15: The MIPP DAQ Readout chain.

contains four differential pairs. Two pairs are bussed; two other pairs are daisy-chained. The controller transmits on the bussed pairs and receives on the daisy-chained pairs (Figure 15). One of the bussed pairs (timing bus) is used to send trigger, timing and initialization (Fast Command, Clk/FC). Control information and requests for status are sent on the other

bussed pair (control bus, Control). The timing bus and control bus require a termination at the further end. The front-ends transmit on the daisy-chained pairs. One is used for sending event data (data chain), the second for sending status information (status chain). The direction toward the readout controller is defined as *downstream*. The number one front-end is defined to be the front-end furthest from the controller (see Figure 15). The signal levels on the pairs within a cable are defined as LVDM, which is designed to drive a double terminated line. Transformer coupling is required on bussed pairs and at least on two chained outputs. The encoding scheme is FM with bits represented as two frequencies: 26.5MHz (logic 1) and 13.28MHz (logic 0) (see Figure 16). Front-ends are required to phase lock their transmit channels to the timing bus clock ( $RF/2$ ). Data transmitted by the front-ends will be at a known frequency, and a fixed but unknown phase with respect to the synchronous link. The block diagram of the MIPP Readout Controller is shown in Figure 17.

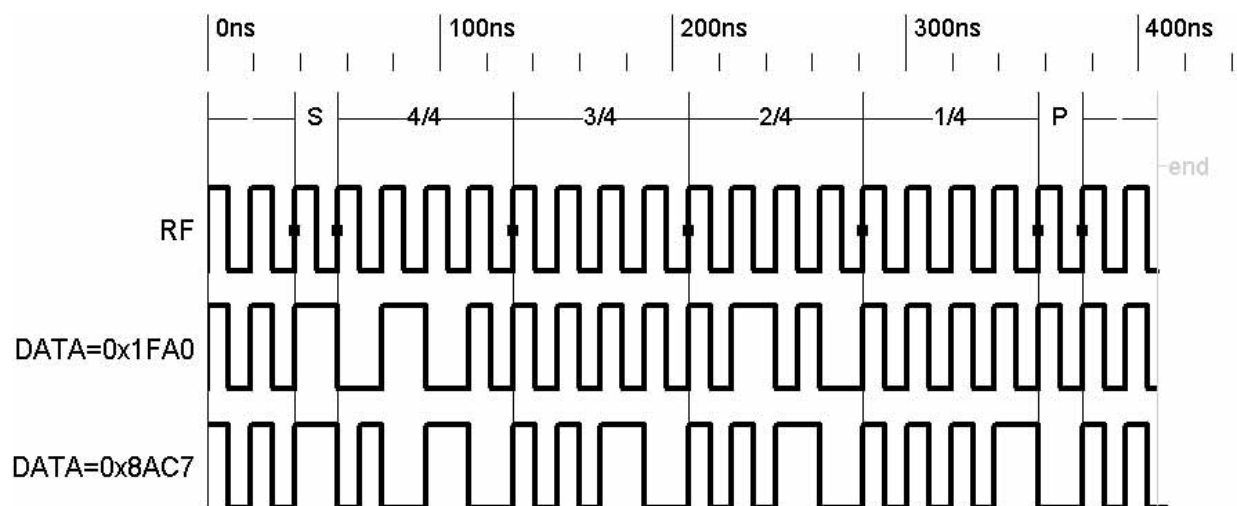


FIG. 16: FM Encoding scheme.

We briefly outline the changes to the detector DAQ here.

### 1. Triggering

We will trigger MIPP using silicon pixel systems that were developed for the BTeV experiment. We will have one pixel plane before the target and two after the target. We will have a trigger scheme that will project on the downstream pixels planes the expected

907 TPC/TDC Readout Card Block Diagram

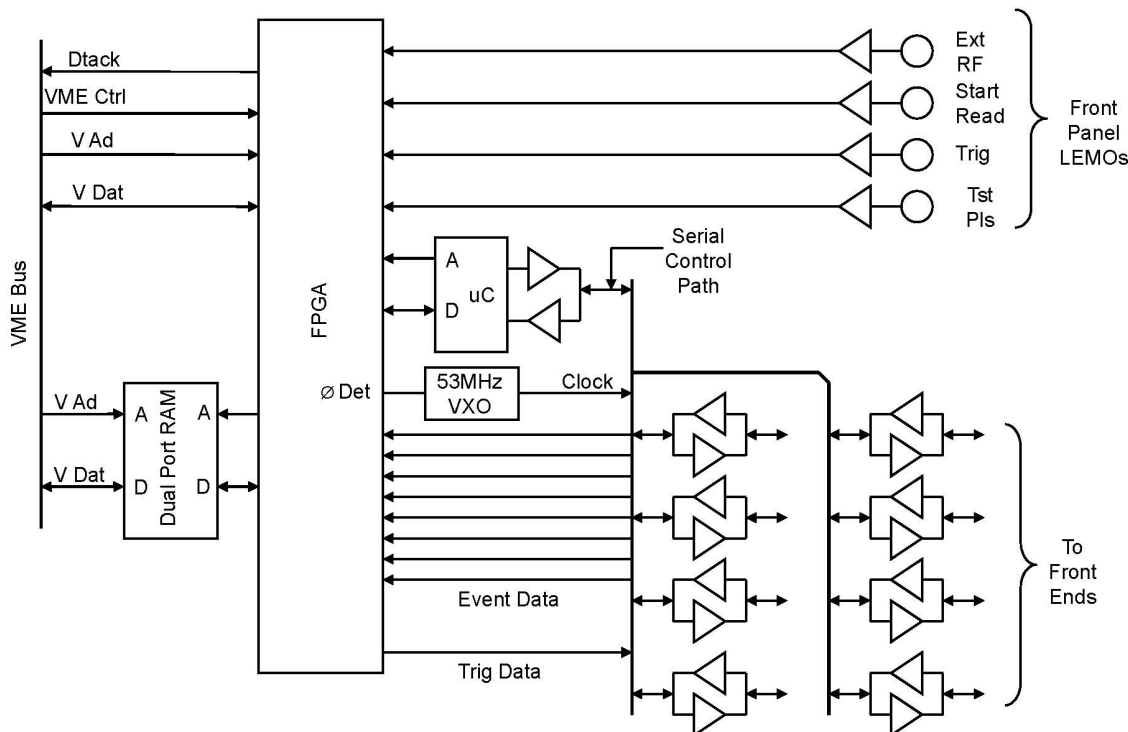


FIG. 17: MIPP Readout Controller card schematic.

un-interacted beam position (the bulls-eye) and trigger the experiment if pixels outside this bull's eye are hit. This scheme will enable us to trigger on low multiplicity events (including elastics) in an unbiased fashion. This would improve the existing MIPP trigger system that utilized a combination of a scintillator counter in conjunction with the first drift chamber multiplicity to provide the interaction trigger. While this system performed satisfactorily in our first run, it suffered from Landau fluctuations in the scintillator and periodic over-efficiency in the wire chamber. The digital nature of the pixel signal eliminates Landau tails completely.

## 2. Chamber electronics

We propose to replace the aging drift chamber electronics (remnants of the E690 system) with a more modern electronics system designed and built in-house at Fermilab. We will

use the same electronics for the Proportional chambers to replace RMH electronics.

The current drift chamber electronics with a large power consumption stresses the air conditioning in MC7 to the limit. The new electronics will cause significantly less heating.

The Chamber electronics will utilize the same MIPP Readout Controller cards as the new TPC electronics. This reduces initial design costs and also simplifies the detector readout.

### *3. Time of flight system and threshold Čerenkov detector*

We propose to replace the ToF and Čerenkov detector readout electronics with electronics designed and built in-house. This design will also utilize the same MIPP Readout Controller cards as used for the TPC readout.

### *4. Calorimeter/Plastic Ball readout scheme*

We have designed a readout board for the plastic ball that has both time digitization and ADC. A variant of this board will be used (ADC only mode) for the EM and hadronic calorimeters.

## **E. Upgrading the beamline to run at lower momenta**

The MIPP secondary beamline performed very well during our physics run which concluded in March 2006. Figure 18 shows a cut view of the beamline elements. During our run, we managed to operate the beamline as low as 5 GeV/c and as high as 120 GeV/c for the NuMI target run (The secondary beam production target was removed and a pinhole collimator inserted to reduce the Main Injector intensity). The beamline has been operated as low as 1 GeV/c to measure the flux available, which was adequate. What is lacking is the ability of the magnet power supplies to regulate the very small currents. We propose to add low-current magnet power supplies that are capable of this. We will switch to these power supplies during our low momentum running. The residual field of the iron yokes becomes significant at these low currents. Hall probes will be added to the beamline magnets to monitor their field so that hysteresis effects can be compensated for.

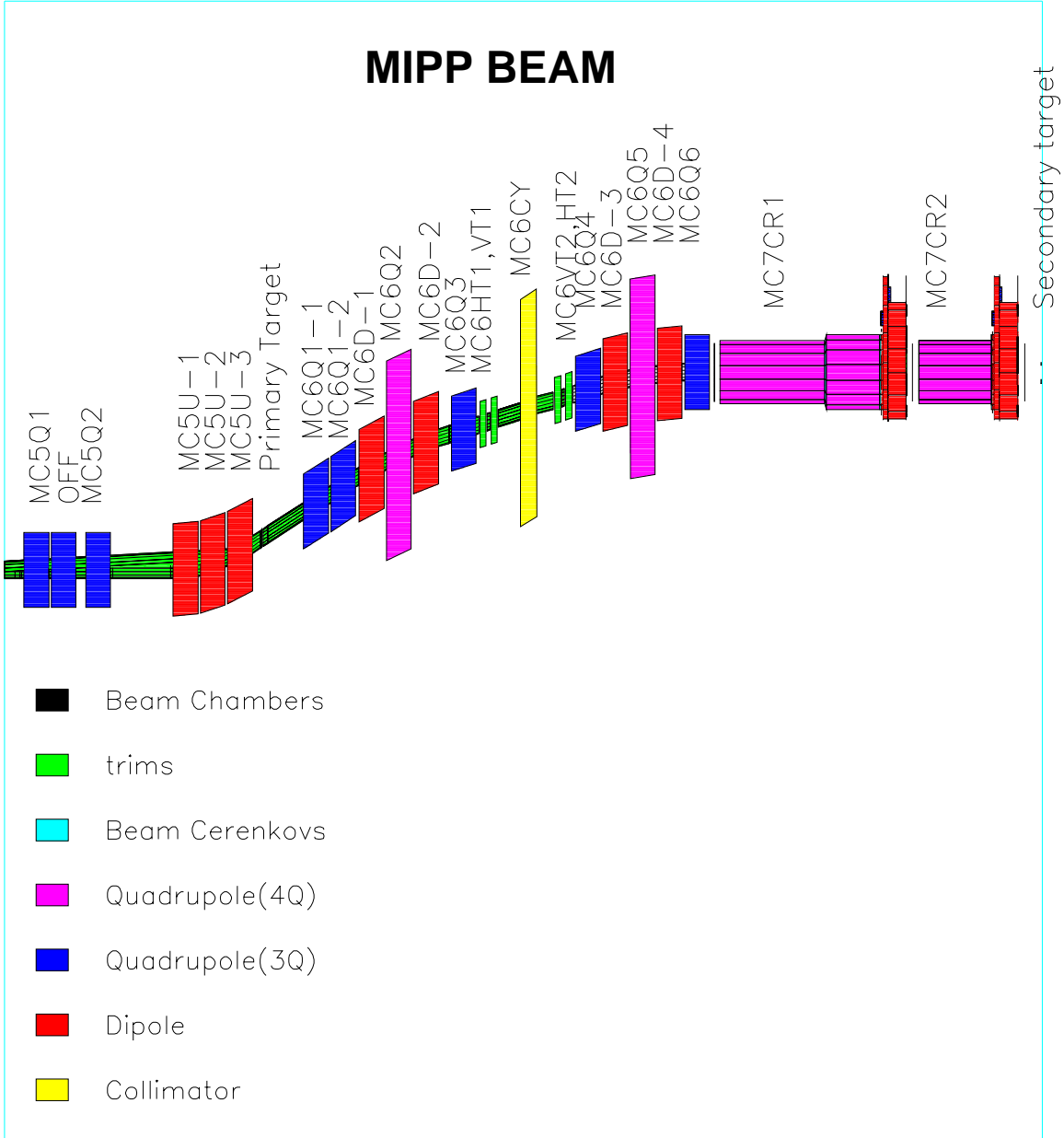


FIG. 18: The MIPP secondary beamline.

## F. Other tasks

We propose several small improvements to the MIPP experiment to increase reliability and maintainability of the experiment. These include several changes to the gas systems, the cryogenic target, and slow monitoring, as well as maintenance on Drift chambers and photomultiplier tubes for the RICH and CKOV detectors.

In the present experiment, we operated a single scintillator veto counter (which had a

hole in it to let the beam through) to guard against beam spray. A veto wall has been built using summer student help. In addition, a recoil detector (the Plastic Ball) will be added to detect low energy particles (both charged and neutral) that are produced at wide angles ( $> 80$  deg to the beam) and miss the TPC.

### III. SUMMARY OF THE PROPOSED PHYSICS FOR THE UPGRADED MIPP RUN

#### A. Particle Production on neutrino targets in the NuMI beam

We outline here the need to measure the particle production on the NuMI targets. In a disappearance experiment such as MINOS, the evidence of neutrino oscillations is obtained from the difference in shapes of the energy spectrum of the neutrino charged current events in the far detector and the near detector. Because of the finite size of the NuMI target and decay region, the angles of the decaying pions that produce neutrinos reaching the near detector have a different distribution than those reaching the far detector. Put another way, the neutrinos that interact in the near detector come from the decay of a different kinematic mix of pions than those that interact in the far detector. It is thus important to measure the dynamics of pion production off the NuMI target.

Figure 19 shows the distributions in longitudinal and transverse momentum of pions weighted by their contribution to the neutrino event rate in the far and near MINOS detectors. These weightings are different in detail. Superimposed on this plot are existing data on hadron production obtained from mainly single arm spectrometer measurements [21], which explains their discreteness in  $p, p_T$  space.

Figure 20 shows the predictions of the absolute neutrino rates in the MINOS near detector using four existing hadron production models [22]. The model predictions differ from the average by as much as 20% as a function of neutrino energy. Figure 21 shows the predictions of the ratio of the far to the near neutrino flux using the same four models. Again, there is considerable uncertainty in the predictions, which increases in the high energy tail of the spectrum. The evidence for oscillations is obtained by normalizing the far detector spectrum to the near detector spectrum ( $\approx 10^6$  more events in the near detector). The shapes of the two spectra have to agree in the high energy tail (no oscillations), before one

## Low Energy Beam

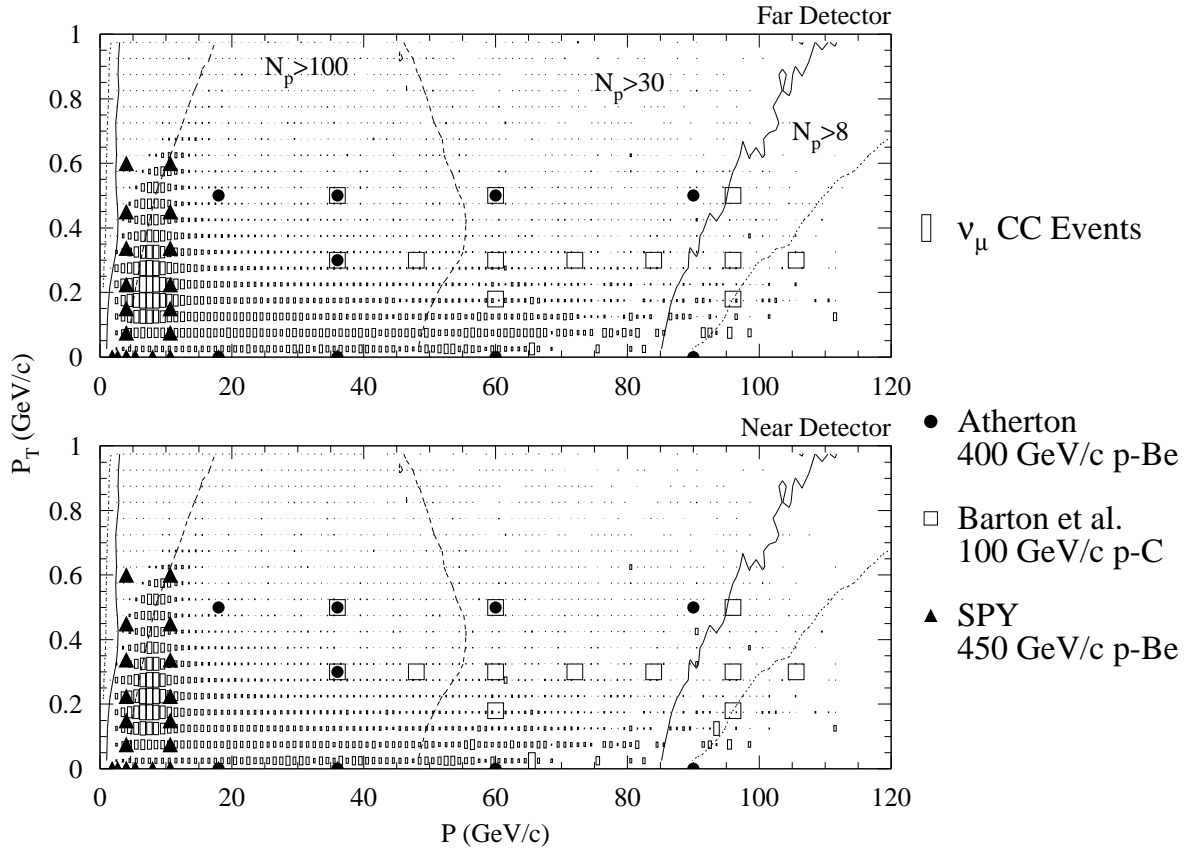


FIG. 19: The distribution in longitudinal and transverse momentum of secondary pions produced on the NuMI target. Secondaries have been weighted by their contribution to the neutrino event rate at the far (top) and the near (bottom) detectors. Overlaid are the locations of existing hadron production measurements.

can take seriously the expected deficit due to oscillations (in the low energy part of the spectrum). Figure 22 shows the variation of the percentage error in the far/near detector ratio as a function of the number of events obtained in MIPP off the NuMI target, for neutrino energies (3-4 GeV, low energy part, oscillation deficit) and for neutrino energies (20-22 GeV, high energy tail). It can be seen that one needs  $\approx 10^7$  events in MIPP on the NuMI target for this percentage error to drop below 3% in the high energy tail. MIPP has obtained 1.75 million events on the NuMI target currently installed in the MINOS experiment using 120 GeV/c protons from the Main Injector.

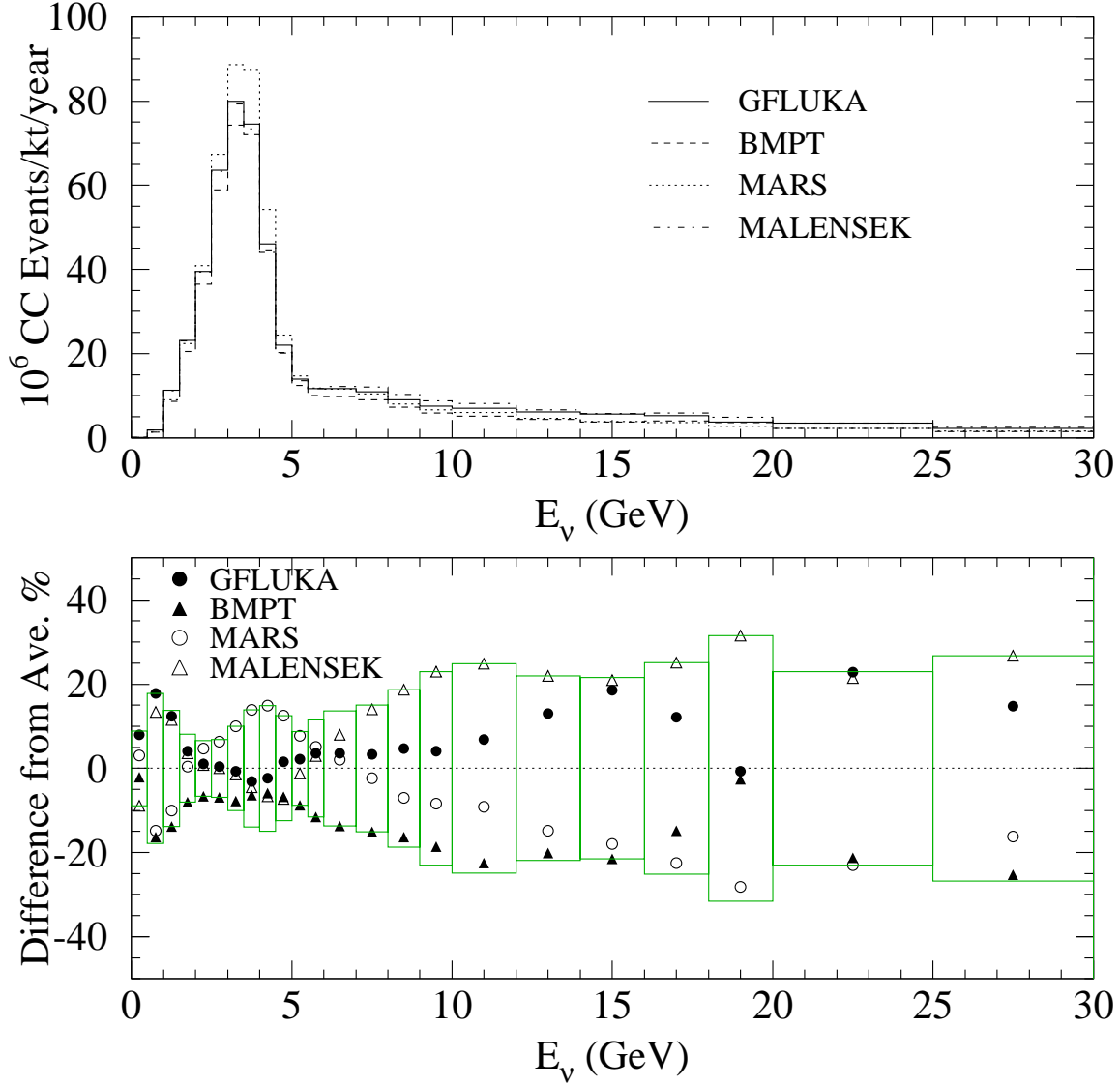


FIG. 20: The predictions of the absolute neutrino rates at the MINOS near detector using various hadron production models.

### 1. MINOS analysis

MINOS has analyzed its near and far detector data and published confirmatory evidence of neutrino oscillations [23] and the best estimates for the oscillation parameters  $\sin^2 2\theta_{23}$  and  $\delta m_{32}^2$ . Details of their near and far detector analysis have been reported at conferences [24]. We reproduce some relevant plots from the analysis done so far to highlight the uncertainties

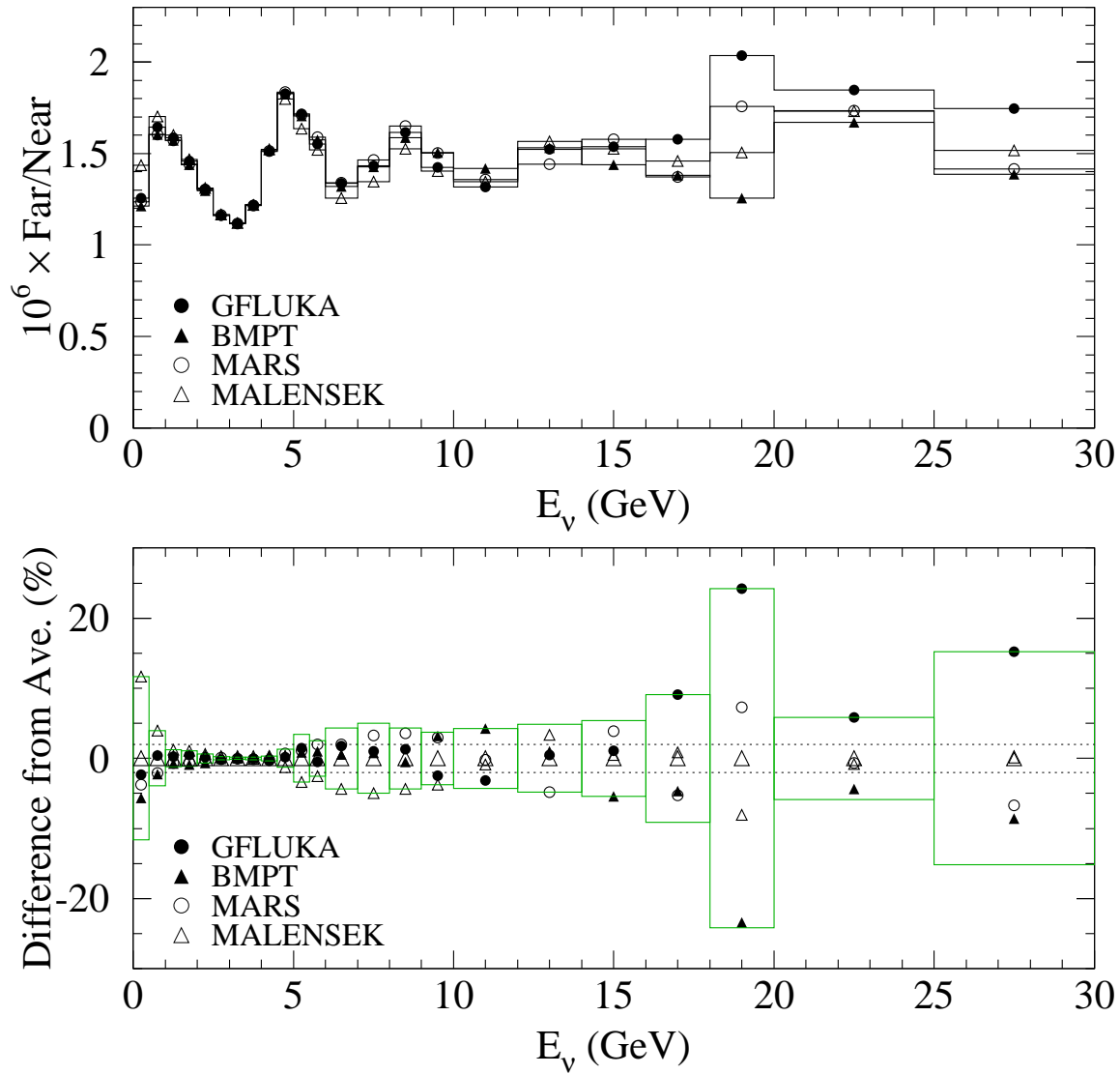


FIG. 21: The predictions for the ratio of the far neutrino flux to the near neutrino flux for various hadron production models.

associated with hadron production Monte Carlos and the need to measure the particle production first hand. Figure 23 shows the prediction of the near detector spectrum using a number of Monte Carlos for the low, medium and high energy NuMI beam settings. The spread in the Monte Carlos is indicated by the shaded error bar. The predictions of the near detector spectra utilize the Monte Carlo fluxes, the neutrino cross section and the detector resolution and trigger efficiencies and acceptances. The Monte Carlos systematically

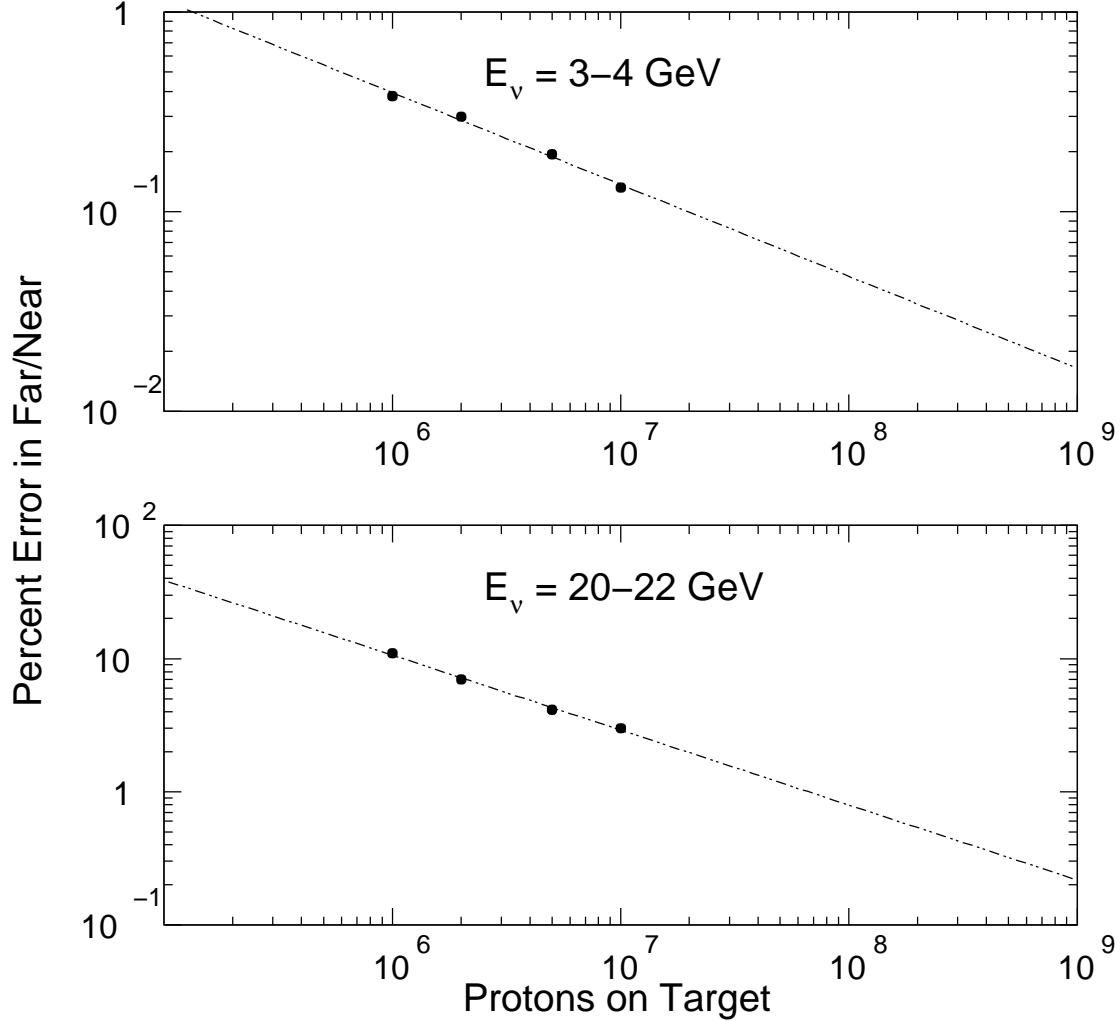


FIG. 22: The percentage error in the far/near ratio as a function of the number of events in MIPP obtained for the NuMI target (labeled protons on target) measurement as a function of the neutrino energy.

underestimate the low energy spectrum in the 6-18 GeV range. They also overestimate the the medium energy spectrum in the same energy range. This leads to the conclusion that the predictions of the hadron spectra are to blame and not the neutrino cross section for the mismatches. MINOS then proceeds to weight the Monte Carlo spectrum to match the near detector events and then uses the re-weighted spectrum to predict the far detector response as a function of the oscillation parameters. Figure 24 shows the predictions of the near/far

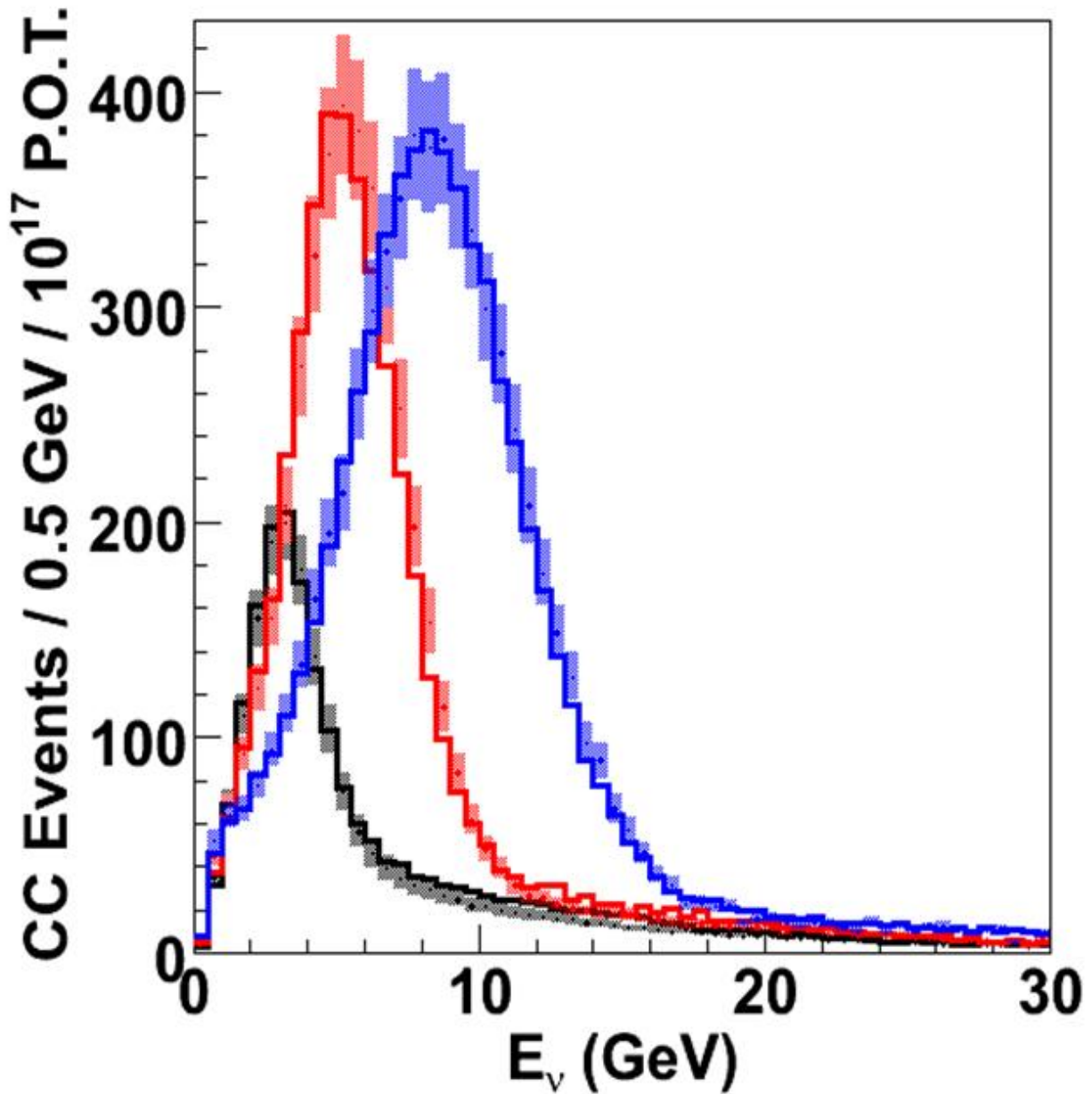


FIG. 23: MINOS predictions of the near detector charged current event spectra compared with data for a variety of Monte Carlos compared with data for the low, medium and high energy NuMI beam settings. The Monte Carlo spread is indicated by the shaded error bars and the data represented by the solid lines.

ratio for three Monte Carlos, FLUKA01, FLUKA05 and MARS. The predictions between FLUKA01 and FLUKA05 differ, even though there has been no new particle production data introduced into the code. The change is purely due to model development. MINOS

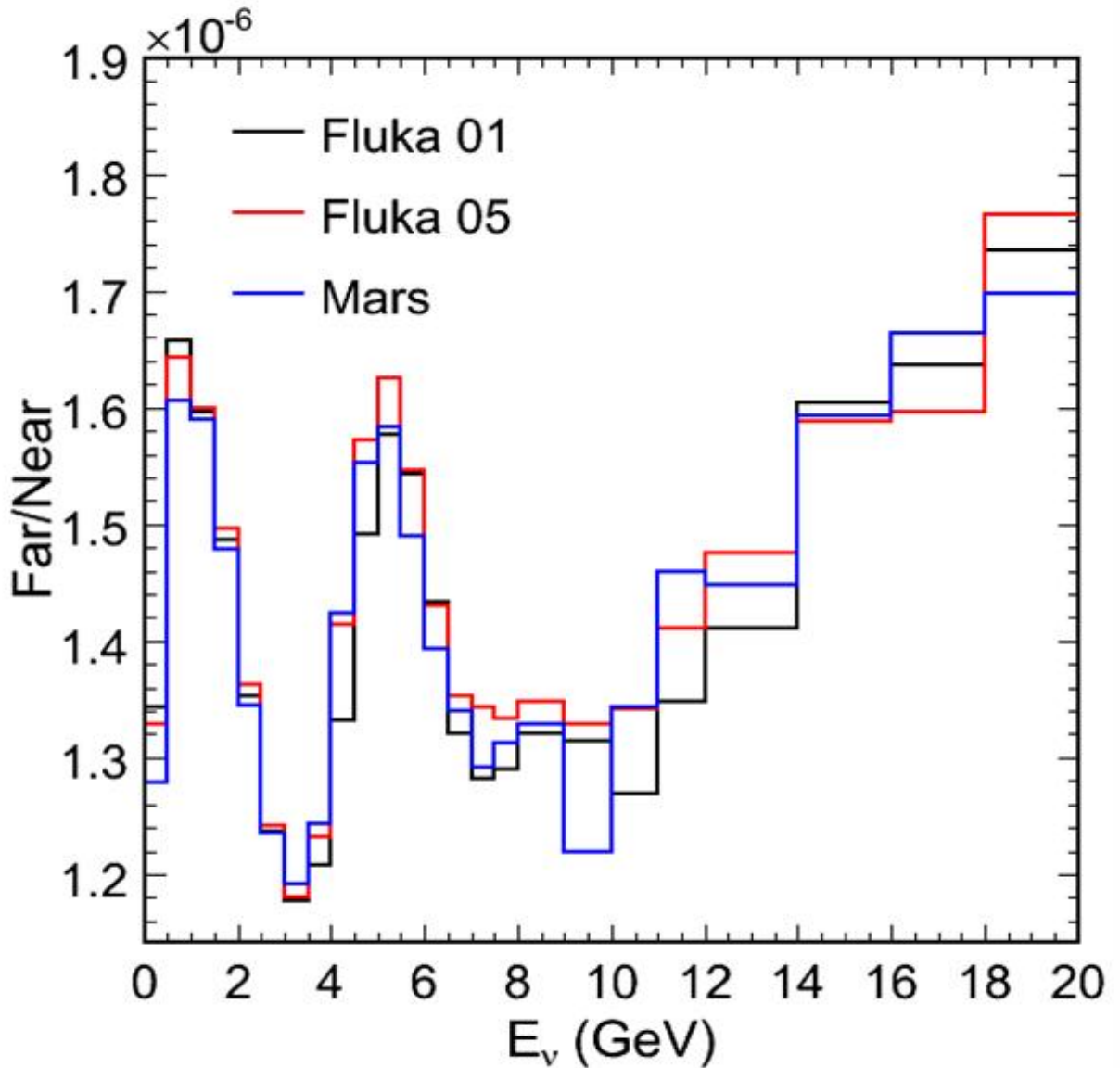


FIG. 24: MINOS predictions of the near/far detector ratio using the Monte Carlos, FLUKA01, FLUKA05 and MARS. The predictions differ between the FLUKA01 and FLUKA05 purely due to algorithmic development and not due to introduction of new particle production data.

has done a more thorough analysis of the near detector predictions as a function of their target position and also the horn current. Figure 25 shows the predictions for the low energy target setting with the target at the “10 cm” position LE10 and the horn current at 185 kA. At the point of maximum disagreement between the Monte Carlo predictions and data, the weight factor is  $\approx 1.4$ . These re-weighting uncertainties in the Monte Carlo are ameliorated in MINOS’s case by the excellent performance of their near detector. It would however

# Results (Including $>30$ GeV)

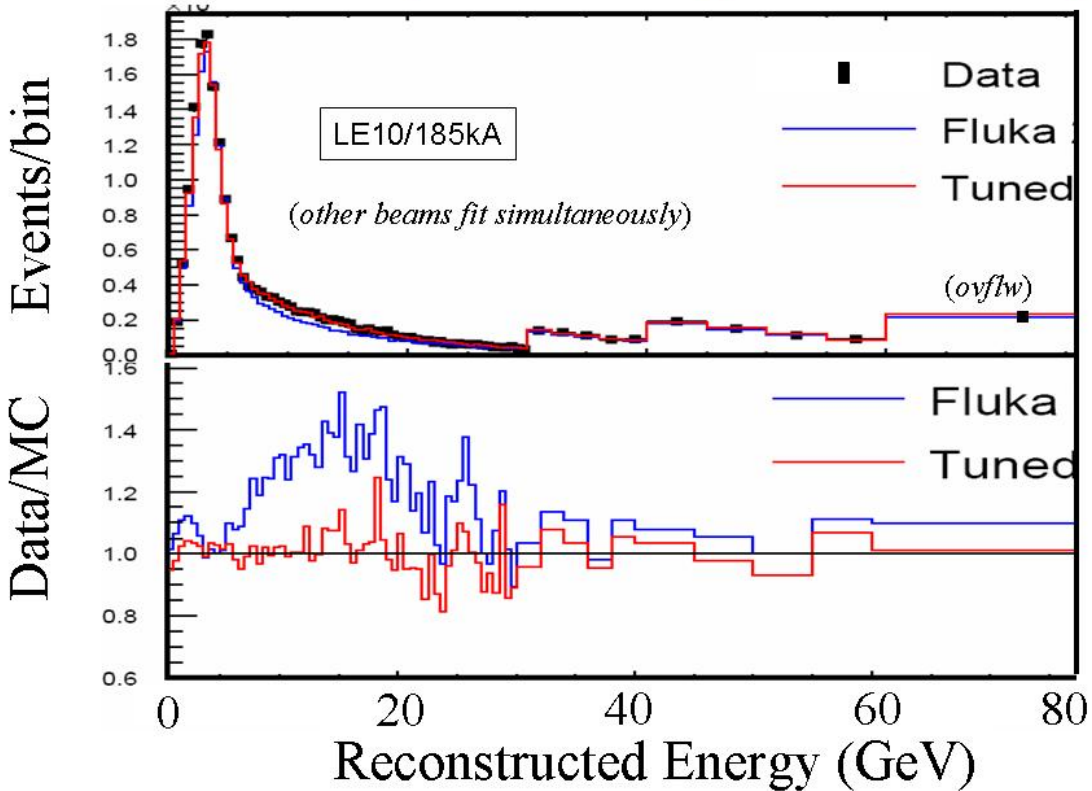


FIG. 25: MINOS predictions of the near detector spectrum for the target at the LE10 setting and the horn current at 185kA. The monte carlo prediction and the weight factor needed to make the Monte Carlo agree with data are shown.

be still desirable to remove all uncertainties by obtaining the needed  $10^7$  events, which the MIPP upgrade can do in 2 calendar days of running.

All of MINOS's largest systematic uncertainties are related in some fashion to neutrino cross section uncertainties and event shape modeling. These will also improve with improved neutrino beam predictions.

## 2. Measuring the $NO\nu A$ / $MINER\nu A$ target

MINER $\nu A$  has requested sufficient running in the NuMI LE beam, as used by MINOS, to measure the low-energy cross sections and nuclear effects so important for MINOS system-

atics. Neutrino cross sections need a first principles measurement of the particle spectrum. Using theoretical models of charged current quasi-elastic events to unfold the neutrino spectrum is hazardous at best, as has been shown recently by MiniBoone using HARP data [25] to measure the CCQE cross section. They observe a cross section higher by 30% than the theoretical predication, an effect they attribute as being possibly due to nuclear collective effects in the target. If this is the case, it will introduce an A dependent systematic to the flux determined this way. The analysis of the acquired MIPP data on the NuMI target will provide MINER $\nu$ A with a first principles calculation of the flux. It will also help MINOS cross check their flux model.

The NO $\nu$ A medium energy target has still to be designed. When it becomes available, MIPP can measure the particle spectrum from this target, obtaining a sample of  $10^7$  events in 2 days of running. This will help the MINER $\nu$ A experiment obtain cross sections using the medium energy target and the NO $\nu$ A experiment with its backgrounds and systematics in its search for electron neutrino appearance.

### 3. *Design of the LBNE target*

Both LBNE and NO $\nu$ A seek to measure the oscillation of the muon neutrino into an electron neutrino. Such experiments, especially the on-axis experiments such as LBNE need to have excellent determination of the electron neutrino background flux produced in their target and surrounding materials. MIPP upgrade will measure the  $K_S^0$  spectrum from the LBNE target and this can be used to infer the  $K_L^0$  spectrum and the  $K_{e3}$  decay rate of  $K_L^0$  which contributes to the electron neutrino background flux.

Equally important to understand is particle production from the material surrounding the target, such as the horn and other supporting structure. Since MIPP upgrade proposes to acquire particle production data on 30 nuclei to improve hadron production models, such data will have a significant impact on this issue as well.

### 4. *Benchmark test of Monte Carlos at the Hadronic Shower Simulation Workshop*

At the recently concluded Hadronic Shower Simulation Workshop at Fermilab [26], a series of benchmark tests were performed to test various Monte Carlo codes. We show

results from one such benchmark that is relevant to the prediction of neutrino fluxes. Data on particle production by 67 GeV/c protons on an aluminum target (60 cm long and 3 cm in radius) obtained in Protvino were compared to the predictions of the MARS and PHITS monte carlos. Figure 26 shows the comparison of the  $\pi^\pm$  spectra with the Monte Carlo predictions and Figure 27 shows the comparison of the  $K^\pm$  spectra with the Monte Carlo predictions as a function of production angle and energy. It is clear that the Monte Carlos disagree with each other and data underscoring the need for a first principles measurement of particle production of neutrino targets.

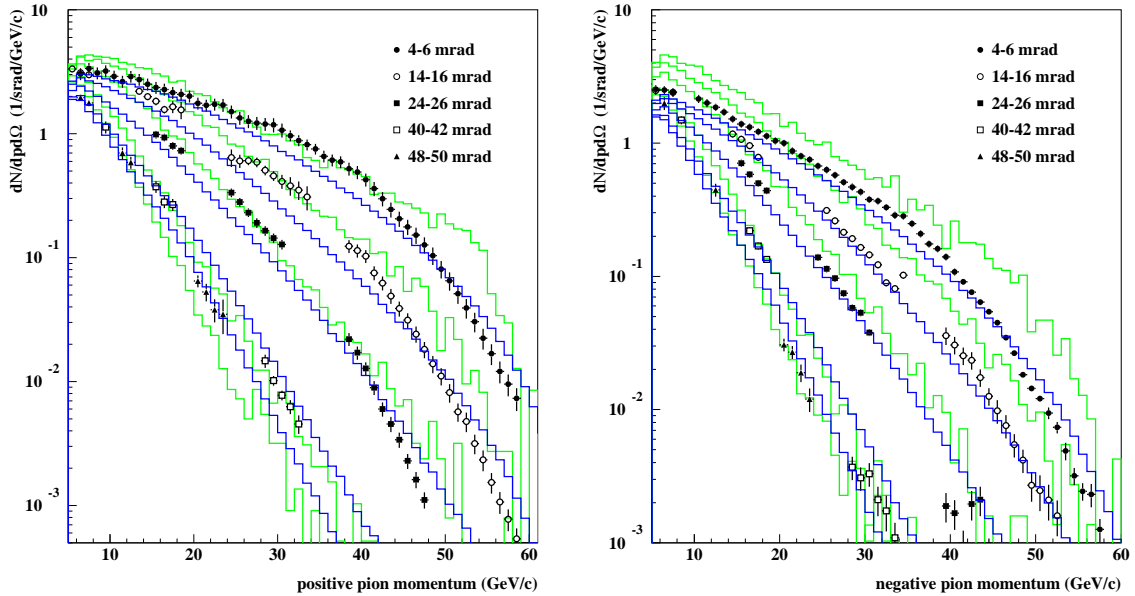


FIG. 26: Comparison of the predictions of the MARS15 (blue) and PHITS (green) Monte Carlos with the production  $\pi^+$  and  $\pi^-$  mesons produced by 67 GeV/c protons on a 60 cm long aluminum target.

## B. Particle production on Nitrogen and the question of Cosmic Ray Showers in the Atmosphere

We propose to measure particle production on a cryogenic nitrogen target using positive and negative beams, which is needed by experiments measuring cosmic ray air showers (Pierre Auger, HiRes etc) and also atmospheric neutrinos (Amanda, Ice Cube, HyperK etc).

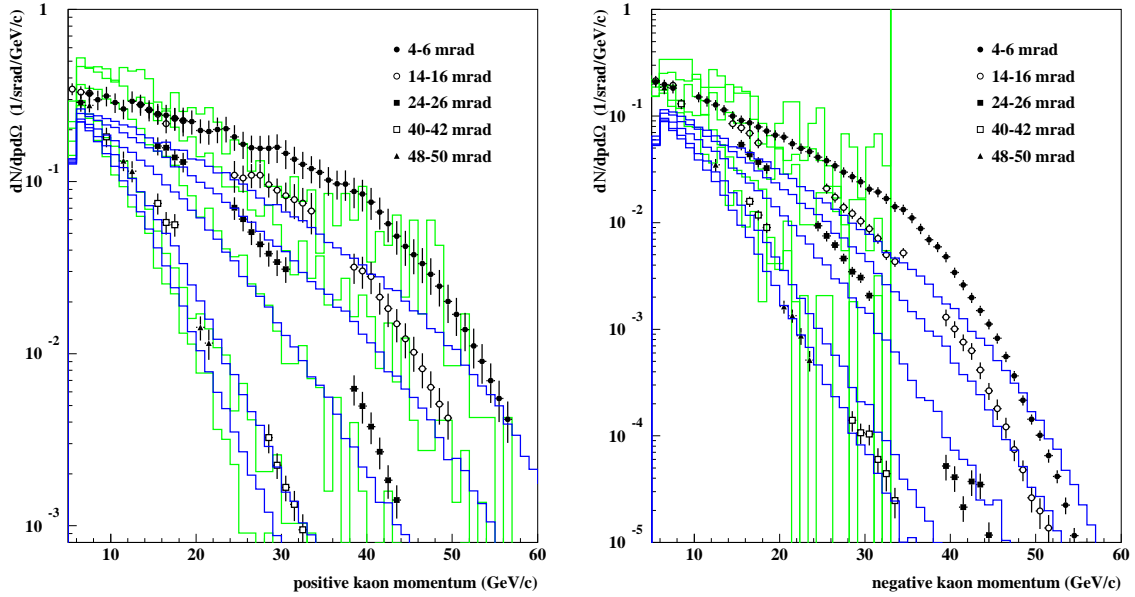


FIG. 27: Comparison of the predictions of the MARS15 (blue) and PHITS (green) Monte Carlos with the production  $K^+$  and  $K^-$  mesons produced by 67 GeV/c protons on a 60 cm long aluminum target.

The problem is illustrated in a recent paper [27] that simulates extensive air showers to illustrate the problem. They simulate the air showers produced by protons of  $10^6$  GeV energy in the atmosphere. The shower goes through several generations of interactions and produce pions and kaons that decay to produce muons and neutrinos. The muons and neutrinos are observed in the detectors and are termed the daughter particles. The mesons that produced the muons and neutrinos are termed the mother particles and the particles that interacted in the atmosphere to produce the mother particles are termed the grandmother particles in their jargon.

Figure 28 shows the energy spectrum of the grandmother particles ( $\pi$ ,  $K$  and  $p$  in an air shower that are produced by a primary proton of  $10^6$  GeV. The spectrum for the pions peaks at 100 GeV and the kaons and protons at somewhat higher energies. These particles interact with the nitrogen (and oxygen) in the atmosphere to produce the atmospheric neutrinos and muons. In other words, the beam energies available at MIPP are relevant to the simulation of the cosmic ray air showers. The muon flux measurement is a critical component of estimating the energy scale of the cosmic ray shower. MIPP measurements

thus will help reduce the systematics in the cosmic ray energy scale measurements. As the primary cosmic ray energy increases, the peaks in this plot do not shift to higher energies. Understanding the shower systematics at the peak of this spectrum (i.e MIPP energies) will help the energy systematics of cosmic rays of all energies. Figure 29 shows the distribution

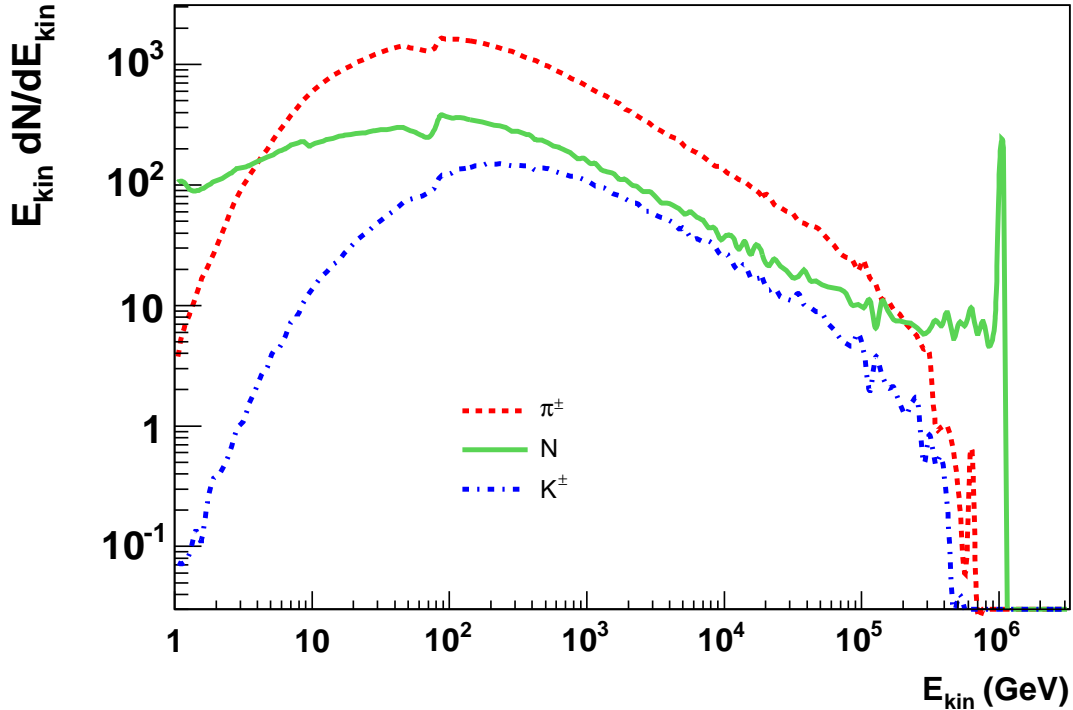


FIG. 28: The energy distribution of the grandmother particles in a vertical air shower produced by  $10^6$  GeV proton interacting in the atmosphere as a function of particle type. These particles interact further in the atmosphere to produce more particles which then decay into muons and neutrinos. The muons are detected at a distance of 0-500 meters from the shower center at ground level. It can be seen that these spectra peak at energies relevant to the MIPP energy scale.

of grandmother particles at different lateral distances from the shower center for all particle types. For the lower energy interactions, the simulation code GHEISHA is used to simulate the interactions of the particles with the atmosphere. For higher energy interactions, the simulation code QGSJET 01 is used. The sharp break in the spectra at 100 GeV is where the two codes meet and disagree at places by a factor of two. This illustrates the problem. These codes at present are “tuned” on single arm spectrometer data and disagree with each

other.

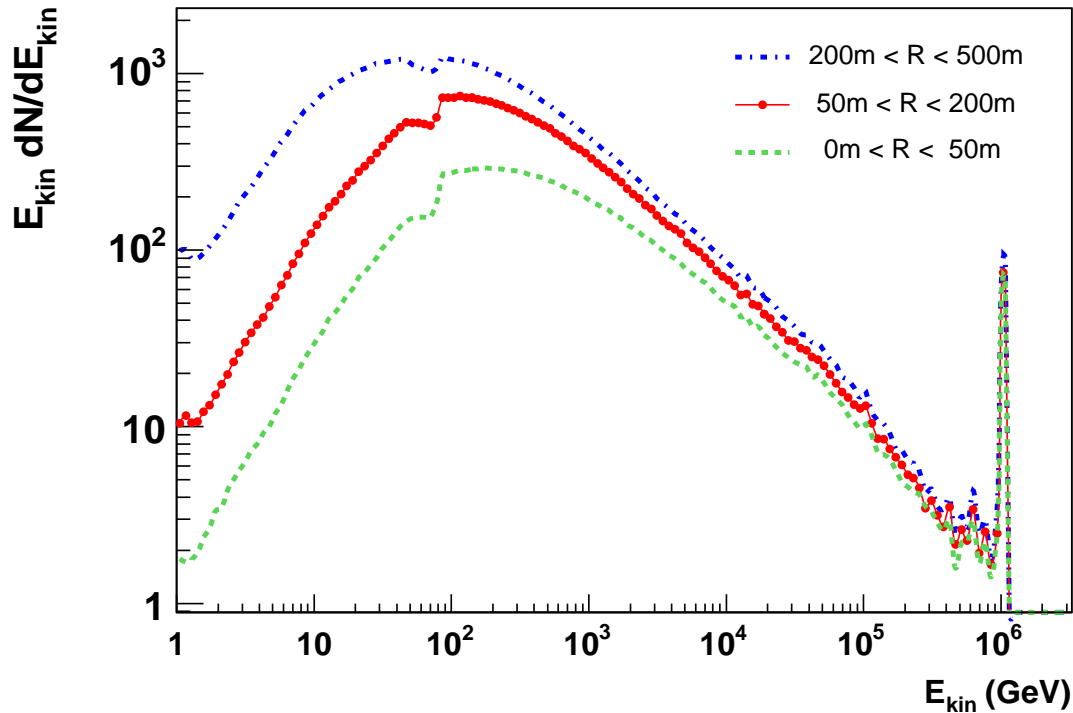


FIG. 29: The energy distribution of the grandmother particles in a vertical air shower produced by  $10^6$  GeV proton interacting in the atmosphere as a function of distance from the shower center. The spectrum peaks at energies relevant to the MIPP energy scale.

Figure 30 shows the momentum of grandmother particles versus the momentum of the mother pions in the air shower and plots the existing data relevant to simulating the process. Most of the data are over 25 years old and were obtained using Beryllium targets and single arm spectrometers resulting in a discrete angular coverage. MIPP will measure the outgoing pion and kaon spectrum for proton and pion beams in its full secondary beam momentum range. These cross sections are the most important in simulating cosmic ray showers in the atmosphere. In addition, it will also have kaon and antiproton interactions on nitrogen of which virtually nothing is known. Being an open geometry experiment, the MIPP angular coverage will be continuous, not discrete. The need for MIPP data is recognized by the cosmic ray community, some of whom have joined this proposal.

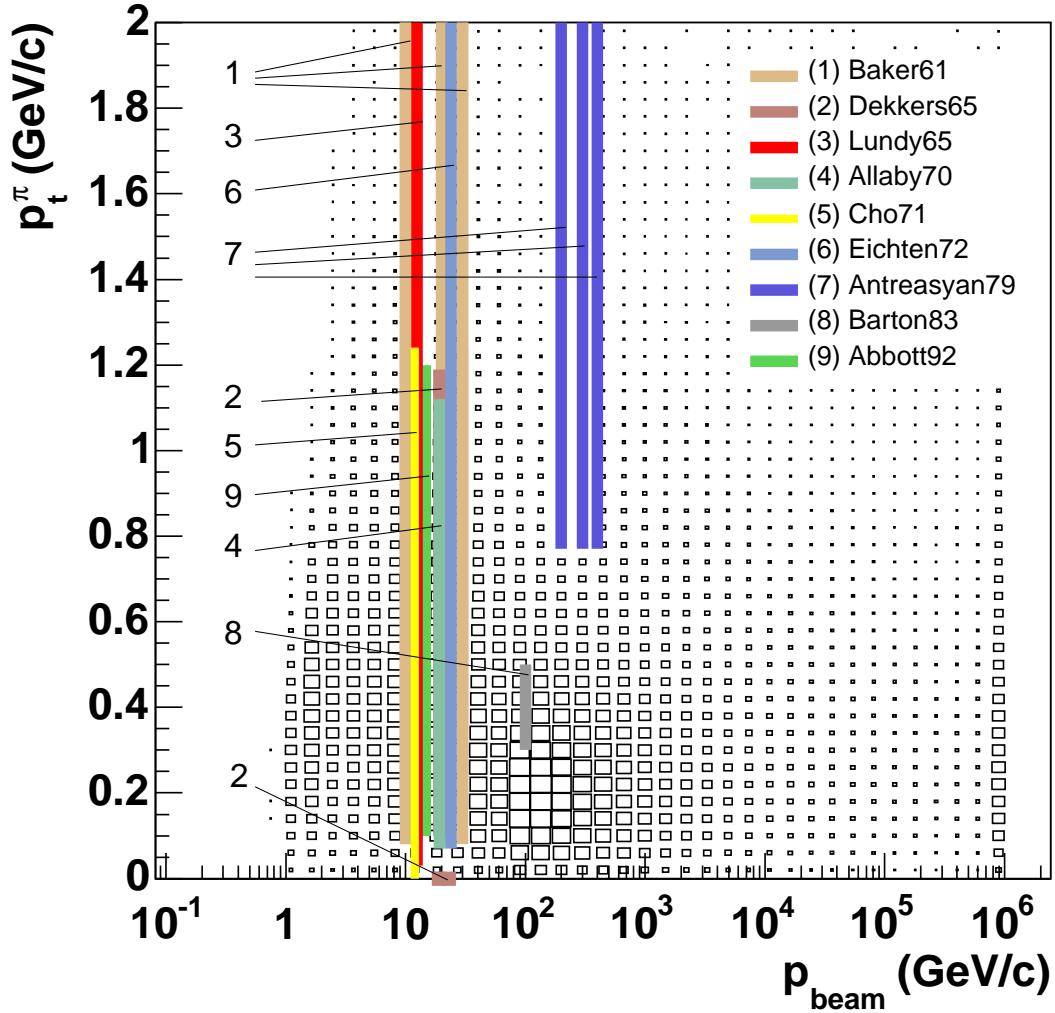


FIG. 30: The momentum of the grandmother particle (abscissa) that interacts to produce the mother pion that decays to produce the muon and atmospheric neutrino. The relevant existing experimental data are plotted. The data are over 25 years old and are often from a Beryllium target and obtained in single arm spectrometers at discrete transverse momenta.

### 1. MIPP Measurement of $\pi/K$ ratios

Because of its excellent particle identification capabilities, MIPP upgrade will measure the ratio of charged kaons to pions as a function of  $p_L, p_T$  of the final state particle. This measurement is of importance to both the NuMI target measurements and the atmospheric

neutrino measurements, since the charged K's produce  $\nu_e$ 's which are a background to the oscillation search  $\nu_\mu \rightarrow \nu_e$ .

### C. Hadronic production on Nuclei and the Hadronic Shower Simulation Problem

At the recently concluded workshop on Hadronic Shower Simulations [26], experts in shower simulation codes from five major Monte Carlos (GEANT4, FLUKA, MARS, MCNPX, and PHITS) (and several less well-known ones) met and reviewed their code status and what needs to be done further to improve codes. It was acknowledged that more particle production data would help improve algorithms a great deal and there were calls for a rapid publication of existing MIPP data and enthusiastic support for the MIPP upgrade.

The problem of hadronic shower simulations stems from our lack of understanding of the strong interaction. Though a theory of strong interaction exists (QCD), it cannot be used to calculate fundamental non-perturbative processes such as elastic cross sections, diffractive cross sections or any of the particle production cross sections that comprise 99% of the total cross section. This is in stark contrast to the simulation of electromagnetic showers where Monte Carlos such as EGS regularly make predictions that can be verified by observation.

The minimum bias cross section is modeled in most of the above mentioned Monte Carlos using the supercritical pomeron (which in itself violates unitarity). By application of the optical theorem, cut pomerons produce the total cross section. The cut pomeron is approximated by a quark gluon string which is then hadronized. This is the basis of the particle production models such as DPMJET and QGSJET which are used in Monte Carlos such as GEANT4 and MARS. The soft part of the scattering and the hard part of the scattering cross section are joined very carefully, but arbitrarily.

Nuclear break-up is handled using a plethora of models that go by the name of binary cascade, Bertini cascade, CHIPS (Chiral Invariant Phase Space), CEM03 and GEM2, each of which have different assumptions on the nuclear break-up mechanism.

Each of these Monte Carlos are “validated” using existing data. Inclusive particle spectra from single-arm spectrometer experiments that are over 30 years old are used. These data are discrete in the transverse momentum variable and have systematics that are significantly greater than open geometry experiments such as HARP, NA49 and MIPP. These models are made to agree with inclusive particle spectra. Predictions of correlations between particles

	Binding Energy	Evaporation n (# neutrons)	Cascade n (# neutrons)	Ionization (#cascade p)	Target recoil
Before first reaction				(250)( $\pi_{in}$ )	
First reaction	126	27(9)	519 (4.2)	350(2.8)	28
Generation 2	187	63(21)	161(1.7)	105(1.1)	3
Generation 3	77	24(8)	36(1.1)	23 (0.7)	1
Generation 4	24	12(3)			
Total	414	126(41)		478(4.6)	32

TABLE I: Destination of 1.3 GeV total energy carried by an average pion produced in hadronic shower development in lead. Energies are in MeV.

are not tested against, since such data do not exist in readily testable form. However, calorimeter designers are currently asking questions such as how wide a hadronic shower is in a calorimeter, which depends on particle correlations.

Another important part of calorimetric simulation of hadronic showers is the nuclear break-up and the number of spallation neutrons and protons emitted, as emphasized by Wigmans [28]. The linearity of the calorimeter and the resolution of the calorimeter depend critically on compensating for the “invisible energy” in a hadronic shower carried away by neutrons and nuclear binding energy. It is important to model these processes correctly. It is not at all clear as to how well the above mentioned nuclear break-up models simulate these processes.

To illustrate this further, table I shows [28] how the energy is deposited by a 1.3 GeV pion in lead. The energy is deposited as ionization  $dE/dx$ , as binding energy required to split the nucleus, as cascade nucleons and evaporation nucleons (isotropic emission). Please note that on average only 478 MeV of a 1.3 GeV pion ends up as ionization energy and the rest is carried away as neutrons and also absorbed as binding energy. The whole question of compensating calorimetry hinges on using the neutrons to produce knock-on protons to compensate for this invisible energy, since energy from the neutrons can be made to be visible by introducing hydrogenous materials in the calorimeter in appropriate proportions, resulting in knock-on protons caused by neutron elastic scattering that deposit visible energy.

The upgraded MIPP spectrometer can measure nuclear multi-particle hadronic production using 6 beam species ( $\pi^\pm$ ,  $K^\pm$ ) and  $p^\pm$  in the momentum range  $\approx 1$  GeV/c-120 GeV/c. The TPC can measure the protons from nuclear breakup that travel forward in the laboratory and the plastic ball detector will detect the evaporation neutrons and protons emitted backwards in the laboratory. We can measure 30 nuclei in 30 days of running and obtain data of unprecedented quality and statistics on nuclei commonly encountered in particle physics detectors.

We propose as a first priority (“A-List”) to measure particle production on the nuclei H<sub>2</sub>,D<sub>2</sub>,Li,Be,B,C,N<sub>2</sub>,O<sub>2</sub>,Mg,Al,Si,P,S,Ar,K,Ca, Hg,Fe,Ni,Cu,Zn,Nb,Ag,Sn,W,Pt,Au,Pb,Bi,U and as a second priority (“B-list”) the nuclei Na,Ti,V, Cr,Mn,Mo,I, Cd, Cs, Ba

These data can be used to validate the Monte Carlos to unprecedented accuracy or may even be usable directly as a library of events in a fast Monte Carlo [29].

It is worth pointing out that the MIPP upgrade proposal represents a unique opportunity to obtain such a dataset. Comparable experiments such as HARP do not possess kaon or antiproton beams and do not have the range in beam momentum (3-15 GeV/c primary momentum). HARP has finished data taking. The NA49 upgrade (SHINE) does not possess the data-taking rate ( $\approx 70$  Hz compared to 3000 Hz in MIPP) nor the particle id capabilities of MIPP (no forward RICH detector), though, being an SPS experiment, it has higher beam momenta (positive beams only, maximum beam momentum 158 GeV/c). Nevertheless, these two experiments will provide valuable data in the near future on particle production.

Lastly, there is a misunderstanding among some that putting test hadronic calorimeter modules in the test beam and comparing the predictions of simulation programs such as GEANT4 and FLUKA to the observed data can help tune the hadronic models in the simulation programs. This myth was debunked at the Hadronic Shower Simulation Workshop, when the Geant4 group collectively answered a question by stating that “We only change our models based on microscopic data” [30]. Upon being asked what “microscopic” meant, they answered, thin target nuclear data. It is difficult to unfold the various nuclear and readout effects in calorimeter data to change the models. In other words, the only way to improve the simulation models is by experiments such as MIPP, HARP and NA49 that measure hadro-production using thin targets.

#### D. Tagged Neutral beams and Calorimeter R&D

The particle flow algorithm (PFA), proposes to measure the energy of jets in an event by using both the magnetic field and the calorimeter. The charged particles are measured using the excellent momentum resolution of the tracker and the neutral particles are measured using the calorimeter. The required fractional energy resolution of a jet is typically  $\sigma_E/E = 0.3/\sqrt{(E)}$ , E in GeV. In order to measure the neutral particle energy using the calorimeter, one needs to separate the charged particle hits and the neutral particle hits in the calorimeter. This dictates a highly segmented calorimeter. In order to test the design, one needs to simulate the widths of the showers of both the charged and neutral particles in the calorimeter. Neutron interactions in the calorimeter cannot be deduced from the interaction of protons below an energy of  $\approx 20$  GeV/c because the limiting fragmentation regime has not been reached at these low energies. It is precisely these energies that are of interest to the particle flow algorithm. This calls for a data-based approach both for charged and neutral hadronic responses. The charged response can be obtained in a regular test beam such as would be available at Fermilab in the M-test area. The upgraded MIPP spectrometer offers a unique opportunity to measure the neutral particle response to three neutral species, the neutron, the  $K_L^0$  and the anti-neutron.

The basic idea is to use the diffractive reactions

$$pp \rightarrow n\pi^+p \tag{1}$$

$$K^+p \rightarrow \bar{K}^0\pi^+p; \bar{K}^0 \rightarrow K_L^0 \tag{2}$$

$$K^-p \rightarrow K^0\pi^-p; K^0 \rightarrow K_L^0 \tag{3}$$

$$\bar{p}p \rightarrow \bar{n}\pi^-p \tag{4}$$

where the beam of protons,  $K^\pm$  or  $\bar{p}$  fragments diffractively to produce the neutral beam. The charged particles in the reaction are measured in the MIPP spectrometer. The beam momentum is known to  $\approx 2\%$ . So the momentum of the tagged neutral particle can be inferred by constrained fitting (3-C fit) to better than 2%, event by event. The tagged neutral particle goes along the beam direction and ends up in a test calorimeter placed in lieu of the present MIPP calorimeter.

This technique demands that the target is a proton and will only work on a liquid hydrogen cryogenic target (that MIPP possesses). The plastic ball recoil detector will act as

TABLE II: Expected number of tagged neutrons,  $K_L^0$ , and anti-neutrons per day with an upgraded MIPP spectrometer.

Beam Momentum	Proton beam	$K^+$ beam	$K^-$ beam	$\bar{p}$ beam
GeV/c	n/day	$K_L^0$ /day	$K_L^0$ /day	$\bar{n}$ /day
10	20532	4400	4425	6650
20	52581	9000	9400	11450
30	66511	12375	14175	13500
60	47069	15750	14125	13550
90	37600	-	-	

an additional veto against neutral target fragments such as slow  $\pi^0$ 's.

The momentum spectrum of the neutral beam is controllable by changing the beam momentum. The method is outlined in detail in MIPP note 130 [31]. The diffractive processes are simulated using the program DPMJET and the event rates estimated for a calorimeter placed in the MIPP calorimeter position. With the MIPP upgrade, it should be typically possible to obtain  $\approx 50,000$  tagged neutrons,  $\approx 9,000$  tagged  $K_L^0$ , and  $\approx 11,000$  tagged  $\bar{n}$  per day in the calorimeter with the beam momentum set to 20 GeV/c. Table II shows the expected number of events/day as a function of beam momentum and beam species. Figure 31 shows the momentum spectrum of tagged neutrons accepted in the calorimeter as a function of the beam momentum. Other similar plots are available in MIPP note 130 [31].

### 1. Observation of tagged neutron events in MIPP

MIPP has observed several tagged neutron candidates in existing data. Figure 32 shows a typical such event with a 58 GeV/c proton beam on liquid hydrogen target. Two positive tracks (11.8 GeV/c  $\pi^+$  and 0.4 GeV/c proton) are observed corresponding to the pion and the proton and a neutral deposit (51.8 GeV in the hadron calorimeter) is observed, with little energy in the electromagnetic calorimeter, signifying a neutron.

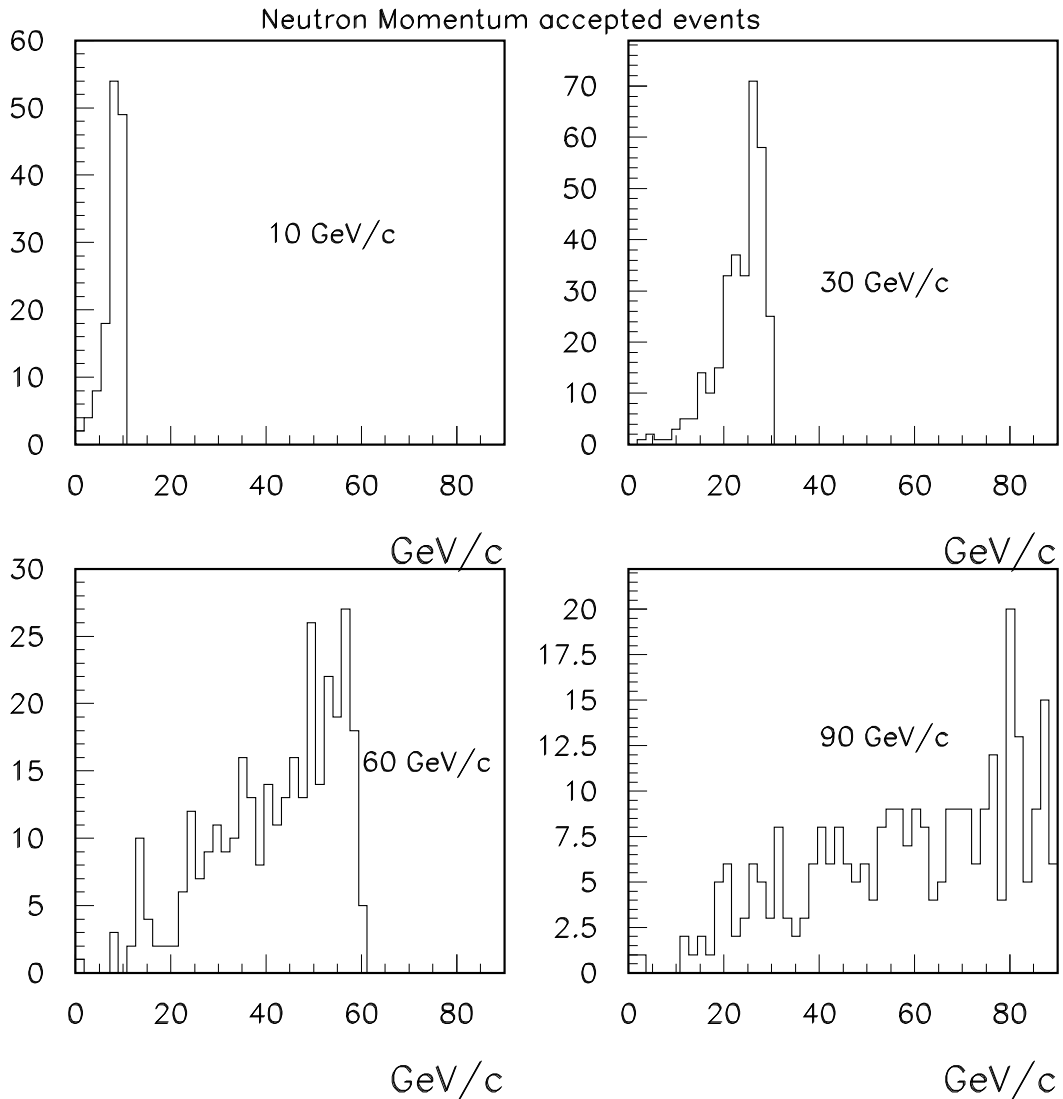
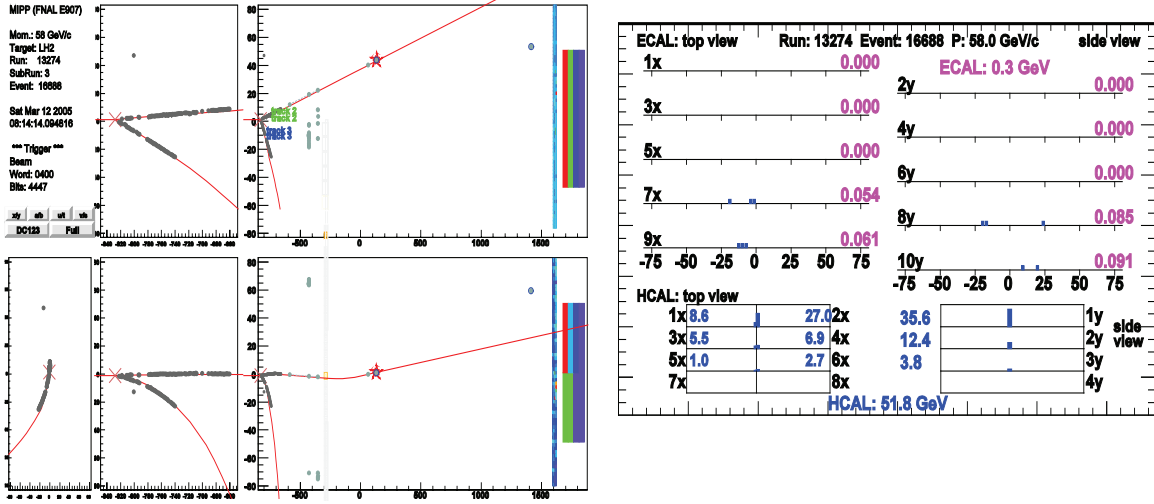


FIG. 31: Momentum spectrum of accepted neutrons for incident proton momenta of 10 GeV/c, 30 GeV/c, 60 GeV/c and 90 GeV/c for the process  $pp \rightarrow pn\pi^+$ .

#### IV. NON-PERTURBATIVE QCD PHYSICS

The upgraded MIPP detector will provide high statistics data using hydrogen and nuclear targets that will permit the investigation of non-perturbative QCD with unprecedented statistics. Here we list a number of such topics that can be addressed by the upgraded spectrometer. Indeed, a large fraction of the liquid hydrogen running can be done symbiotically

### Tagged neutral candidate 2 --58 GeV pp interaction



Tracking Display

Calorimeter display

FIG. 32: MIPP event display of a tagged neutron candidate. There are two positive tracks in the tracking chambers (11.8 GeV/c  $\pi^+$  and 0.4 GeV/c proton) and a deposit consistent with a neutron (51.8 GeV) in the hadron calorimeter.

with the tagged neutral beam running.

#### A. Further testing of a Scaling Law of Hadronic Fragmentation

The scaling law in question [32] states that the ratio of a semi-inclusive cross section to an inclusive cross section involving the same particles is a function only of the missing mass squared ( $M^2$ ) of the system and not of the other two Mandelstam variables  $s$  and  $t$ , the center of mass energy squared and the momentum transfer squared, respectively. Stated

mathematically, the ratio

$$\frac{f_{subset}(a + b \rightarrow c + X)}{f(a + b \rightarrow c + X)} \equiv \frac{f_{subset}(M^2, s, t)}{f(M^2, s, t)} = \beta_{subset}(M^2) \quad (5)$$

*i. e.*, a ratio of two functions of three variables is only a function of one of them. The physics behind the scaling law may be understood by considering inclusive cross sections as the analytic continuations of crossed three body interactions, which factorize into a production term that results in the formation of a short-lived fireball of mass  $M^2$ , which subsequently decays into the subset in question. The formation is governed by  $s$  and  $t$ . The decay term is only a function of  $M^2$ . It should be noted that the physics in question falls outside the scope of perturbative QCD and as such the scaling law is not currently derivable from QCD considerations.

In the MIPP data already taken, we managed to acquire  $\approx 5.65$  million events on liquid hydrogen at beam momenta 20 GeV/c, 60 GeV/c and 85 GeV/c. These are currently being analyzed and will form the basis of testing the proposed scaling law as a function of both  $s$  and  $t$ .

With the upgrade, we can extend the test of the scaling relations with two particle inclusive final states, which will require higher statistics due to the larger number of variables to test against.

## B. Antiproton Interactions in MIPP

The FAIR project has been approved by the German government and will provide a facility for research into anti-proton and ion interactions at GSI Darmstadt. The start of construction is planned for 2007 with the first experiments being set for 2012 and the completion of the project is scheduled for 2014. The cost of the project is  $\approx 1$  billion euros. PANDA [33] is one of the flagship experiments at FAIR and stands for Proton ANtiproton DArmstadt).

The GSI-KVI group are interested in measuring cross sections of antiprotons on hydrogen and other nuclear targets in MIPP to help them design the PANDA detector. MIPP has antiproton beams with momenta as high as  $\approx 60$  GeV/c and as low as  $\approx 3$  GeV/c. The excellent particle identification capabilities of MIPP will enable a systematic study of anti-proton interactions in particular the annihilation cross section.

The PANDA experiment proposes to measure  $p\bar{p}$  interactions in the charmonium range and higher. They are also interested in the magnitude of open charm production in  $p\bar{p}$  interactions of which little is known in this energy range. The presence of pixel planes in MIPP might facilitate a measurement of these rare processes.

### C. High Multiplicity Events in MIPP and the question of bosonic condensation

We propose to investigate the production of high multiplicity events in  $pp$  interactions where excesses may exist due to the occurrence of Bose-Einstein interference [40] in multipion production. This study can be done on the large sample of  $pp$  interactions we will collect using the liquid hydrogen target.

The goal is to investigate collective behavior of particles in multiple hadron production in  $pp$  and  $pA$  interactions at the beam energy  $E_{lab}=30 - 120$  GeV. We will study the domain of very high multiplicity (VHM) for  $z > 4$ , where  $z = n / \langle n \rangle$ . At large multiplicities, near the threshold of reaction, all particles will have small relative momentum with respect to each other. In a thermalized cold and dense hadronic gas a number of collective effects listed below may show up as a consequence of multiboson interference.

- A large increase of partial cross section  $\sigma(n)$  of  $n$  identical particles production is expected, compared to the commonly accepted extrapolation.
- Formation of jets consisting of identical particles may occur (pionic laser).
- Large fluctuation of charged  $n(\pi^+, \pi^-)$  and neutral  $n(\pi^0)$  components, onset of Centauros or chiral condensate effects may occur.
- Increase of the rate of the direct photons as the result of the bremsstrahlung in partonic cascade and annihilation  $\pi^+ + \pi^- \rightarrow n\gamma$  in dense and cold pionic gas or condensate is expected. The creation of a multipion bound state is possible which in the course of its formation emits soft photons.
- In the domain of high multiplicity, the major part of the center of mass energy is materialized leading to high density of hadronic system. At this condition a phase transition to cold Quark Gluon Plasma may occur.

- The momenta of produced particles in the center of mass system in the VHM domain are small. Then the multi-particle Bose-Einstein correlation may be readily seen. The latter can lead to the “hadron laser” effect, and the enhancement of soft gamma-quanta production.
- We expect a uniform energy distribution over produced particles due to thermalization in this regime.

The process of energy dissipation in hadron interactions poses a complicated problem for theory. For instance, the event generator Pythia gives the  $pp$  cross section  $\sigma(z)$ , at  $z > 2$ , two order of magnitude lower than the experimental value, see Figure 33. Hence further experimental and theoretical investigations are crucial to solve this problem. It may be closely connected to the vacuum structure of QCD and the confinement phenomenon. MIPP can investigate the properties of multiboson systems in the domain of low temperature and high density where pions may be in a state of boson condensation. The estimates shows that the temperature of the hadronic system becomes lower than 25 MeV at a multiplicity of  $z = 5$ . At such a temperature, the pionic gas may be in a condensate state. MIPP offers a unique opportunity to investigate the above-mentioned problems. Using the partial cross section extrapolation (Figure 33) one can estimate the counting rate in the VHM domain. As an example, for  $z=4$ , the partial cross section is  $\sigma \approx 0.2 \mu b$ . In a 10 day run on the hydrogen target, we will collect 50 Million events, in which there will be  $\approx 300$  events with  $z \geq 4$ . According to theoretical estimates, the multiparticle enhancement effects could become prevalent in the multiplicity domain  $z \geq 4$ , resulting in a greatly increased rate in this region.

#### D. Baryon Spectroscopy with the upgraded MIPP

Partial-wave analyses of  $\pi N$  scattering data have yielded some of the most reliable information about nonstrange baryon resonances. These analyses provide information about resonance masses and total decay widths (or their pole positions) and  $\pi N$  branching fractions. In order to determine resonance couplings to other channels, it is necessary to study inelastic  $\pi N$  scattering reactions, such as  $\pi^- p \rightarrow \eta n$ ,  $\pi^- p \rightarrow \pi^+ \pi^- n$ , and  $\pi^- p \rightarrow K^0 \Lambda$ , to give only a few of many possible examples. Important information is also provided by

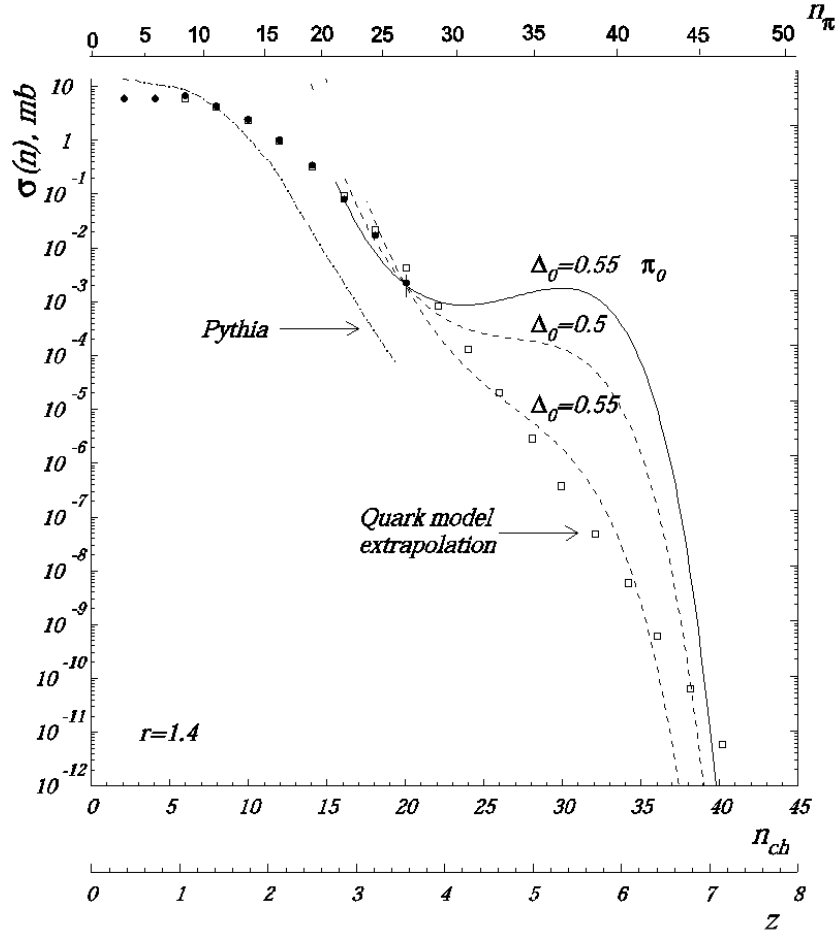


FIG. 33: Multiplicity distribution in  $pp$  interactions at 70 GeV (solid points). the curves marked by the parameter  $\Delta$  are model calculations accounting for identical pions interference.

meson photoproduction experiments, such as  $\gamma p \rightarrow \pi^0 p$ ,  $\gamma p \rightarrow K^+ \Lambda$ , and  $\gamma p \rightarrow \pi^+ \pi^- p$ . These hadronic and electromagnetic reactions are all linked by unitarity of the S-matrix, and modern coupled-channel analyses attempt to describe data from both hadronic and electromagnetic channels within a single consistent framework.

The data obtained from  $\pi N$  scattering and meson photoproduction experiments provide crucial information about QCD in the nonperturbative regime. One of the important issues concerns how many internal degrees of freedom are really needed to describe baryon resonances. Essentially all of the known baryon resonances can be described as quark-diquark states, whereas quark models predict a much richer spectrum involving three dynamical quark degrees of freedom. That is, quark models predict many more states than have been

observed experimentally. These states are commonly known as “missing resonances”. There are two likely solutions to this puzzle: (1) the missing states simply do not exist; or (2) the missing states have not been seen because they couple weakly to the  $\pi N$  channel.

MIPP data with pion beams less than 5 GeV/c on liquid hydrogen will permit coupled channel partial wave analyses to be performed on a variety of channels such as

$$\pi^- p \rightarrow \pi^- \pi^0 p$$

$$\pi^+ p \rightarrow \pi^+ \pi^0 p$$

$$\pi^- p \rightarrow \pi^+ \pi^- n$$

$$\pi^+ p \rightarrow \pi^+ \pi^+ n$$

where the missing neutral is detected by the missing mass.

### E. Missing Cascades

As discussed in the nonstrange (S=0) baryon spectroscopy part of this proposal, discovery of the excited states of the nucleon, the  $N^*$ 's and the  $\Delta^*$ 's, has come from partial wave analyses of these states being formed from pion-nucleon scattering. Likewise, strange (S=-1) baryon spectroscopy, the  $\Lambda^*$ 's and  $\Sigma^*$ 's, has relied primarily on direct formation of these states via  $K^- p$  scattering, e.g.  $K^- p \rightarrow (\Lambda^* \text{ or } \Sigma^*) \rightarrow \text{decay products}$ . However, discovery of the excited states of S=-2 baryons, the  $\Xi^*$ 's (cascade hyperons), has been obtained primarily from production mechanisms. Production of these states via the  $K^- p \rightarrow K^+ \Xi^*$  reaction is proposed here for the MIPP upgrade program.

Again, a concise review of the status of our knowledge of  $\Xi$  resonances is found in the *Review of Particle Physics* [41]. Quoting, “Not much is known about  $\Xi$  resonances. This is because (1) they can only be produced as a part of a final state, so the analysis is more complicated than if direct formation were possible, (2) the production cross sections are small (typically a few  $\mu\text{b}$ ) and (3) the final states are topologically complicated and difficult to study with electronic techniques. Thus early information about  $\Xi$  resonances came entirely from bubble chamber experiments, where the numbers of events are small, and only in the 1980's did electronic experiments make any significant contributions. However, nothing of significance has been added since our 1988 edition.”

By SU(3) flavor symmetry, the spectrum of  $\Xi^*$  states has a one-to-one correspondence

with  $N^*$  and  $\Delta^*$  states. In the conventional quark model, the  $N^*$ 's are radial and rotational excitations of  $udd$  and  $uud$  configurations and the  $\Xi^*$ 's are excitations of  $uss$  or  $dss$  combinations. Thus, the same question of “hidden” or “missing” resonances appears. Only 11  $\Xi$ 's are listed in Ref. [41] (including the ground state), while 44 are predicted. These states are much narrower than the  $N^*$ 's (tens of MeVs rather than hundreds), making them easier to identify and distinguish. Hence, the study of the spectrum of doubly strange hyperons provides advantages in understanding the spectroscopy of all hadrons in particular and nonperturbative QCD in general.

A Monte Carlo simulation, see Fig. 34, indicates that the MIPP beam momentum resolution is a critical factor in resolving these states. Simulated here are the lowest three  $\Xi$ 's listed by the PDG [41], assuming their values for the masses and widths. The middle state in Fig. 34, the  $\Xi(1620)$ , is a one star resonance, meaning that “evidence of existence is poor”. If it exists, it presents a particular problem for quark models because of its low excitation (only 300 MeV above the ground state). In contrast, the first excited  $N^*$  state is the Roper resonance at 1440 MeV, 500 MeV above the ground state.

The missing cascade problem can be investigated in MIPP using low energy  $K^\pm$  beams.

## V. HARDWARE DETAILS OF THE MIPP UPGRADE

This section describes in detail the proposed upgrades and repairs of the Jolly Green Giant magnet coils, the TPC Front End electronics and upgrades and additions to the rest of the data acquisition and detector systems. We also discuss modifications to the MIPP beamline.

### A. Jolly Green Giant repair

The Jolly Green Giant magnet (JGG) provides the magnetic field for charge and momentum measurement of particle tracks in the TPC. The aperture of the JGG magnet is large enough to fit the TPC. The magnetic field of 0.7 T is (except for distortions) vertical and parallel to the electric drift field inside the TPC.

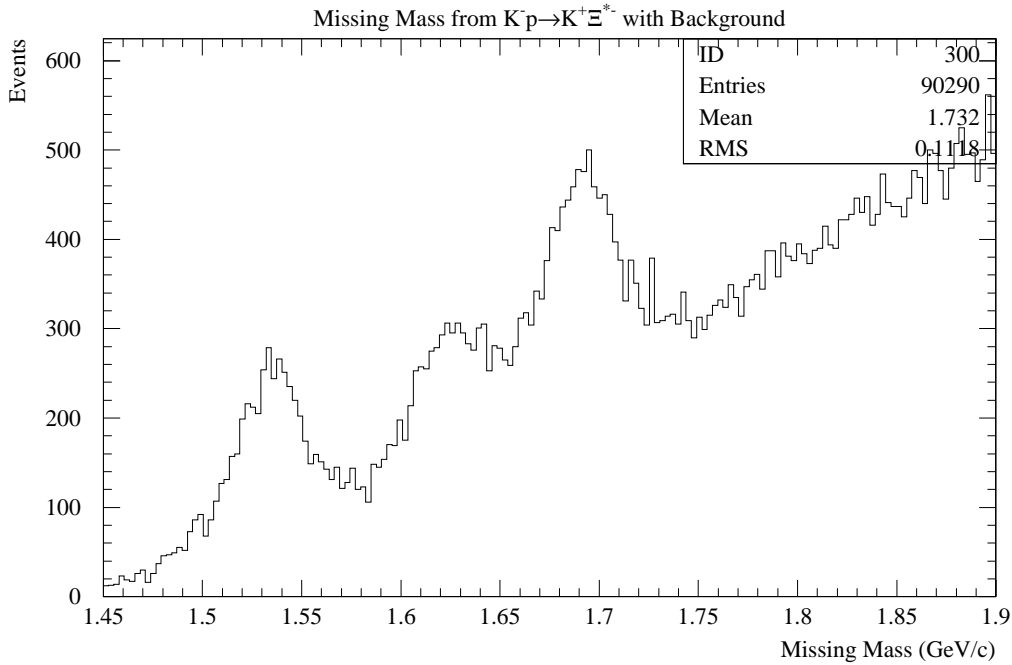


FIG. 34: Monte Carlo simulation of  $K^-p \rightarrow K^+\Xi^{*-}$ . The simulation includes a total of 100000 events with an assumed 5% signal at each of the three resonances  $\Xi(1530)^-$ ,  $\Xi(1620)^-$ , and  $\Xi(1690)^-$  from  $K^-p \rightarrow K^+\Xi^{*-}$ . The assumed background is 34%  $K^-p \rightarrow K^+K^-\Lambda$ , 34%  $K^-p \rightarrow K^+\Xi^-\pi^+\pi^-$ , and 17%  $K^-p \rightarrow K^+\Xi^-\pi^0$ . The lab momentum is 3.0 GeV/c. Masses and widths were taken from Ref. [41] estimates. A 0.5% beam momentum uncertainty was assumed, and the momentum resolution of the final state  $K^+$  was estimated by tracking it through the MIPP Monte Carlo, counting the number of pads digitized and applying multiple-scattering and digitization errors.

### 1. Former state of the JGG

The JGG magnet used to have two pairs of water cooled copper coils with a total of 1024 coil turns. Turns are insulated from each other with sheets of G10 and epoxy. The coils have been power cycled many times and have been operated for a long time over the past four decades. A failure in one of the coils was repaired before the first MIPP run. The magnet was then used in MIPP for three years. During this time we have had electrical turn-to-turn coil shorts and water leaks in the coils four times. Three times the magnet was restored to

an operational state. The failing coils were bypassed with external jumpers. The operating current was then increased to obtain the same magnetic field as before each failure. The last failure close to the end of the first run completely destroyed the bottom two coils.

## *2. New coil design*

The need to replace the JGG coils opened up the possibility for improvements. The magnetic field of the JGG is not very uniform. The region of interest is the rectangular active drift volume of the TPC centered in the magnet aperture. It extends 164 cm along the beam direction, 104 cm horizontally perpendicular to the beam, and 90 cm vertically. Within this volume the magnetic field components perpendicular to the electric field of the TPC reach up to 20% of the magnetic field component parallel to the electric field (see figure 35). The perpendicular components introduce distortions in the TPC track data of up to 5 cm[42]. These distortions can be corrected but residuals of up to 1.4 mm remain. This impacts vertex reconstruction and momentum determination. A more homogeneous magnetic field results in better data.

The width of the coils is given by the shape of the magnet yoke. It is hard to change. The pole pieces are 60 inches wide. This 1.46 times the width of the TPC drift volume. The length of the coils can be expanded more easily with new coils expanding symmetrically upstream and downstream of the yoke. Currently the pole pieces extend only 48 inches along the beam. This is only 74% of the length of the TPC drift volume. The effect of larger coils on field uniformity was modelled for several sizes of extensions in spring and summer of 2006[42]. An extension of the coils by 9 inches on each end gains a significantly more uniform magnetic field and does not interfere with the placement of the detectors downstream of the JGG. The further gains for extensions larger than 9 inches are smaller. With the new coils the pole pieces now have the same size along the beam direction as the TPC drift volume. The resulting  $E \times B$  distortions will be less than 3 cm throughout the drift volume of interest, half of the distortion with the old coils. After correcting for the new distortions remaining residuals will be at most 0.5 mm. This is more than twice as good as the results with the old coil.

Besides this work on the coil geometry a lot of work was done on the detailed design of new coils. For cost reduction the new coils have been made from aluminum rather than

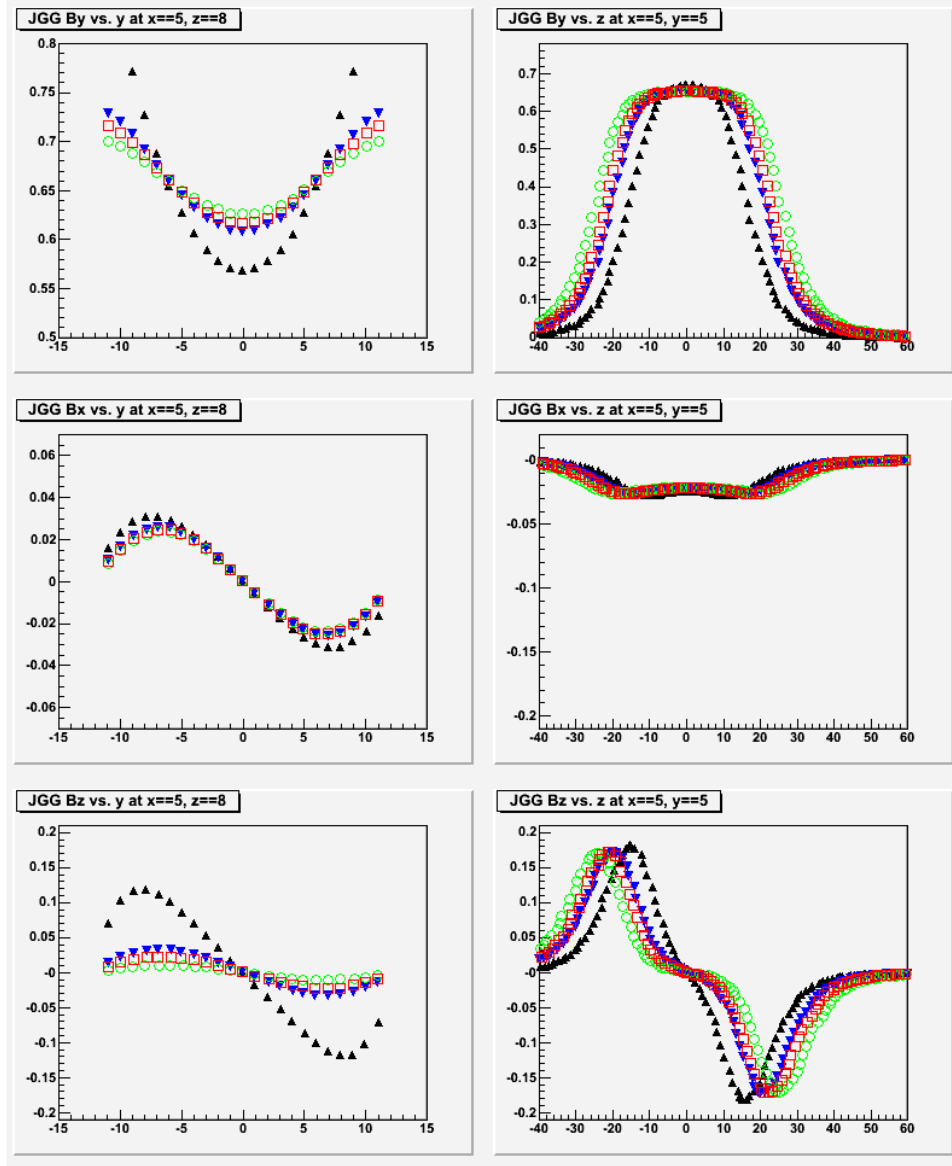


FIG. 35: Components of magnetic field in the JGG in tesla plotted against grid positions (two inch per grid space). Black triangles show the current coils. Blue inverted triangles show the model for nine inch extended coils. Squares and circles show extensions of 12 inches and 18 inches, respectively. The field shapes due to the 9 inch version are considerably better than the original field in that the extent of the bending field  $B_y$  is greater and the the other components  $B_z$  and  $B_x$  are better behaved.

copper. The coil conductor has a larger cross section. Two new coils will have 360 turns in five layers. The heating calculation for the final design has been performed and found to be satisfactory. The impact on the magnet power supply and power bus was evaluated. The

new coil specifications are listed in MIPP Note 137[43].

### *3. Coil replacement*

The new coils were fabricated and have been installed in the magnet. Figure 36 shows the magnet with new coils installed.

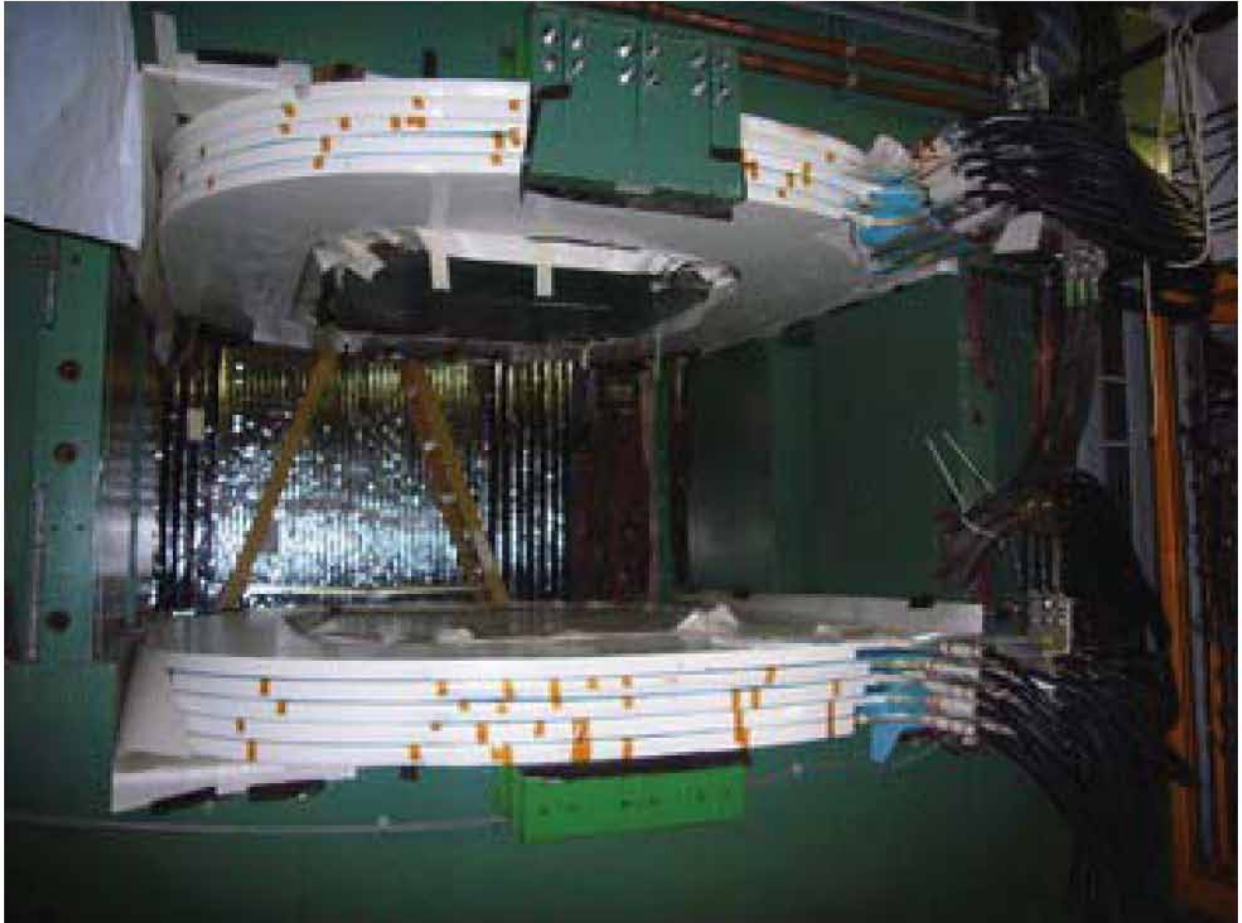


FIG. 36: Photograph of the Jolly Green Giant Magnet with new coils installed (2010).

### *4. Ziptracking the new magnetic field*

The magnetic field of the JGG with new coils has to be mapped. We have upgraded the Ziptrack system so that it is now driven by a modern PC using Labview (as opposed to Assist on DOS 3.1) and the digitization accuracy and slop in the motion of the cart along the string direction have been completely ameliorated by a linear encoder of accuracy  $40\mu\text{m}$ .

## B. The TPC Front End Electronics Upgrade

We discuss below the details of the scheme to speed up the front-end electronics of the MIPP TPC. This is done by acquiring 1100 ALTRO/PASA chips originally designed for the ALICE experiment at the LHC. The STAR experiment at Brookhaven ordered  $\approx 10,000$  ALTRO/PASA chips for upgrading the electronics of its TPC. MIPP acquired 1100 ALTRO/PASA chips in the same chip production run thereby reducing the cost (by a factor of  $\approx 5$ ) by sharing the overhead with the STAR collaboration.

### 1. Brief Description of the MIPP TPC

The MIPP TPC [19] was originally designed and used at LBNL in the EOS (E987) experiment and later at BNL (E895). The TPC encompasses an active gaseous volume of 96 cm wide by 150 cm long by 75 cm high (the drift direction), corresponding to a maximum collection time of  $16 \mu\text{sec}$ . To minimize space charge build up, the TPC incorporates a gating grid (currently limited to a maximum pulse rate of 3 kHz) which is pulsed to allow only ionization related in time. Because of limitations in the readout electronics described below the trigger rate is presently limited to about 30 Hz. Figure 37 shows the MIPP TPC as viewed from the upstream end.

The information from the 15,360 channels in the TPC is used to determine with high precision, in three dimensions, charged particle tracks emerging from the target station mounted on the front aperture of the detector. This chamber has the ability to independently record over 3,800,000 individual data points for a single interaction event and forms the basis of the precision momenta and  $dE/dx$  measurements for each particle trajectory. The original device that was refurbished for MIPP was designed with a readout system that limited the total data acquisition rate to a maximum of 60 Hz. Redesign and updating of the TPC front end electronics, replacing the aging 20 year old components with new high density components, is projected to allow a 100 fold increase in the maximum readout rate of the detector to a theoretic limit of 3 kHz.

Currently the readout of the TPC is limited by the multiplexed serial readout system which operates on non-zero suppressed data samples for each given event. In this manner the maximum readout speed is limited to 60 Hz, due to the high channel count readout



FIG. 37: The MIPP TPC.

and slow (1 MHz) multiplexing/digitization system. The observed occupancy however, for a typical interaction event in the TPC is only on the order of 5% of the total channel count. This results in the possibility of greatly increasing the readout capabilities of the detector by performing the initial data filtering on board the front end electronics and reducing by at least an order of magnitude the data through-put that is currently required for a single system read. The readout can be further enhanced by improving the digitization time required for each pad row and increasing the over all parallelization of the readout system.

The design goal of the proposed electronics upgrade is to bring the speed of the readout system to 3 kHz for normal operation of the system. Operation of the system at 3 kHz requires that sustained readout of the chamber be accomplished in less than 0.3 ms. Non-uniformities in event rate induced by beam structure, restricts this rate in such a manner that the operational time for full event readout should not exceed 0.2 ms during burst

operation for sustained high speed data acquisition.

The average zero suppressed data size for events as measured during the MIPP physics run was determined to be on the order of 115 kilobytes for a multi-track interaction event. The raw data rate when combined with transaction overhead results in the requirement that the output data pathway be designed to accommodate a single spill burst data rate of 575 megabytes/s. The proposed upgrade addresses this throughput via a minimum 5-way parallelization of the output data-way, resulting in a requirement of only 115 megabytes/s per primary data pathway which is compatible with commercial data bus implementations.

The upgrade of the TPC front end cards (FECs) to meet these requirements has been studied using a pair of custom designed ASICs that have been engineered, tested and produced for A Large Ion Collider Experiment (ALICE) collaboration at the LHC for use in their more than 570,000 channel time projection chamber. The system incorporates two separate chips, “PASA” an analog preamp/shaper and “ALTRO” a fast ADC/filter which provides event buffering, baseline corrections, signal filtering and zero suppression. The two chips are integrated in a standardized front end card with a dedicated data bus that is synchronized to the main data acquisition system via a series of readout control units (RCUs). The system has also been adopted by STAR collaboration at BNL, the BONUS at Jefferson Lab, as well as by the TOTEM experiment at CERN.

## 2. ALICE ASICs

To accommodate the readout of 570,136 charge collection pads, each sampling a maximum of 1000 samples per event, the ALICE collaboration designed and engineered two custom ASICs to operate in the high rate environment of the LHC heavy ion program. The ALICE readout design, as would be incorporated into the upgrade of the MIPP TPC would replace both the analog and digital portions of the current front end electronics cards. Each of the existing 128 analog/digital electronic “sticks” would be removed and replaced in a one to one manner with an ALICE FEC ( both of which are shown in Fig. 38), redesigned to match the physical dimensions of the aluminum cold plate upon which the current electronics are mounted. Additionally the cards would be fitted to use zero insertion force (ZIF) socket compatible with the current TPC chamber connections and interlocks. This redesigned FEC follows in all other respects the electrical design and characteristics of the current CERN

board layouts.

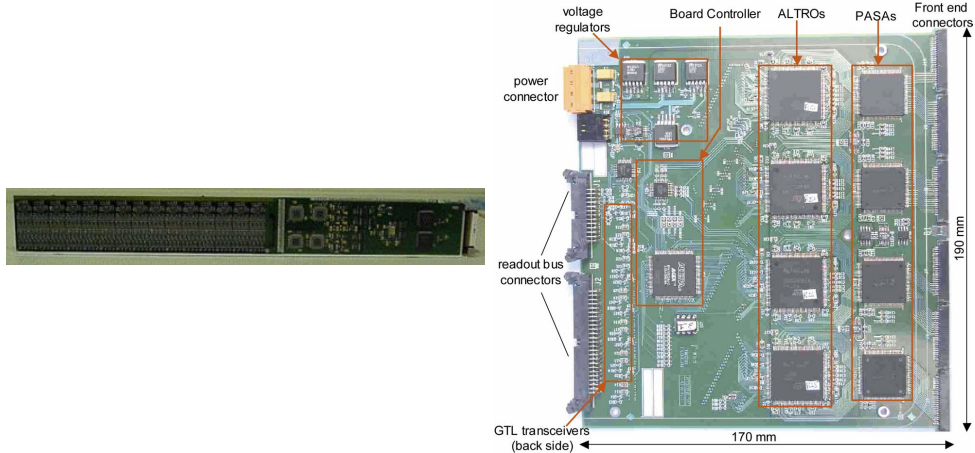


FIG. 38: TPC front end electronics boards for MIPP and ALICE. The difference in physical form factor requires a redesign of the ALICE board to match the MIPP cold plates and connectors. Note that the two boards are not to scale and the MIPP TPC stick is roughly as long as half the TPC width.

The ALICE system as shown in Fig. 39 is divided into two stages. The raw signals from the detector pad rows are first fed into a custom designed integrated circuit referred to as “PASA” which serves as the preamp and pulse shaper for each channel[44]. The raw charge collected from the sample window is reshaped into a sharply peaked output distribution of width  $\mathcal{O}(190 \text{ ns})$ , as shown in Fig. 40, which is matched to the input requirements of the ALTRO chip for accurate digitization. Each PASA chip services 16 readout pads and is matched to the ADC inputs of the ALTRO chips shown schematically in Fig. 41 for a single digitization channel. The ALTRO ASIC as shown in Fig. 42 is a 16 way parallel system including on each channel a 10 MHz ADC, digital signal processor, and memory buffer. The operation of the chip is compatible with normal fixed-target data acquisition operation. Although the signals are sampled continuously the data is processed (pedestal subtraction, shaping and sparsification) only upon receipt of a Level 1 trigger signal. The processed data is stored in the memory buffer upon receipt of a Level 2 accept signal or otherwise discarded.

Implementation of the ALICE front end electronics in the MIPP TPC requires that several additional modifications be made to match the operational needs of the existing hardware. The time window for event scanning and digitization will be reduced from 1000 samples per event to 250 samples to match the drift time over the active volume of the detector. The

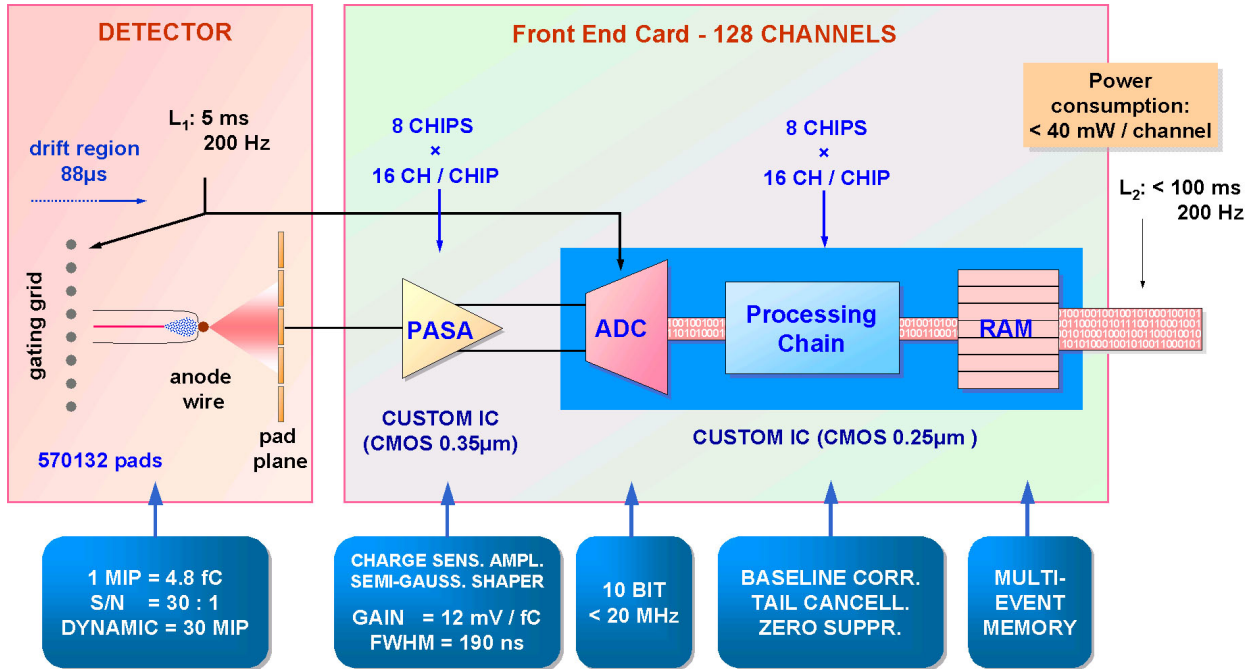


FIG. 39: ALICE front end card and readout system block diagram[46].

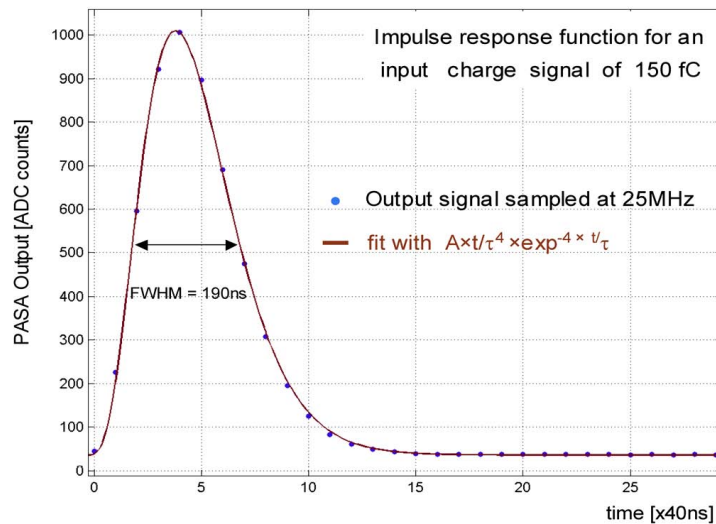


FIG. 40: PASA output function for an initial test charge of  $150 \text{ fC}$ [47].

reduced number of samples then allows for additional segmenting of the ALTRO event buffer in such a manner that the FEC cards will be able to fully buffer 8 events at a once. To ensure that the heat load generated by the new front end boards is compatible with the existing cold plates and water cooling system, provisions have been made to operate the ALTRO bus at

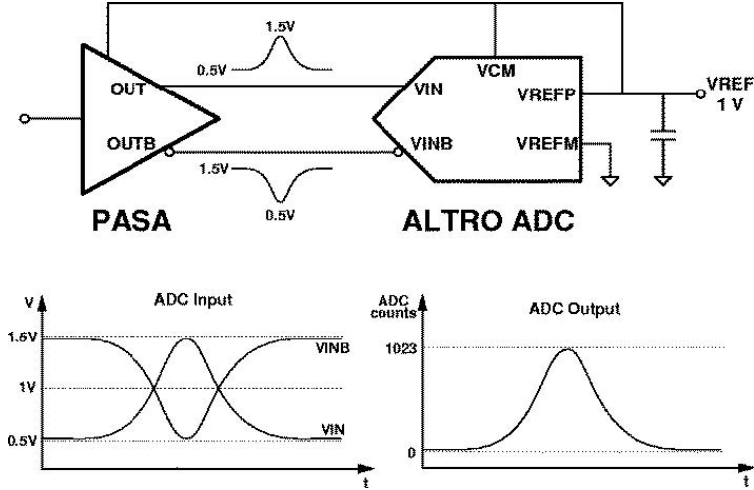


FIG. 41: PASA to ALTRO digitization logic[48].

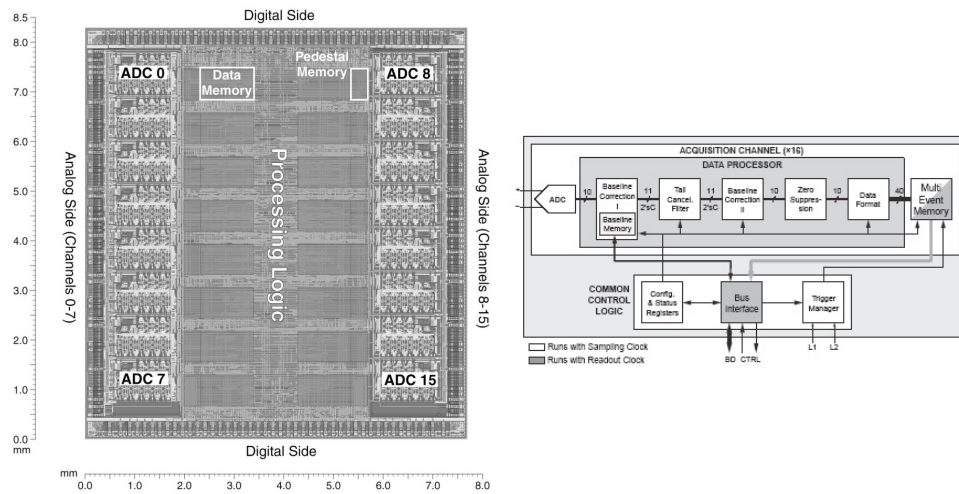


FIG. 42: The ALTRO chip developed at CERN services the readout of 16 channels by integrating a fast ADC, signal processing and event buffering in a single package with interface to a high speed data bus and programming lines.

20 MHz instead of the 40 MHz design frequency. These modifications are projected to both increase stability and retain the utility of as much of the existing equipment as is possible. The component requirements for the full system upgrade of the time projection chamber are listed in Table III. The projected yield for the PASA and ALTRO wafers based upon the previous production run is estimated at 82%. When yield is included, it is estimated that

Component	Channels	no. Per FEC	Total Required
Front End Circuit Board	120	1	128
ZIF Sockets		1	128
Preamp/Shaper (PASA)	16	8	960
ADC/Filter/Memory (ALTRO)	16	8	960
Readout Control Units (RCU)		1:16	8
Single Board VME PCs			1
Gigabit Network Switch			1

TABLE III: Component requirements for upgrade of the MIPP time projection chamber for operation at 3 kHz.

1200 raw dies would be required to obtain enough components to instrument the detector.

The cost per channel for the ALTRO electronics solutions, dependent upon chip yield, is estimated at \$10 per channel based upon the electronics costs for instrumenting the BONUS TPC at Jefferson lab. The total cost of the front end electronics modifications is estimated at a direct cost of \$180,000 without contingency. Additional cost is incurred in the procurement of single board VME style computers for event filtering and synchronization. The single board processor is estimated to cost \$4800 dependent upon final specifications and memory buffering requirements. The total direct cost of equipment for upgrading the MIPP time projection chamber is estimated at \$190k without contingency.

The contract signed by CERN and Fermilab delivered the 1100 ALTRO/PASA chips needed by this upgrade scheme after they were tested and verified to work. Faulty chips will be replaced by CERN.

Fermilab has built a complete prototype of the the TPC front end board using the ALTRO/PASA chips. Figure 43 shows the complete TPC stick using ALTRO/PASA chips. Figure 44 shows the detail of the layout for one ALTRO/PASA unit. Figure 45 shows the prototype of a buffer board that receives and stores the data acquired from a single stick during a 4 s spill.



FIG. 43: Prototype of the TPC stick using ALTRO/PASA chips that will house 8 daughter boards. Each daughter board consisting of a single ALTRO/PASA unit is removable for repair.

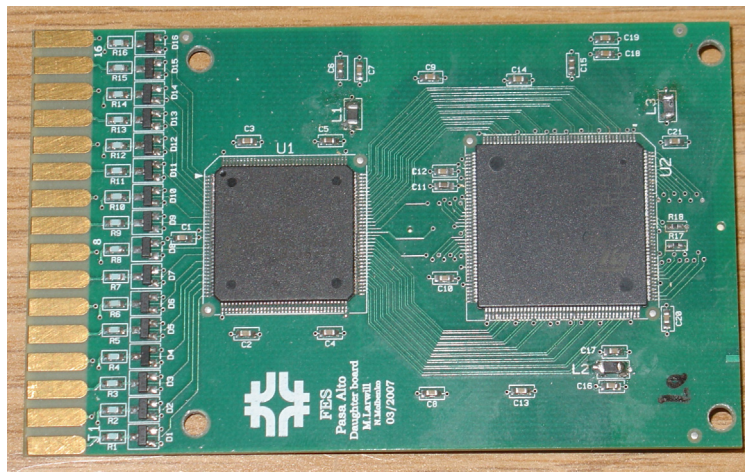


FIG. 44: Prototype of the daughter board using a single ALTRO/PASA unit.

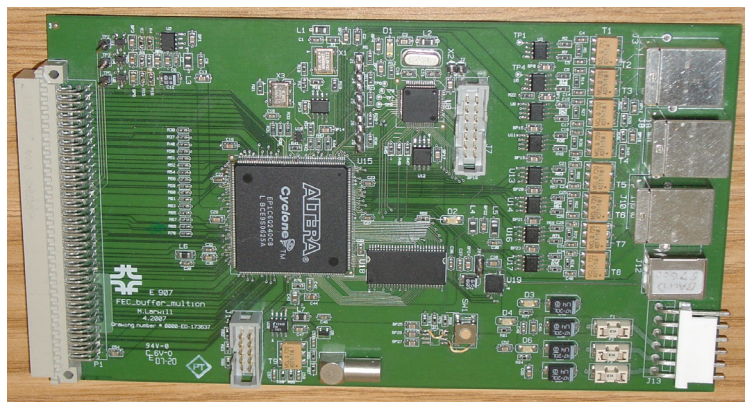


FIG. 45: Prototype of the buffer board that receives and stores data from a single stick.

### C. MIPP trigger system upgrades

MIPP trigger consists of two parts. The raw beam trigger is formed by coincidence between scintillator counters (TBD and T01) placed at the entrance of the MIPP hall and just before our interaction target respectively. Particle identification is performed on the beam using the information from the beam Čerenkov system for higher energy beam and by the time of flight counters for lower energy beam. We were thus able to trigger on 6 species of beam particles ( $\pi^\pm$ ,  $K^\pm$  and  $p^\pm$ ). The interaction trigger in MIPP consisted of information from a scintillation counter (SCINT) placed after the target combined with information from the first drift chamber downstream of this. This interaction trigger has performed well during our physics run but its purity/efficiency suffered for lower multiplicity events due to the inability to tell apart single and multiple tracks in SCINT because of Landau tails in the pulse height distributions. It also suffered from occasional oscillatory behavior in the drift chamber. These inefficiencies will be corrected during offline analysis of the present run to obtain the correct multiplicity cross sections. The SCINT counter also introduced 0.5% interaction length, which would result in triggers caused by interactions in the counter.

In the upgraded MIPP experiment, we propose to remedy these defects by a new interaction trigger based upon the fPix Silicon pixel detectors developed for the BTeV experiment.

#### 1. Interaction Trigger

There will be one Silicon pixel plane upstream of the target and two planes downstream of the target. Each layer will consist of an array of six by eight fPix chips. The pixels on each chip are  $400\ \mu m$  by  $50\ \mu m$ , with the finer segmentation in the y vertical direction. The fast chip hit signals from each fPix chip will all be independent so that it can be input to a trigger processor, but the readout of each individual chip will be coupled across the rows so that each silicon detector plane provides six rows to read out. The fast chip hit signal will be latched on the rising edge to be 50 ns wide. The fast chip hit signal will be inactive for 130 to 200 ns. With our planned 300 kHz beam rate with the beam being spread over four chips, this will not impose any substantial dead time limitations. Approximately 86% of the beam will hit four chips upstream of the target. The two planes downstream of the

target will be used to form track-pointing to make sure that the interactions come from the target and not from the 300  $\mu\text{m}$  silicon or other material.

Several different categories of triggers will be used. The first type are non-interacting beam tracks that go without interacting in our 1% target and hits are observed in a “bull’s eye” in the downstream pixel counters where we expect beam. These non-interacting beam triggers are highly pre-scaled and used for monitoring the experiment. An interaction trigger is formed when we do not have a beam track in an expected “bull’s-eye” region. This bull’s eye region is defined in a dynamic way for each beam track depending on its point of impact in the first silicon plane. The other trigger planned is based on total multiplicity of hits in the two pixel planes downstream of the target. The interaction trigger logic on the fPix signals will be performed in a custom interaction trigger board.

The trigger schematic is shown in Figure 46.

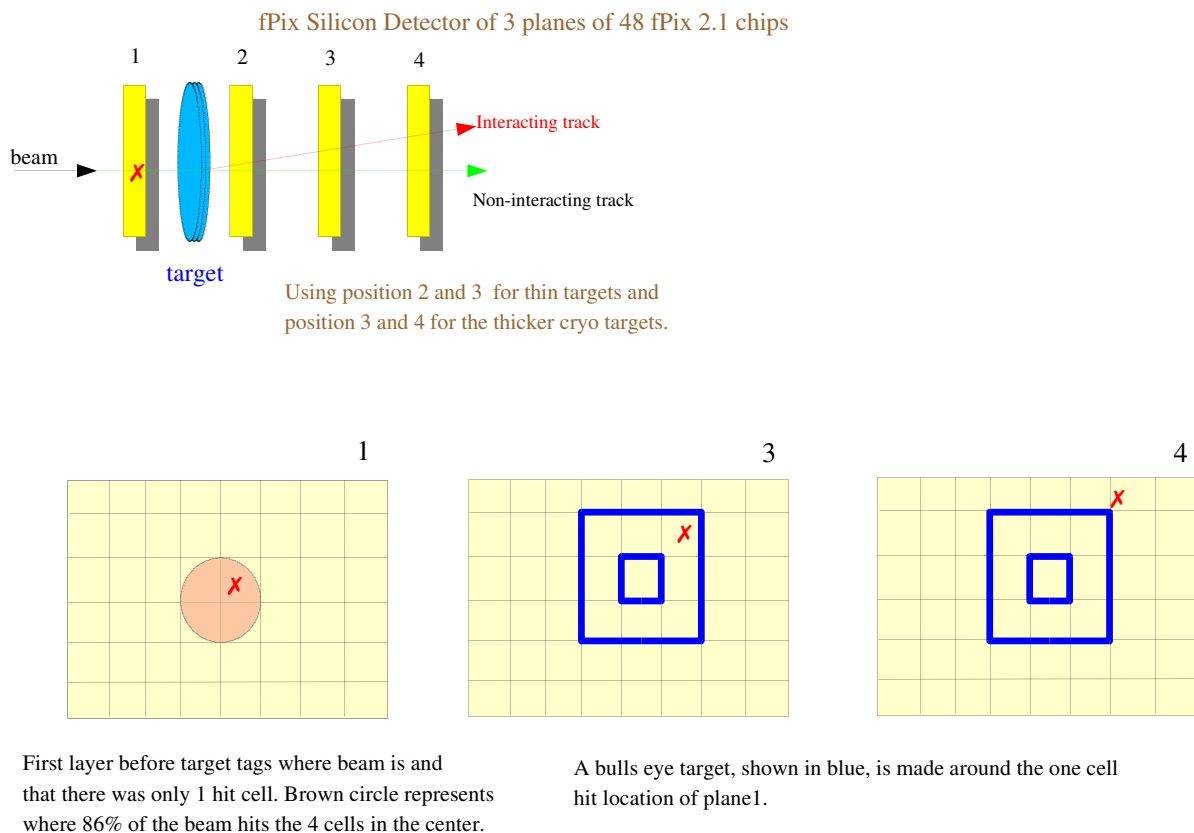


FIG. 46: Schematic of the new silicon based trigger system.

Equipment	Cost
3 Planes of fPix detectors	\$87,100
fPix mounting, cooling, LV, bias and PCI boards	\$50,000
Interaction Trigger logic board	\$8,800

TABLE IV: Equipment summary for trigger upgrade.

As in the original MIPP trigger system, we will keep the ability to pre-scale triggers so that we take 80% of events that have an interaction trigger with an equal amount of pions, kaons and proton interactions. The other 20% will be un-interacted beam triggers, to monitor the efficiency and performance of detector, trigger efficiency and dead time. It should be pointed out that this trigger scheme will have greater efficiency in triggering on low multiplicity events and so is of importance for the ILC tagged neutral beam events which have two charged tracks and one missing neutral.

## 2. MIPP Trigger Electronics

The MIPP trigger electronics will largely be replaced by a custom design MIPP trigger module. The main goal will be to streamline the trigger system and remove some problematic modules which have dead channels from the two years of usage during the previous run. The new custom trigger board will replace hard to maintain NIM and CAMAC electronics, allow readout of trigger data (beam flux scalers, etc.) in the new readout scheme, and incorporate the new veto wall and fPix chip hit signals as the new interaction trigger.

As in any cross section measurements we plan to take  $\approx 10\%$  of all triggers as empty targets. For the experimental operation with thin nuclear targets this will be done by taking a spill with one target, (12,000 events in a 4 second spill every 2 minutes) and the target wheel will automatically be advanced to the next target. The wheel consist of 8 slots one of which will be empty. By moving the target automatically between spills, we plan to make the most effective use of the beam and have empty target runs that reflect the beam quality backgrounds.

Table IV gives a summary of the equipment needed for the trigger upgrade.

#### D. MIPP Trigger Module

The MIPP Trigger module is designed to control upgraded MIPP Data Acquisition System (DAQ). It generates and distributes through MIPP DAQ system timing synchronization and trigger signals. The requirements for the MIPP trigger system are described in the MIPP internal document [36]. The MIPP DAQ system is built using a unified MIPP Readout Controller Module. The Readout Controller Module distributes timing synchronization and trigger signals in a form of encoded signals synchronous to the distributed RF/2 (26.55 MHz) clock. The description of the encoding scheme and implemented signals can be found elsewhere [39].

The current MIPP trigger system uses the following sources of the detector signals to generate a trigger:

- 12 Time-Of-Flight scintillation counters with PMTs
- 20 Veto scintillation counters with PMTs
- 4 Beam Cherenkov counters with PMTs

The PMT signals will be discriminated by commercial electronics modules available from Fermilab PREP. The logic combinations of the discriminators outputs will be used to generate trigger output signals using MIPP Logic module. The MIPP Logic module will provide the following functionality:

- Double width 6U VME module
- 32 NIM/TTL programmable logic inputs with LEMO connectors
- 4 NIM programmable logic outputs with LEMO connectors
- 8 channels of 0.5 ns time measurements for selected input channels
- Internal memory storage for default power-up configuration

The module has a VME slave interface and implemented as a double width 6U VME board. The outputs of the MIPP Logic modules will be fed to the MIPP Trigger module. This module will be responsible for the generation and distribution of the trigger signals to the MIPP Readout Controller modules. The MIPP Trigger module will provide the following functionality:

- Double width 6U VME module
- 16 trigger logic NIM/TTL signal inputs with LEMO connectors
- Two Beam synchronization signals (RF, TCLK) with LEMO connectors
- TCLK events decoder
- One RJ-45 input connector
- 8 RJ-45 output connectors
- Programmable trigger pre-scalers
- Various input/output signal scalers
- Internal FIFO memory for the trigger condition of the individual triggers
- Internal memory storage for default power-up configuration

The MIPP Trigger module generates a sequence of timing control signals encoded into the RF/2 clock. The two main signals are Begin Spill and End Spill, which indicate the beginning and the end of the active beam cycle respectively. Asynchronous to the beam INIT, CSTAT and TEST signals are also encoded and can be generated by the module. Logic level Global Reset and Read Event signals are distributed directly via RJ-45 connector. These signals are to be received and encoded by the Readout Controller Module, and distributed to the front-ends along with the other clock-embedded timing signals. The Readout Controller Module may also generate these two signals independently. The Trigger Module has an internal quartz oscillator, which could be either locked to the accelerator RF or set to a free running mode. The timing sequencer generating beam related signals could be synchronized to the BSCLK events (e.g. §75) or set to run free with a programmable repetition rate.

The module also receives and encodes 16-NIM/TTL input signals as experiment triggers. The definition of various triggers is provided in reference [36]. The encoded trigger signals should be generated only between Begin Spill and End Spill signals. The MIPP Trigger module has one RJ-45 input and eight RJ-45 output modular connectors. It can be used as a fanout module do distribute timing and control signals within MIPP DAQ crates. The module has a VME slave interface and implemented as a double width 6U VME board. Figure47 shows the block diagram of the MIPP trigger module.

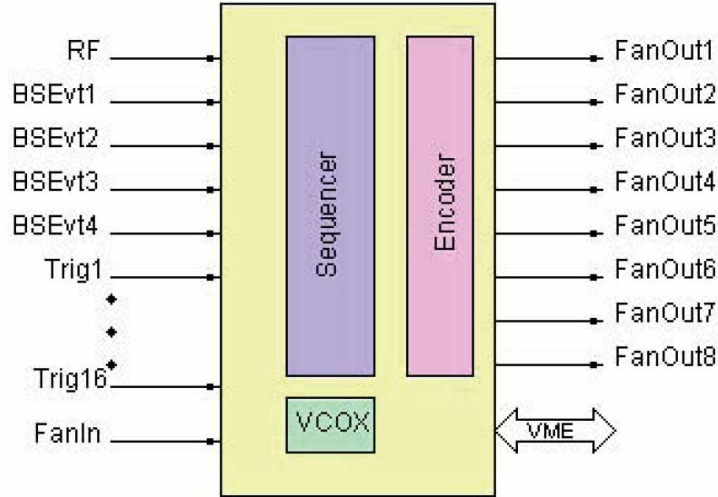


FIG. 47: Block diagram of the MIPP trigger Module.

### E. Upgrade for Chamber Readout Electronics

Currently the drift chambers are read out through pre-amplifiers and discriminators inherited from the E690 experiment that use CAMAC TDCs.

The large MWPC's are read out through RMH electronics that have not been supported for several years.

This system was maintainable through the first MIPP physics run and produced good data from three beam chambers and six tracking chambers downstream of the experimental target. However, there are several issues that need to be resolved.

We managed to keep the RMH system in working order up to now using spares. However, it is not possible to guarantee that this readout system will work through another run.

The readout of the CAMAC TDCs currently uses the CES CBD8210. This system is obsolete and not maintainable any more. CAMAC hardware in general is becoming less well supported. Currently the TDCs are read out without the use of DMA. The current readout system could perhaps be upgraded to transfer data in DMA mode. A new solution for the CAMAC readout and the change to DMA transfer would likely be sufficient to obtain a readout time as needed for operation at 3000 Hz. However, a new readout will provide much more flexibility at only incrementally higher cost.

The existing system uses a large number of high current low voltage power supplies. Each

drift chamber uses two 5 V and one 10 V supply. All of these supplies are aging and several have failed during the past run resulting in minor downtimes.

The current system dissipates a large amount of heat in the area of the experiment between the two analysis magnets. This has caused significant problems with air conditioning in MC7. The air conditioning itself is an old system. With the present heat load the air conditioning system in MC7 would need to be upgraded.

In preparation for the first MIPP physics, new electronics for the RICH detector readout were built. The RICH readout uses front end boards that read out the RICH PMT's and send data to MIPP Readout Controller boards. This solution has been working well and essentially the same readout board will be used for the new TPC electronics. This readout can be adapted for all chambers.

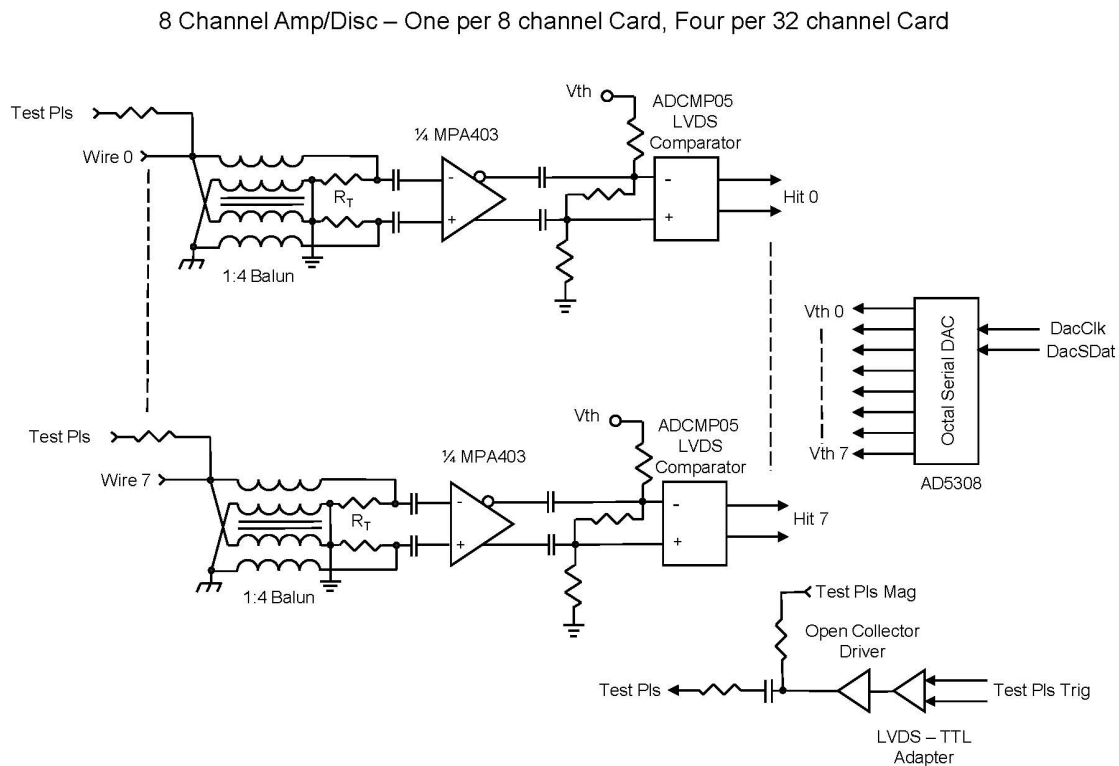


FIG. 48: Chamber pre-amp card schematic.

For the new readout, we propose to build new pre-amp cards with 8 and 32 channels

High-Speed Differential Interfaces  
 "Cyclone II devices can transmit and receive data through LVDS signals at a data rate of up to 640 Mbps and 805 Mbps, respectively. For the LVDS transmitter and receiver, the Cyclone II device's input and output pins support serialization and de-serialization through internal logic."

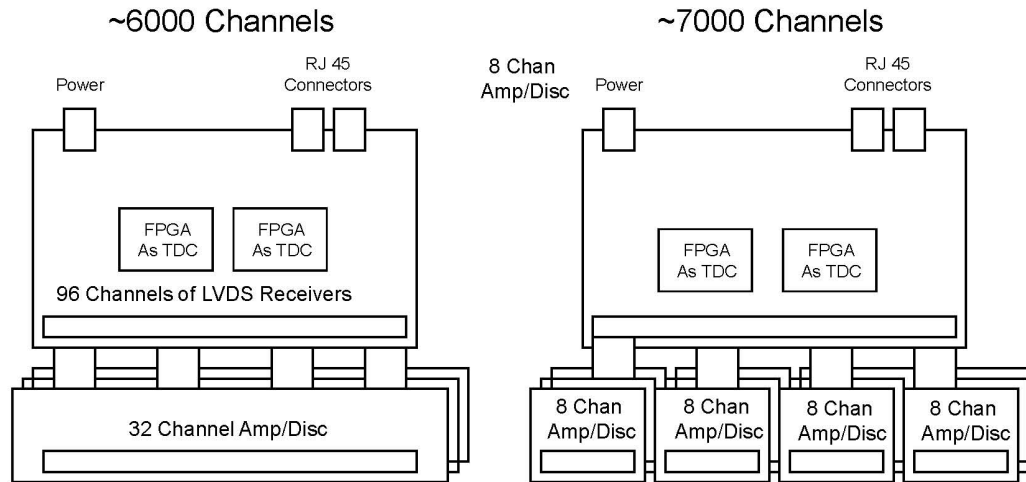


FIG. 49: Chamber pre-amp and discriminator cards. The 32 channel pre-amp cards will be used with the MWPCs. The 8 channel cards are for drift and beam chambers.

per card for the drift chambers and MWPC's, respectively (see figure 48). These cards will be mounted on the chambers in the same way that preamp cards are mounted presently. Several of these daughter cards will connect to 32 channel TDC front end cards as shown schematically in figure 49. These cards will be based on the RICH front end cards. The RICH cards provide a latch for each channel whereas the new chamber cards will use TDCs. Each card will hold enough memory to buffer data for an entire 4 second slow spill.

The Chamber front end cards will be daisy-chained (see Figure 50) onto a total of five MIPP Readout Controller cards in the same way that multiple RICH front end cards are read out. We have built prototypes of all cards necessary for the drift/wire chambers. Figure 51 shows the prototype of the 8 Channel amplifier board. Figure 52 shows the prototype of the 32 channel amplifier board. Figure 53 shows a prototype of the 96 Channel TDC board.

## TDC Card Arrangement

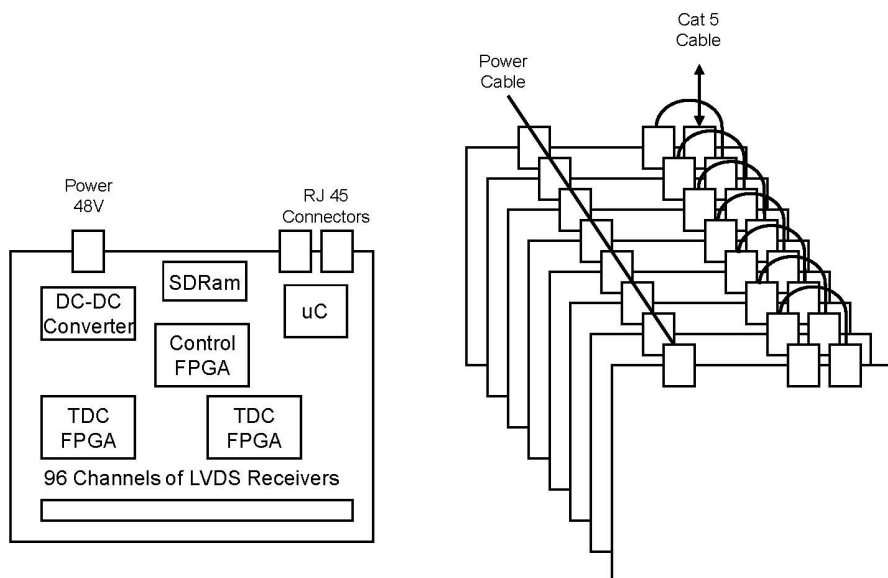


FIG. 50: Chamber TDC cards schematic.

The total cost for the new chamber readout electronics is estimated at \$121k for material and \$29k for labor. The labor cost is low due to the simple design of the new readout based closely on existing electronics designed by the same engineers. The largest material costs are \$56k for 1100 daughter cards and \$49k+\$7.5k for 325 front end TDC cards and mounting structures/mechanical protection.

A detailed list of tasks is included in the Gantt chart.

### F. Time of Flight, $T_0$ , and threshold Čerenkov Readout

The current Time of Flight (ToF) readout uses LeCroy 2229 CAMAC TDCs. The 2229 modules have a long conversion time when used in full range mode as is desired by the MIPP experiment. The Time of Flight signals are also read out with LeCroy 4300 ADCs needed for slew corrections on the TDC signals. These ADCs are FERA modules, but are currently

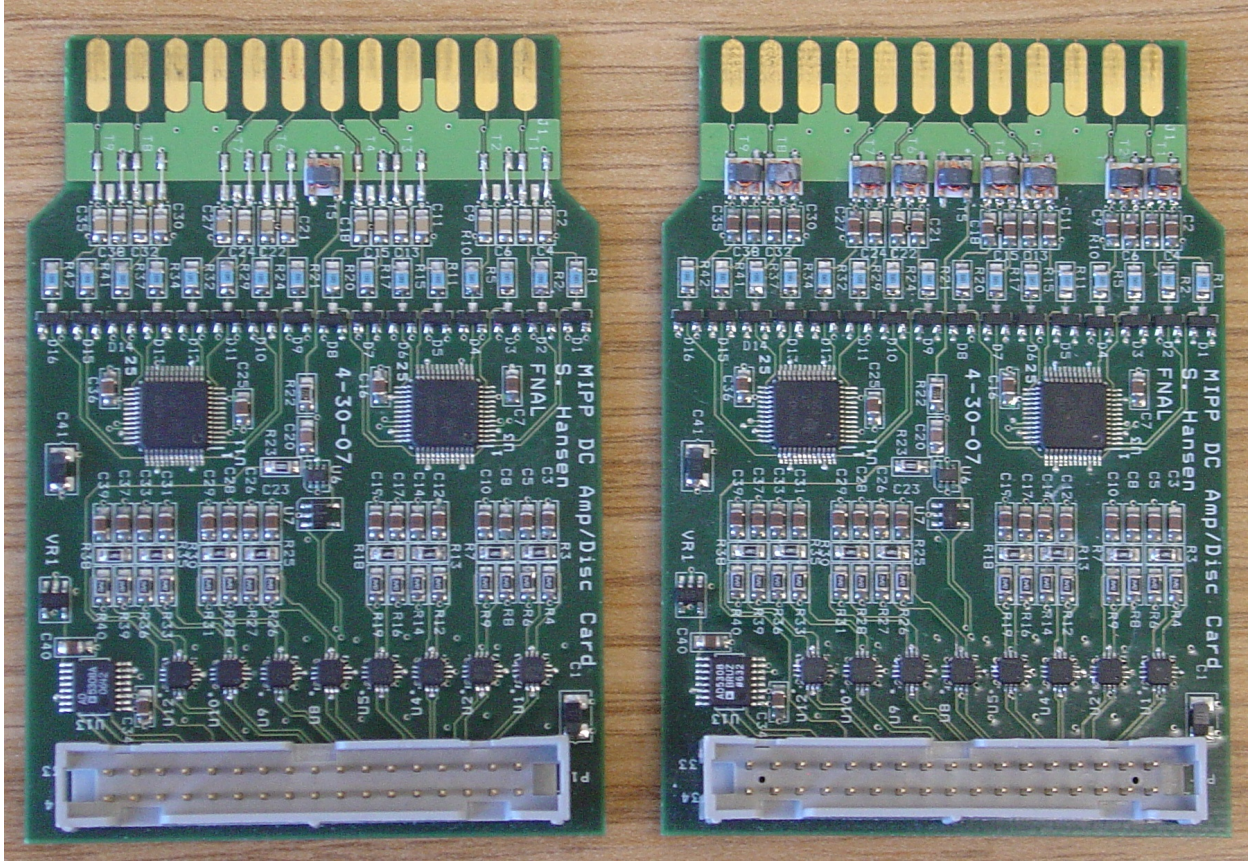


FIG. 51: Prototype of the 8 Channel amplifier card.

read out through the CAMAC backplane.

Long delay cables are used in order to receive a trigger for the common TDC start and ADC gate. These ribbon cable delays are sensitive to the environmental temperature. This causes fluctuations in the timing response that are large compared to the timing resolution needed for ToF particle identification. Although much work is being done to correct for these fluctuations in offline analysis, a change in the readout to eliminate these temperature dependent variations will make the ToF system more robust and significantly simplify the offline analysis, reducing both time and man-power needed for data analysis.

The threshold Čerenkov (CKOV) detector is read out through ADCs and multi hit TDCs. It has 96 channels. The current readout uses CAMAC hardware.

The T0 detectors in the beamline provide the beam definition for the trigger and the timing mark of the interaction in the target. They are also used at low beam momentum for beam particle identification. A total of three scintillators in the beam line is read out with 12 photomultiplier tubes. With proposed modifications to the trigger we would need

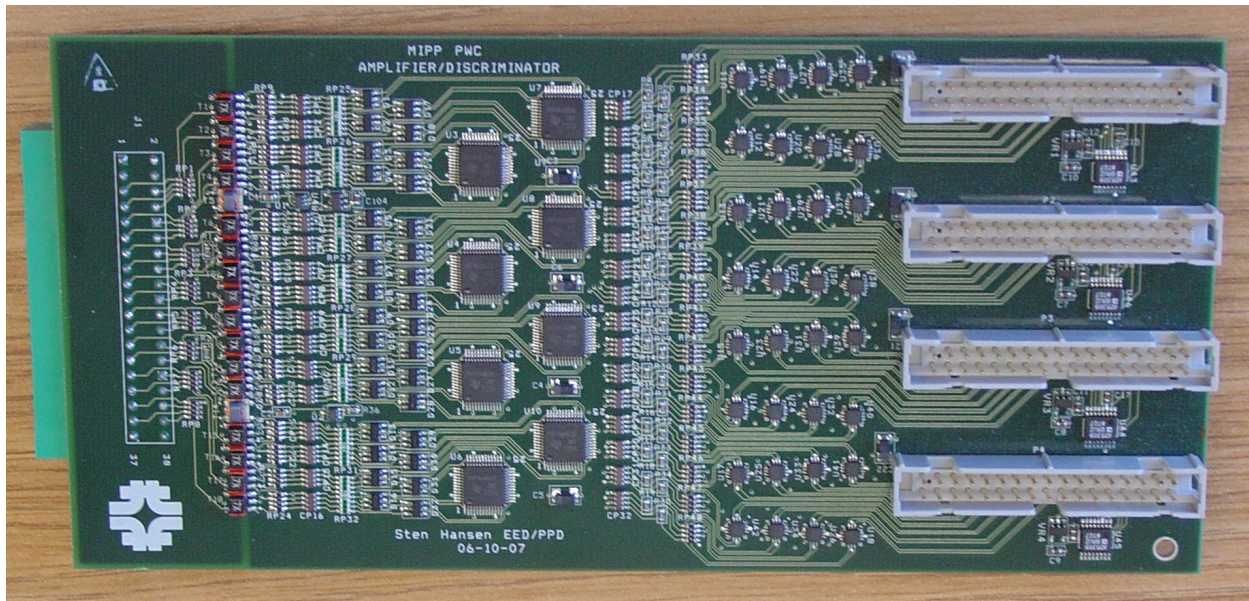


FIG. 52: Prototype of the 32 Channel amplifier card.

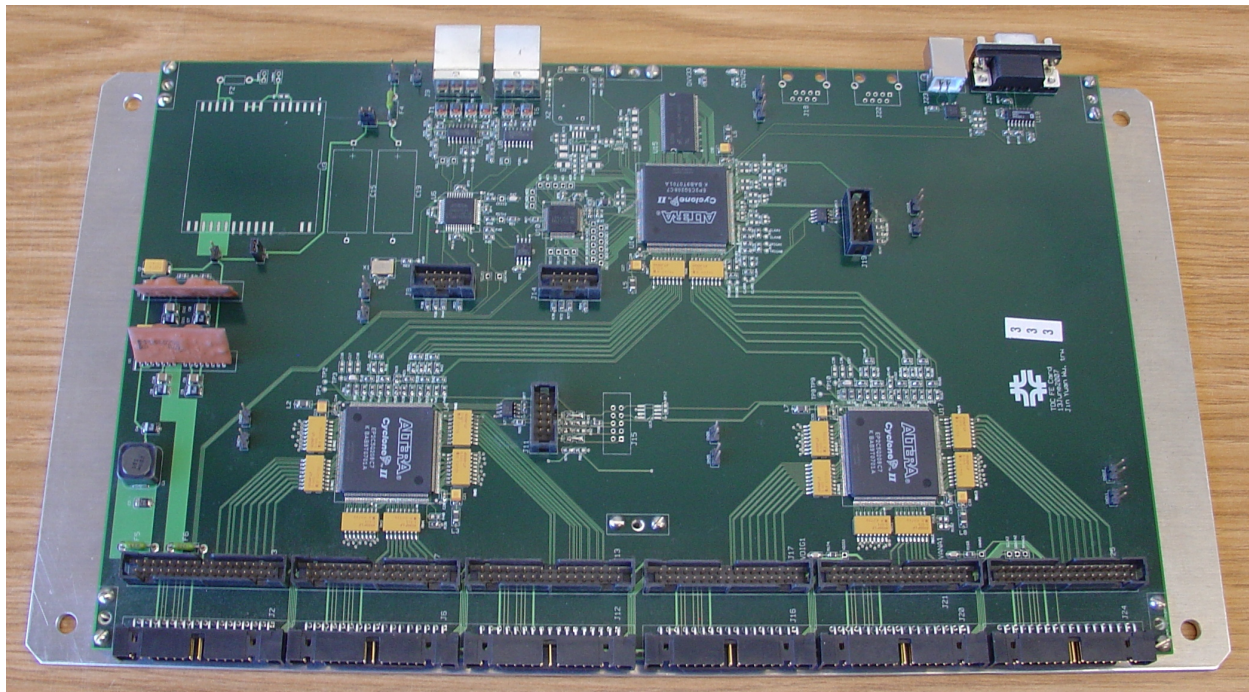


FIG. 53: Prototype of the 96 Channel TDC card.

to add delay to the signals of the T0 system. This would degrade timing resolution.

If the CAMAC readout was to be maintained we would need to obtain new readout for four CAMAC crates for the ToF readout and for two CAMAC crates for the CKOV readout. The currently used CES CBD 8210 module is no longer maintainable. The new solution

for CAMAC readout is the Hytec1365 module. It provides readout for one CAMAC crate, but does not allow to put multiple crates onto a CAMAC branch. Thus the experiment would need to purchase six of the Hytec1365 modules to read out the ToF and CKOV. These modules by themselves would cost \$30k. The total upgraded readout system for these detectors would be more expensive.

Instead we propose to build a new readout for these detectors. Again the back-end will be provided by the MIPP Readout Controller cards that are also used by the TPC and chamber readouts. The front end boards will be similar to the front end cards used in the RICH and proposed for the chamber readout with the difference that ToF and CKOV need ADC readout and the ToF needs high resolution TDC readout.

Front end boards with the TripT chip (also used by the MINER $\nu$ A experiment) and a high resolution TDC chip (the TDC-GPX chip from ACAM GmbH, also used by LHC-b) will provide 30 ps timing resolution for the ToF (better than the 2229 currently used) and multihit capability needed for the CKOV. The TDC-GPX chip can be operated in different modes. The mode with 30 ps resolution and 2 channels per chip fits the needs of the ToF while coarser resolution with 8 channels per chip reduces cost for the CKOV. The new electronics will be able to buffer hits. The delay cable on the ToF can be eliminated.

Design of the front end cards for the ToF and CKOV is expected to not pose significant challenges. The TripT chip and the analog part of the circuit will essentially be copied from a MINER $\nu$ A design and the TDC-GPX chip is entirely digital.

The total cost of the new readout for the ToF and CKOV is estimated at \$34k. The production cost is small because the total number of channels is small (106 ToF + 12 T0 + 96 CKOV + spares). The design cost is small because the system uses components that are common to other systems.

### **G. The Plastic Ball Recoil Detector**

The Plastic Ball detector was originally built at GSI, Darmstadt to study high multiplicity heavy ion collision events for the BEVALAC experiment at LBNL. It then moved to CERN to be in the WA80 experiment in the early 80's [49]. After the completion of the CERN-SPS heavy-ion experiment, WA98, the plastic ball moved to KVI, Gröningen, Netherlands. KVI have informed us that it is available for use at Fermilab, having finished its physics run at

KVI. The GSI, Darmstadt group is interested in measuring antiproton cross sections using the upgraded MIPP spectrometer as this will enable them to better design the PANDA [33] detector.

The fully configured plastic ball consists of 815 “phoswich” modules, one of which is shown schematically in Figure 54. The module consists of a  $CaF_2$  scintillator sandwiched to a plastic scintillator, both of which are readout with a single photomultiplier tube. The photomultiplier signal is measured using two gates with different widths. Light from  $CaF_2$  is slow (1250 ns gate) and that from the plastic scintillator is fast (250 ns gate). The fast gate measures the plastic scintillator light only and the slow gate measures both the plastic scintillator and the  $CaF_2$  light. The charged particles deposit energy in both layers where as the neutral particles such as neutrons deposit energy in the hydrogen rich plastic scintillator.

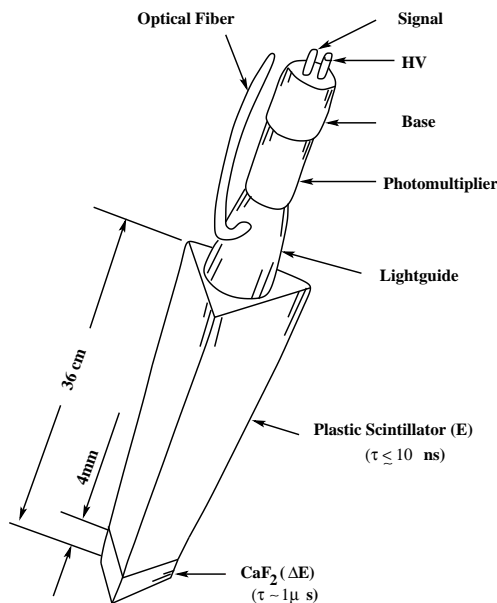


FIG. 54: Schematic of a single plastic ball phoswich module. The detector consists of a scintillator sandwich of a  $CaF_2$  module and a Plastic scintillator, readout through the same photomultiplier.

Figure 55 shows the identification of particles using the plastic ball by comparing the two signals. One can see the separation between the proton signal which is seen in both scintillator layers where as the neutral signal is seen only in the plastic scintillator. The neutrons and photons are distinguished further by time-of-flight.

Figure 56 shows the full plastic ball detector as configured at KVI. Figure 57 shows

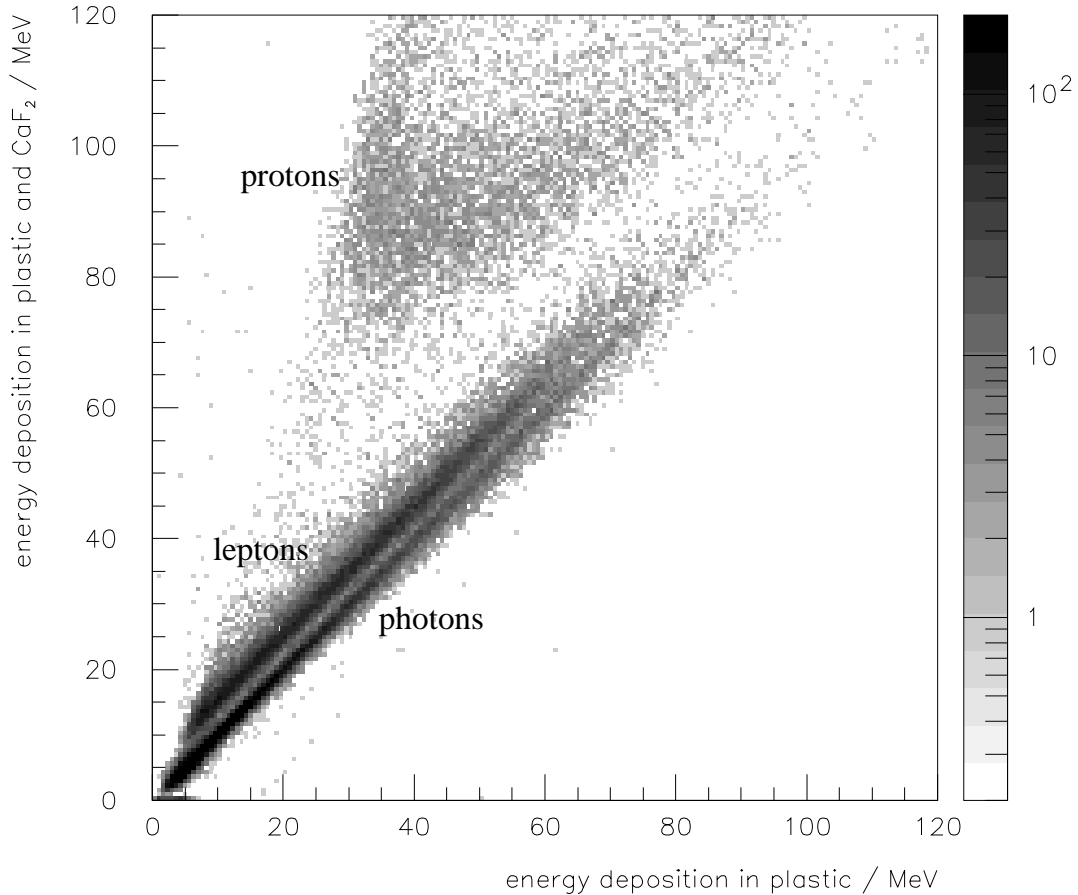


FIG. 55: On the ordinate is plotted the sum of the energies deposited in  $\text{CaF}_2$  and the plastic scintillator and on the abscissa is plotted the plastic scintillator energy only. The protons are clearly separated from the photons.

a schematic of 340 phoswich modules arranged as a hemisphere. This is similar to the configuration we would use in MIPP, with the hemisphere covering the target upstream of the TPC.

### 1. Transportation to Fermilab and Integration into MIPP

We have estimated a cost to transport the Plastic Ball to Fermilab, after talking to Fermilab engineers. The Plastic Ball detector has to be mounted in a removable fashion such that the TPC may be repaired. During NuMI target running, the Plastic Ball has to be removed from the beamline as well, since the NuMI charged tracks produced at the

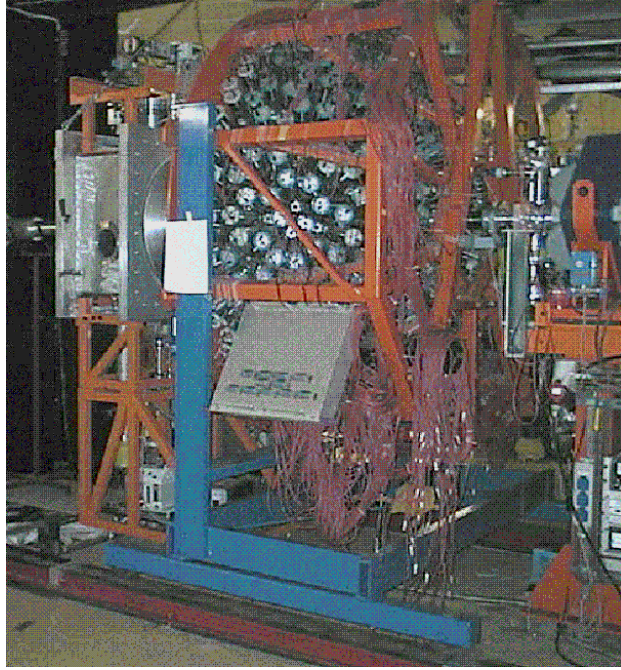


FIG. 56: Photograph of the fully configured plastic ball at KVI.

upstream end of the long target need to enter the TPC without encountering the Plastic Ball.

#### H. Plastic Ball Electronics [35]

The upgraded MIPP DAQ requires trigger rates up to 3 kHz with minimum interval between triggers of  $16 \mu\text{s}$  and trigger decision time of  $2 \mu\text{s}$  [36]. The extracted beam spill may be up to 6 seconds long. This requires for the front-ends to store up to 20000 events per spill. Stored events are to be read out during between spill intervals of 54 seconds. An 8-channel prototype of the Plastic Ball Front End (PBFEE) board is being developed and tested. See Figure 58. The specified interval between triggers of  $16 \mu\text{s}$  allows implementing deadtime-less front-end electronics design similar to the D0 Muon Electronics readout [37]. Such an approach requires continuous digitization of the detector signal and allows using reliable digital pipelines to compensate trigger decision time. A block-diagram of the Plastic Ball Front-End board is shown in Figure 59. The photomultiplier signal is split by a passive splitter with integration and differentiation times of  $\approx 20 \text{ ns}$ . The differentiated signal is discriminated for time measurement and sent to one of the four TMC304 inputs [38]. The

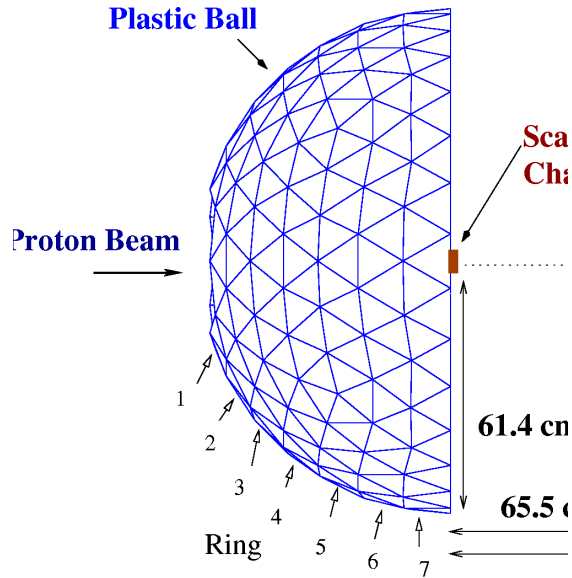


FIG. 57: This hemispherical arrangement of 340 phoswich modules would be similar to the way we would use it in MIPP, upstream of the TPC.

TMC chip allows high precision time measurement of rising and falling edges with  $\approx 100$  ps resolution and has internal digital pipeline. The integrated portion of the signal is digitized at 26.55 MHz by Analog Devices AD9229 12-bit pipelined 4-channel ADC. The ADC output is de-serialized and delayed by an external digital pipeline. When the trigger signal arrives it generates a trigger gate which controls ADC and TMC data transfer to the external event memory. A SPICE simulation of the passive signal splitter outputs with differentiation and integration time of 20 ns and 5 meters of RG-174 cable is shown in Figure 60. The photomultiplier signal was simulated by a current source with a rise time of 10 ns and fall times of 10 ns and 500 ns. The plots labeled dif and int show differentiated and integrated outputs of the splitter respectively. Additional study with the actual detector signal is necessary to finalize the value of the time constant of the splitter.

A detailed block diagram is shown in Figure 61. The TMC chip has an internal pipeline of 128 cells which provides maximum delay of 4.8 s at clock frequency of 26.55 MHz. The pipeline for the ADC data is implemented in a FPGA. At the arrival of a trigger signal the digitized data from the TMC and ADC pipeline outputs is temporarily stored in FIFO

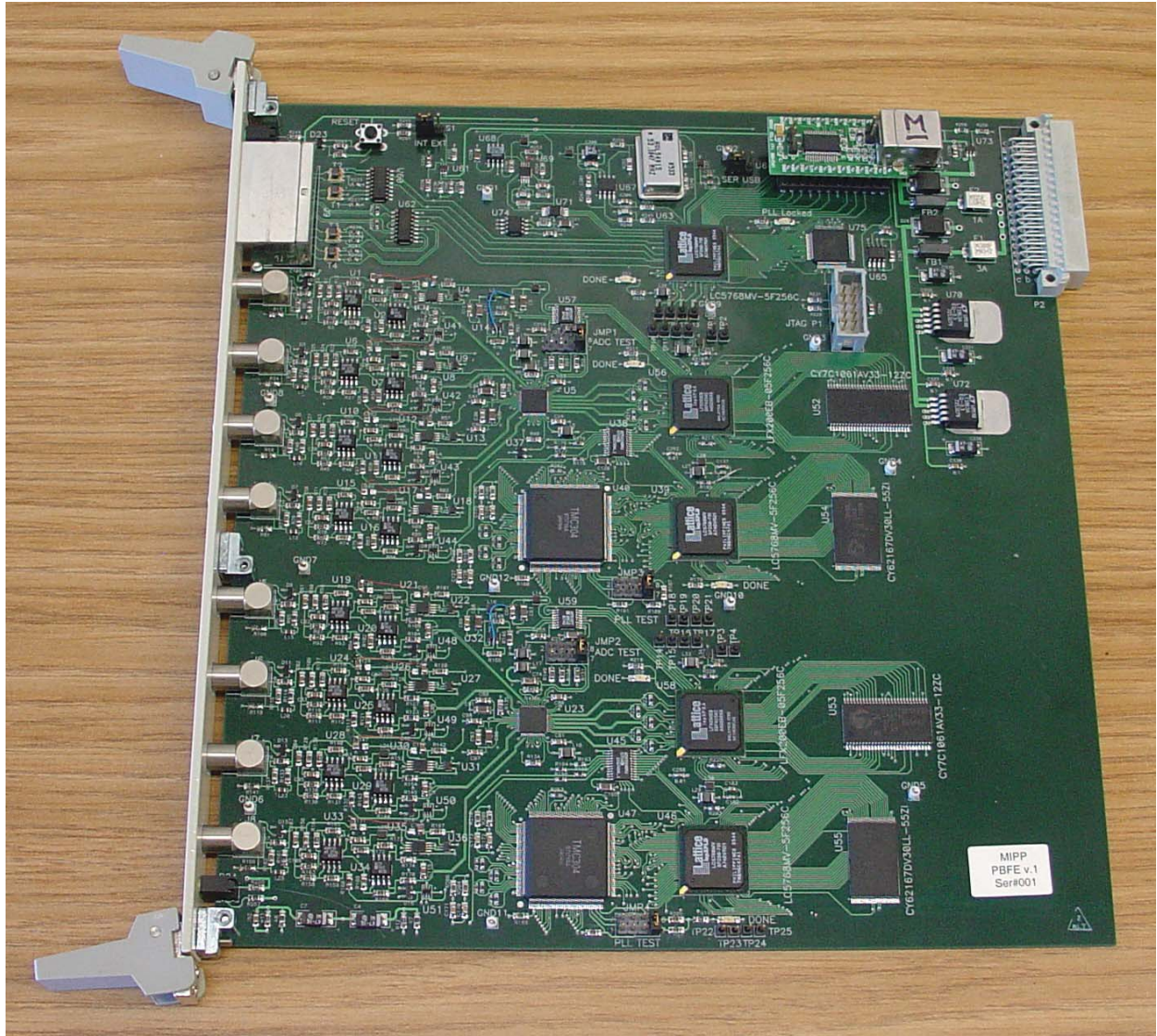


FIG. 58: Prototype of the Plastic Ball Front End Electronics board.

memories. The duration of the trigger signal determines how many data words are written to the memory. Zero suppression is done during this process using hit bit for the TMC data and internally generated tag bit for the ADC data. The tag bit is generated individually for each channel by a programmable one-shot (see Figure 62). Using this procedure, only non-zero data words are stored in FIFOs. At the end of a trigger gate the event sequencer writes the event data from FIFOs to the external RAMs. Writing event data to RAMs takes less than specified minimum interval between triggers, and the front-end is ready for the next trigger before it may arrive. This guarantees downtime-less operations of the front-end.





FIG. 60: SPICE simulation of the passive signal splitter.

A different version of the control firmware is required for the UM245R interface. An event is formed by the event sequencer upon readout request from the DAQ controller. The sequencer reads event length from each RAM and calculates total event length. The event then is transmitted via serial interface. The event format includes leading word count, event header, variable segments of ADC and TMC data for each channel that has a valid hit, and a global checksum. The event header includes 32-bit time stamp and status information. Each front-end has a time stamp counter which is sampled at the arrival of the trigger. The time stamp counter is reset at the beginning of the spill. The PBFEE board features programmable on-board test pulse generator with individual 12-bit DAC control and mask bit for each channel. Each channel has an individually programmable 8-bit threshold DAC. Two prototype boards are assembled and tested using auxiliary USB interface. The DAQ software is in preparation for testing the board with Plastic Ball detectors in cosmic rays.

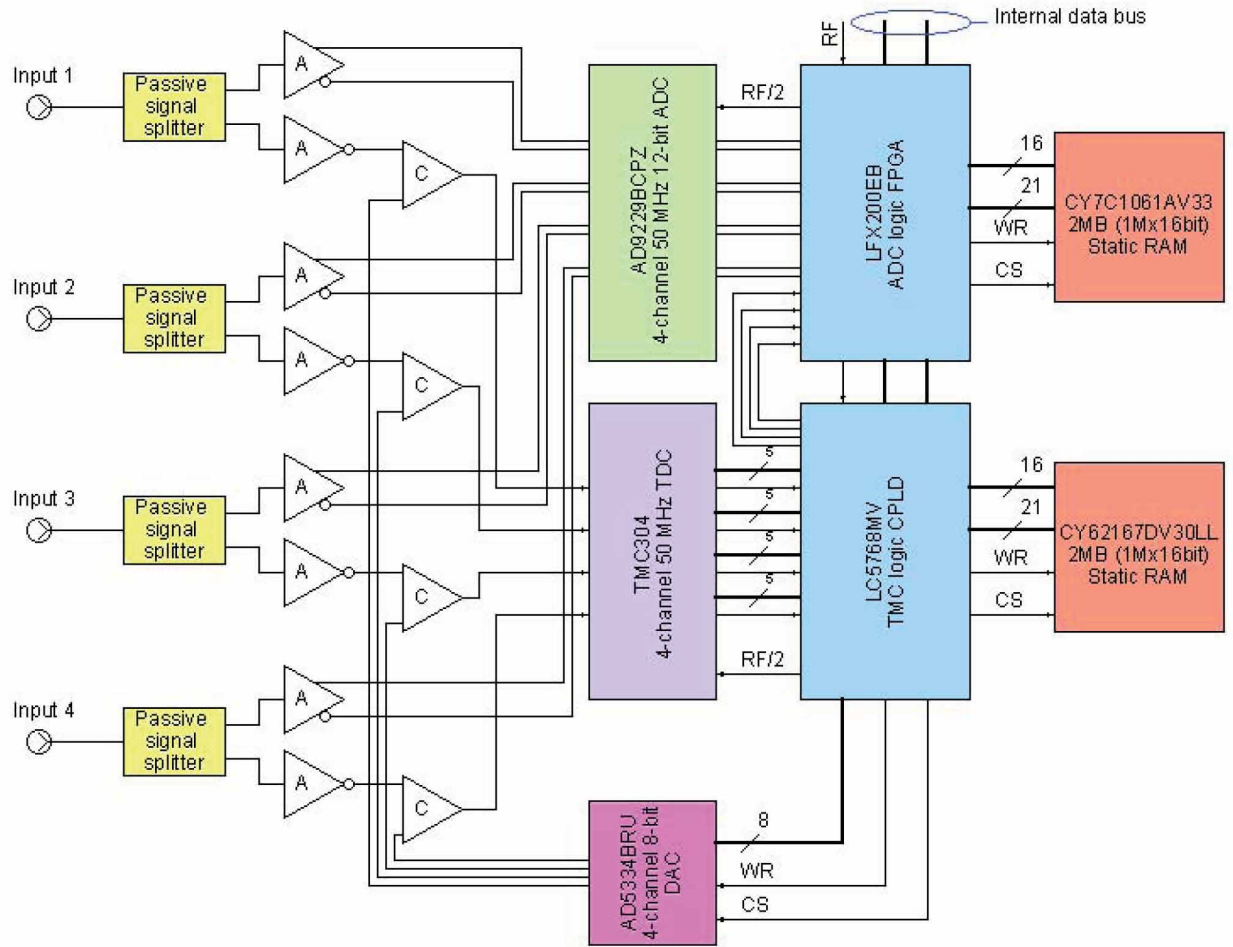


FIG. 61: Detailed block diagram of four channels.

## I. EM Calorimeter Electronics

Similar by design to the PBF board, a 32-channel prototype front-end board for MIPP EMCal has been developed and tested. The board has differential analog inputs and receives signals from four 8-channel wire amplifier boards. The power to the wire amplifier boards is provided via 26-pair twisted-and-flat cable. The EMCal wire amplifier board is shown in Figure 63. The wire amplifier board provides initial gain and integration of the wire chamber signal which in turn is continuously digitized by the ECFE board Analog Devices AD9229 12-bit ADC at 26.55 MHz clock frequency. The amplifier baseline is measured by using ADC samples occurred before actual wire signal. The ADC samples are delayed by a digital pipeline and the rest of the board is very similar to the PBF design. Each ADC channel

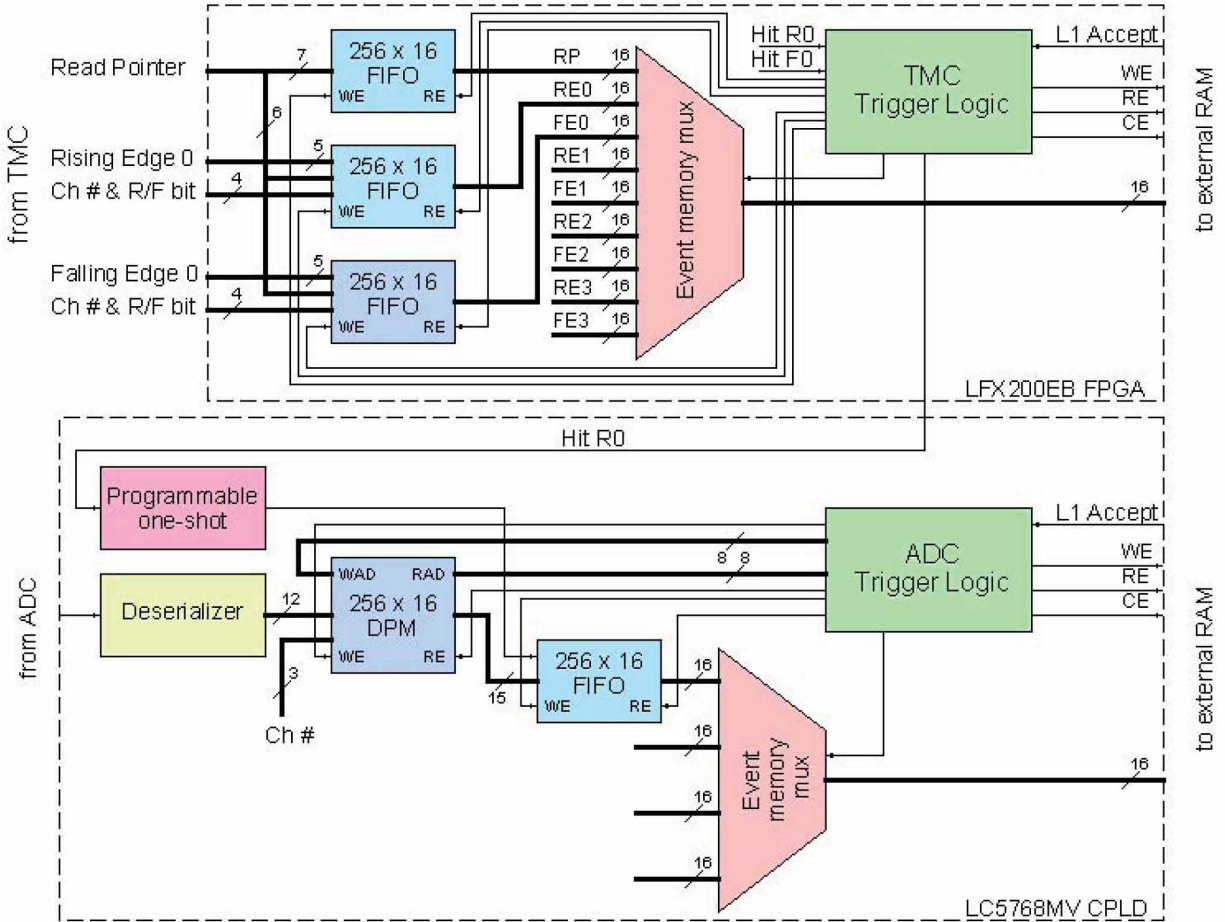


FIG. 62: Details of the trigger logic.

has a discriminator associated with it to provide zero suppression. Only digitized signals above the programmable threshold are stored in the event memory. The block diagram of the ECFE board is shown in Figure refemcalblock. The board also features test pulse control of the pulser incorporated on the wire amplifier board. The test pulse amplitude and channel mask are programmable as well. The prototype ECFE board is shown in Figure 65.

## J. Upgrades to the Online Data Acquisition System

The MIPP DAQ system used in the 2004 to 2006 runs was originally designed and coded in 2003. It utilized components that were readily available at the time such as the CES CBD8210 CAMAC branch drivers, six VME power PCs and assorted other electronics. The

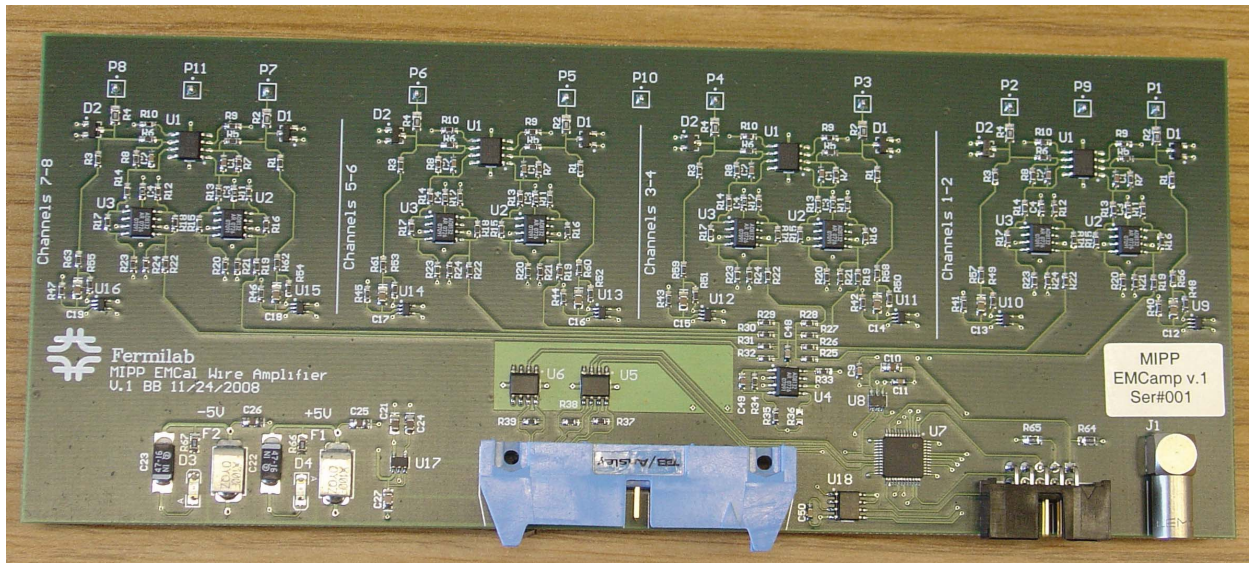


FIG. 63: An 8-channel EMCAL wire amplifier board.

B Baldin  
11/12/08

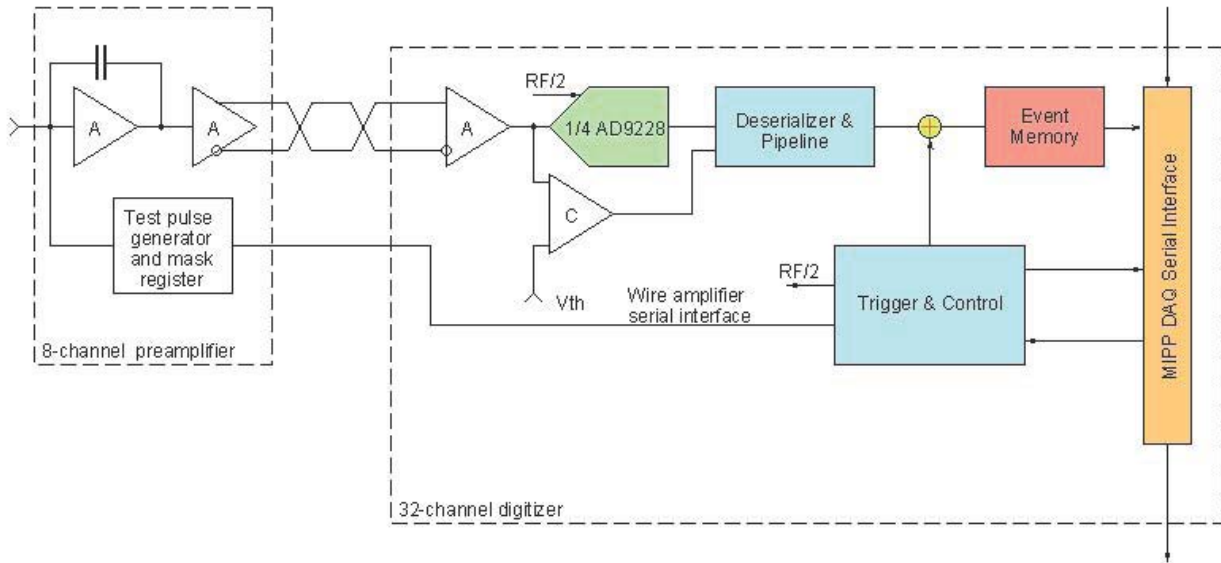


FIG. 64: Block diagram of the EMCAL front end board.

DAQ system itself used the Fermilab CD event builder of that time (r2dm) which during the run constrained our system to remain at RedHat Linux 7.3 operating system (due to

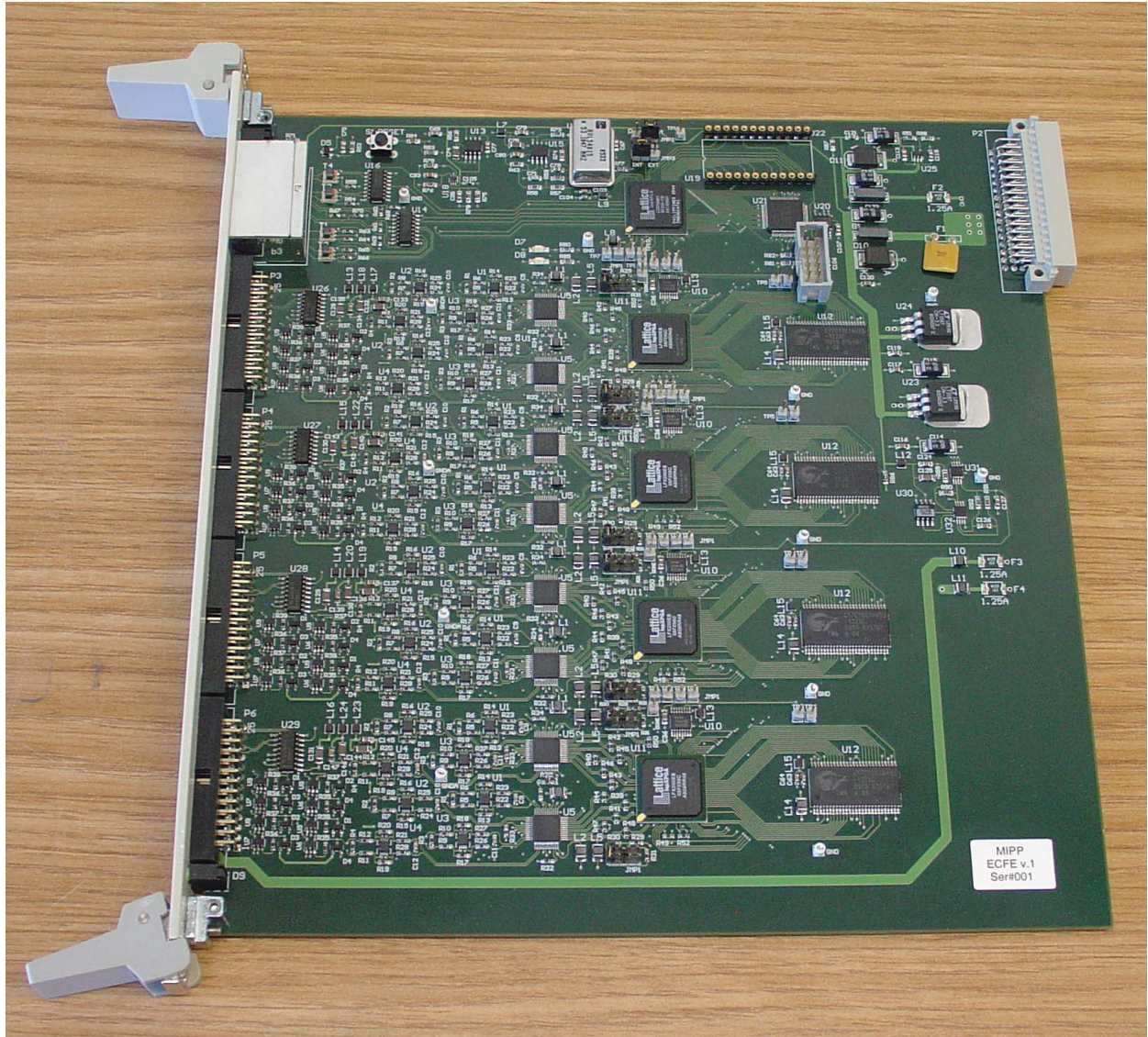


FIG. 65: Prototype EM Cal Front End board.

ACE/ITC). The CBD8210 CAMAC branch driver can no longer be maintained nor are the old power PCs capable of being upgraded to the newer operating systems. Hence the DAQ system for the upgraded MIPP experiment is in need of a major overhaul. This is important not only for the larger physics data set expected in the upgraded MIPP experiment which is 100 times more demanding at 3 kHz than the old system running at 30 Hz, but also in sight of the long term use of the MIPP experiment when eventually the calorimeters of the MIPP experiment will be replaced by ILC test calorimeters for tagged neutral beam studies. So having a DAQ system whose electronics and operating systems can be maintained for

several years is of importance.

From May to September 2006 a group of MIPP physicists and the Fermilab Computing Division met weekly to determine the route that this MIPP DAQ upgrade should proceed. It also involved discussions with the PPD electronic engineers who are building new electronics for the TPC and wire chamber readout. Further discussions were held in Summer of 2010. The new DAQ can be broken up into three groups: VME, fPix and computers. In addition there are requirements that we wish to address for local data storage, long term data storage for Physics analysis, network infrastructure and long term data analysis CPU needs.

The DAQ hardware upgrades consist of replacing the old Power PC's with a newer single board computer VME controller, and interfacing the new equipment being built. Most of the work on the DAQ upgrade is in software code development for the new common backend readout. We will continue to use the DAQ user interface and run control code from the existing MIPP DAQ system. The experiment will continue to maintain these parts of the code and the code specific to the readout of all detector systems.

### *1. The VME systems*

Currently MIPP has the RICH PMT readout in a VME crate shared with the power PC and the old CBD8210 CAMAC branch driver. The RICH PMT readout board will remain and additional VME modules designed by the PPD electronic shop for TPC and wire chambers will be added. The current six power PC's (four for the old TPC electronics and two for the CAMAC and RICH readout) will be replaced by two newer single board computers. There is no need to upgrade the old RICH readout boards except to read them out on an event by event basis during the spill with the new single board computers. The new TPC, wire chamber, TOF, Ckov, Calorimeter, and Plastic Ball readout will have event buffers for the spill so that at the end of each spill the sparsified data will be sent by the data transfer process of VME modules to the the DAQ central computer with the single board computers processing the data.

## 2. *fPix readout*

A new tracking silicon detector system is planned for the target region. These will be used as part of the new interaction trigger system which is described in the trigger section, but its readout will need a dedicated PC computer with an extended PCI bus that can handle 18 PCI cards, one for each row of fPix chips of the 3 silicon planes. During the spill the dedicated fPix computer will constantly readout each event into a local memory or a disk file. This will then be transferred at the end of the spill to the central DAQ computer.

## 3. *DAQ system Computer*

The central DAQ computer will receive and assemble event data and copy it to tape storage. The computer must be fast enough to be able to readout the Power PC 5500 single board computers with TPC, wire chamber, and other detector data, and the fPix computer. This will be done through an upgraded event builder.

The expected data rate is 1 Gbyte per spill. This must be transferred and handled by the computers before the next spill, i.e. within 56 seconds. The nominal rate is that MIPP will get a 4.0 second spill every two minutes, but during some fraction of data taking the system must be able to handle one spill every minute. All processors have Gigabit and 100 Megabit fast ethernet ports and should be able to handle the highest rate expected in only a few seconds to get the data to the main DAQ computer and enable out-of-spill calibration and monitoring data acquisition. The main DAQ computer should be able to process the spill through the event builder in the remaining 56 seconds and store it onto a mirrored disk system. The local disk system needs to have a capacity of 10 TB to provide local storage for  $\sim 1$  week of data. The local storage will allow continued data taking in case of network problems between the experiment and the tape backup at FCC.

This computer also has to provide access to the data for online monitoring. This is presently done through a cross mounted disk using NFS. Another model would be for the DAQ software to send a data stream to the monitoring PC through the network, thus avoiding double disk access for monitoring.

A separate PC will run the graphical human interface to set up run conditions, start and stop runs, perform pedestal runs, etc. For the main DAQ computer a dual CPU system

with a 3 GHz processor with a high speed bus can provide sufficient computing power to support event building and data transfer to Feynman and the monitoring PC.

#### *4. Monitoring Computer*

In order to reliably monitor data quality, two approaches are used. Summary histograms with event statistics provide data on dead/hot channels and similar statistics for all events in the last spill which will be displayed and compared to reference plots for presentation to the shift operator on five display monitors. The computer will automatically do a comparison of these distributions and audio alarms will be provided when there is an obvious problem. Also a fraction of the events have to be fully reconstructed and displayed constantly on a monitor for full event data validation. This track reconstruction is CPU intensive but we would expect that 10 events out of the  $\sim 10000$  taken each spill need to be fully reconstructed to monitor physics quality.

This set of tasks is best handled by a multi-core CPU computer that receives a copy of the data stream. The system also will need six monitors that the computer can display the data on at the end of each spill.

#### *5. Data transfer to ENSTORE, Data storage in Feynman Computer center and Offline analysis needs*

Our average event size is 100 kBytes. The 3 kHz event rate expected in the upgraded MIPP experiment results in 1.2 Gbytes of data per spill. With 58% accelerator uptime we will receive 420 spills per day and record 500 Gbytes of data per day. We expect to transfer this data to the Feynman Computing Center ENSTORE tape robot continuously during the day. A 6 Mbytes/second transfer rate through the site network and into ENSTORE is needed. The CDF and DØ experiments currently obtain 30 to 60 Mbytes/second. Thus the existing ENSTORE system should be sufficient. For offline storage and CPU needs, please see the discussion in the section entitled “Proposed Run Plan”. See table V for a summary of the DAQ equipment costs. See Figure 66 for a schematic of the proposed MIPP data acquisition system.

Equipment	breakdown	Cost
4 Power PC 5500	4x\$4800	\$19200
2 3 GHz PC	2x\$2750	\$5500
2 10 Tbyte disk	2x\$1000	\$2000
6 displays+drivers	6x\$700	\$4200
1 PC for fPix	\$1700	\$1700
2 13 slot PCI extender	\$1999	\$3998
Total		\$36598

TABLE V: Equipment summary for DAQ upgrade equipment.

### 6. DAQ Task Summary

The MIPP/CD DAQ group has identified the following tasks as being central to the upgrade.

- Update event builder for the new kernel and operating system (Estimate 6 weeks of 1 person full time.)
- Get the Linux kernel operating on the two new Power PC 5500 (Estimate 8 weeks of 1 person full time in two blocks of 4 weeks, with a spare 2 weeks at the end)
- Modify the DAQ for the new TPC(12 weeks), and wire chamber readout modules (4 weeks), and CKOV, ToF, Calorimeter readouts (4 weeks)
- Modify the Event Monitor(2 weeks)
- Test the electronics modules being re-used (4 Weeks)
- Maintain all associated NIM and VME modules.
- Maintain custom electronics built for RICH, TPC, wire chambers, Interaction Trigger and TOF-TDCs.

We foresee a  $\sim 6$  month commissioning run during which work will continue to integrate the new pieces of software together. See section on “Proposed Run Plan” for a discussion of these issues.

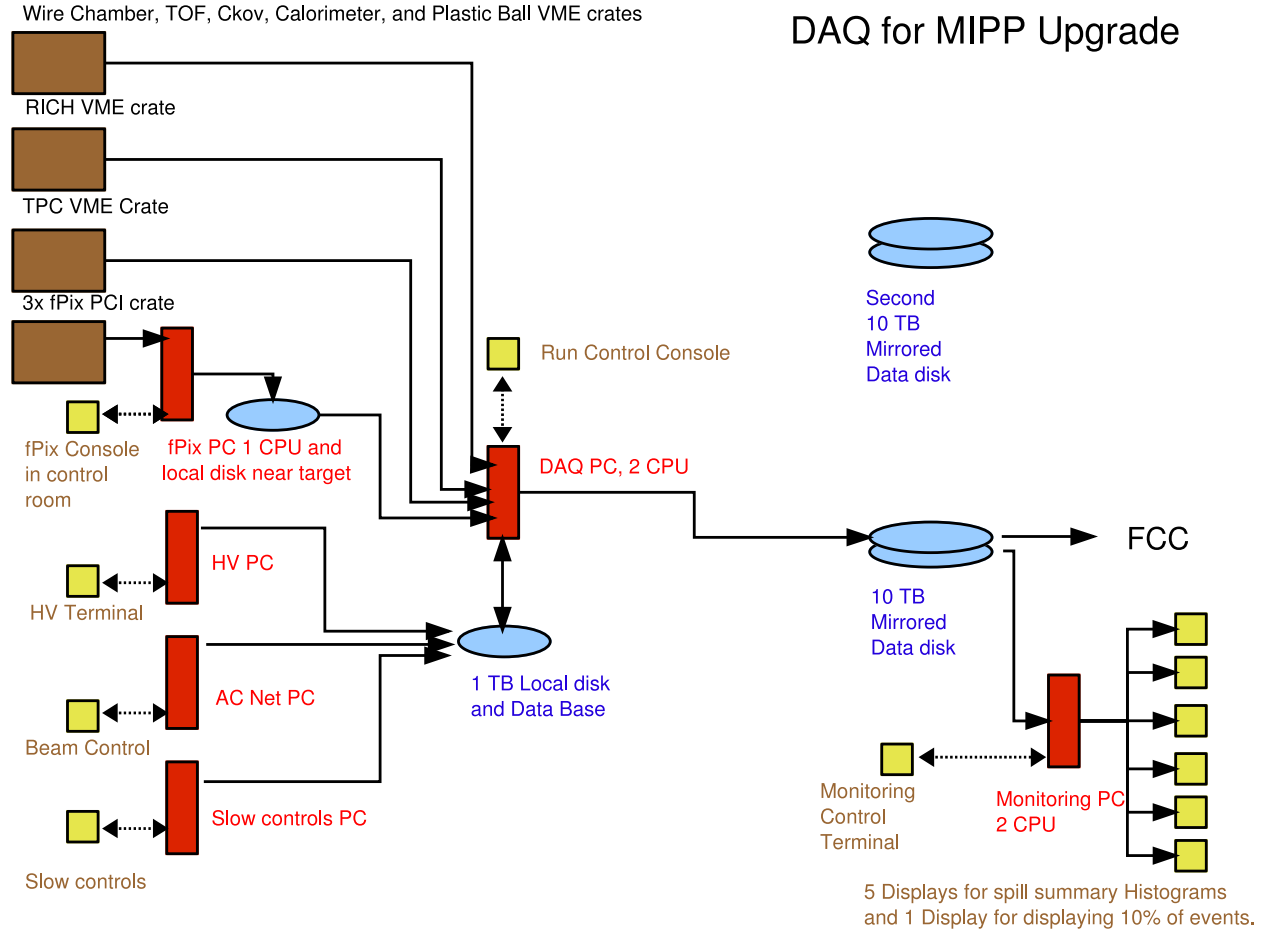


FIG. 66: Schematic of the Upgraded MIPP DAQ system.

## K. Cryogenic Target Upgrade

### 1. Modifications to the Cryo-target

The cryogenic target and refrigeration system built for MIPP worked well during the commissioning and physics run. MIPP has acquired over 5 million events on liquid hydrogen. There are, however, some design changes we would like to perform. The target volume is contained in a vacuum space connected to the cryogenic system through a transfer line. The beam has to travel through part of this transfer line to get to the target. The inner diameter of the transfer line, based on the E690 design is currently small. A very small fraction of the beam particles in the tail hit the transfer line (with the exact fraction depending on the beam tune) and causes triggers. This causes a large background none-the-less because

the experimental target is 1% of an interaction length thin, while beam particles encounter a much larger fraction of an interaction length if they hit the transfer line. The existing transfer line also is not compatible with the Plastic Ball detector that we plan to install as a recoil detector just upstream of the TPC to cover the hemisphere upstream of the target. In addition to the new transfer line the mounting structure of the refrigerator on the JGG magnet yoke will have to be modified to be compatible with the extended JGG coils and the Plastic Ball. These modifications will cost \$51k in material and labor.

### *2. Modifications to operate with cryogenic Nitrogen*

The cryogenic target system will need to be modified to allow for cryogenic Nitrogen operation. Liquid nitrogen is heavier than liquid hydrogen or deuterium and it is warmer. Thus a new target flask will have to be designed and fabricated and the target control system will have to be expanded to allow control at liquid nitrogen temperature. The cost for material and labor for this upgrade will be \$33k. This target can also be filled with liquid Argon.

### *3. Cryocooler*

One component of the cryogenic target system is the cryocooler. It has been working up to now. However, it is old and we do not have a spare. We have identified the cryocooler as a single point of failure that could result in significant downtime to the experiment. A new spare cryocooler will cost \$40k. Additional parts and labor to make the new cryocooler compatible with the existing target will cost \$20k.

## **L. Gas System and Slow Control Upgrades**

The detectors in the MIPP experiment use a variety of gases and gas mixtures. These are provided by an extensive gas system. Overall this gas system has been working well. However, there are some aspects to the system that we propose to improve further.

### 1. *Ckov gas purification system*

The performance of the multicell Čerenkov detector detector has been lagging in MIPP compared to results reported by other experiments that used the same detector. The reason for this performance degradation has been identified to be contamination in the radiator gas. Thus gas purification has to be added to the Ckov gas system. A paper by Ullaland [50] shows (in figure 6) gas transparency improvements in the UV for C4F10 gas (as used by MIPP) purified by molecular sieves and activated carbon filtration compared to the gas as delivered by the manufacturer.

### 2. *Methylal bath system*

The drift chambers operate on a mixture of Argon, Isobutane, and a small fraction of Methylal. The Methylal is added by flowing a fraction of the mix of the other two gases through a bubbler in a liquid Methylal bath.

The Methylal refrigerator on the drift chamber gas mixing system requires frequent maintenance due to water ice building up. It also needs to be filled frequently due to its small reservoir size. We propose to upgrade the Methylal refrigerator to a system that fills automatically from a larger reservoir and works with less maintenance. This will make the system more reliable and also reduce contact of shift personal with the Methylal, thus increasing safety. We estimate the cost for this task at \$12k.

### 3. *RICH Vessel Fill Automation*

The RICH vessel is filled with CO<sub>2</sub> at slightly above atmospheric pressure. It was designed to be a gas tight vessel to keep constant gas density in the radiator volume. The vessel has a small leak that could not be found. This is not a problem because the changes in gas density can be computed from temperature and pressure of the gas, both of which get monitored electronically. However, the system needs to be maintained above atmospheric pressure to avoid oxygen contamination of the CO<sub>2</sub>. This requires manual intervention weekly to bi-weekly depending on the weather. In order to minimize the pressure fluctuations and hence the corrections to the data we propose to install an automated CO<sub>2</sub> fill system. This system will cost \$8k in material and labor to implement.

#### 4. *Other Gas Upgrade*

The TPC is operating with P10 gas, a mixture of 10% methane in Argon. We developed a mixing system for this gas mixture. When we had problems with breaking wires in the TPC we switched to a backup system of premixed P10 cylinders. The existing system was designed as a backup to the mixing system rather than a primary supply system. A cylinder lasts only two days. The bottle pressure is not monitored electronically. The overhead for bottle changes and gas orders was significant. The system allows for the introduction of air contamination into the P10 during bottle changes that could result in broken wires. We propose to upgrade the P10 system to be supplied from a semitrailer.

The beam Čerenkov detectors (BCkov) use vacuum pumps to run below atmospheric pressure. The vacuum pumps can fail and in worst case introduce oil into the BCkov vessels. With upgraded vacuum instrumentation any such failure can be detected early. This will increase system reliability and significantly reduce the chance of a failure that would result in a long downtime.

#### 5. *Slow Controls Upgrades*

The temperature in the experimental Hall is currently being monitored in several places. Due to the sensitivity of some of the detectors to temperature we propose to add more temperature probes throughout the experimental hall and especially in the region around the time of flight detector.

The threshold Čerenkov detector pressure sensors need to be replaced before the next physics run. These and other sensors need to be recalibrated.

Control and monitoring of new components for the gas system and cryogenic target require additional slow control infrastructure. These upgrades will cost \$34k.

#### **M. Photomultiplier Tubes for RICH and Čerenkov detectors**

The RICH detector images Čerenkov rings with an array of 96 columns of 32 half-inch diameter photomultiplier tubes. Currently 15 columns are instrumented with 12 stage Hamamatsu R560 PMT's and 52.5 columns utilize 10 stage FEU60 PMT's. The remaining 912 positions in the RICH are not instrumented due to the loss of PMT's in a fire during commis-

sioning of the MIPP experiment in Spring of 2004. The remaining PMT's were distributed over the RICH array. With the present configuration, the RICH performed well during the MIPP physics run in 2005/2006. However, rings with a small diameter from particles near the Čerenkov threshold will be fit with better precision and accuracy if the readout is instrumented completely. The 12 stage PMT's provide a better sensitivity for single photons than the 10 stage PMT's.

The threshold Čerenkov detector provides particle identification for particles with a momentum close to 10 GeV/c. It contains 96 cells, each read out with a two inch diameter PMT. Seven of these 96 PMT's need to be replaced to obtain a fully working Čerenkov detector.

#### **N. Modifications to the beam line**

We propose to add low-current power supplies (Lambda- Genesis) as in M-test to run our beamline in the low momentum mode. During low momentum running, we will switch from the regular power supplies to these new ones for all the magnets in the secondary beamline. In addition, we plan to add Hall probes to each magnet to monitor the field to avoid hysteresis effects due to iron yoke residual fields to ensure that each magnet is set to the correct field appropriate for the particular beam momentum setting.

#### **O. Beam Veto upgrade**

In the first MIPP physics run some of the triggered events, especially at low beam momentum, have beam halo and spray particles hitting the experiment in coincidence with events of interest. The beam background particles can be separated from the events of interest when they are significantly out of time with the triggered event. But additional tracks within several 100 ns cannot always be separated from the primary event vertex in the TPC. ADC gates of other detectors in the experiment are 400 ns long. The energy deposit of background inside this window cannot be distinguished from the event signals.

The experiment is currently using a beam veto counter to inhibit the trigger when spray is present. However, this counter covers only an area around the beam of approximately 1 ft<sup>2</sup>. In the upgrade the experiment will read out at a rate of approximately 100 times the

rate of the first run. Thus the beam intensity has to increase by a similar factor. The beam backgrounds will also increase.

We propose to expand the beam veto counter into a veto wall that will cover the area of the TPC and the proposed recoil detector. This is an area of  $48 \times 60$  in<sup>2</sup>. The signals from spray particles need to be collected in time for the trigger formation. An array of six 10 inch wide fast plastic scintillator paddles with light attenuation  $>100$  cm will satisfy these requirements. The Rexon RP420 scintillator is a good inexpensive choice. For reliable light detection, each paddle will be read out with photomultiplier tubes on each end. The 12 signals will be latched and processed by the upgraded trigger electronics to form the trigger inhibit signal. High Voltage for the PMT's will be provided through the existing LeCroy 1440 HV system.

### **P. Rewinding the TPC**

The TPC contains three planes of wires. Charged particles ionize the P10 gas inside the TPC drift volume. Ions drift up to the solid cathode at the top of the drift volume. The cathode is at -10 kV. Electrons drift down to the ground plane of wires. Just above the ground plane is a plane of wires used to gate the TPC. This gating grid is transparent to the drifting charges when all of its wires are at the surrounding potential  $V_0$ . Outside the gate window half of the wires in this plane are put at  $V_0 - 150$  V and alternate with the other half of wires at  $V_0 + 150$  V so that drifting electrons terminate in the gating grid wires. When the grid is gated, electrons drift through the gating grid and through the ground plane into the amplification region. Anode wires at +1250 V form the third plane of wires. They are just below the ground plane to create a large gradient in the amplification region. Drift electrons get multiplied in this region and terminate on the anode wires. They create image charges on the TPC pad plane just below the anode wire plane. These pads are read out by the TPC electronics. The anode wire plane actually consists of anode wires alternating with field shaping wires at ground potential.

During commissioning for the first MIPP physics run several wires in each of the wire planes broke. The TPC was opened multiple times and broken wires were carefully extracted. Figure 67 shows a section of wires during the repair. The wires broke due to contaminations in the gas. All wires were exposed to this gas. Some of the anode HV sections can not

be operated at the full 1250 V. This results in gaps in sensitivity in the TPC. Due to the mounting of the wire planes it is not possible to replace anode wires without removal of the two upper wire planes.

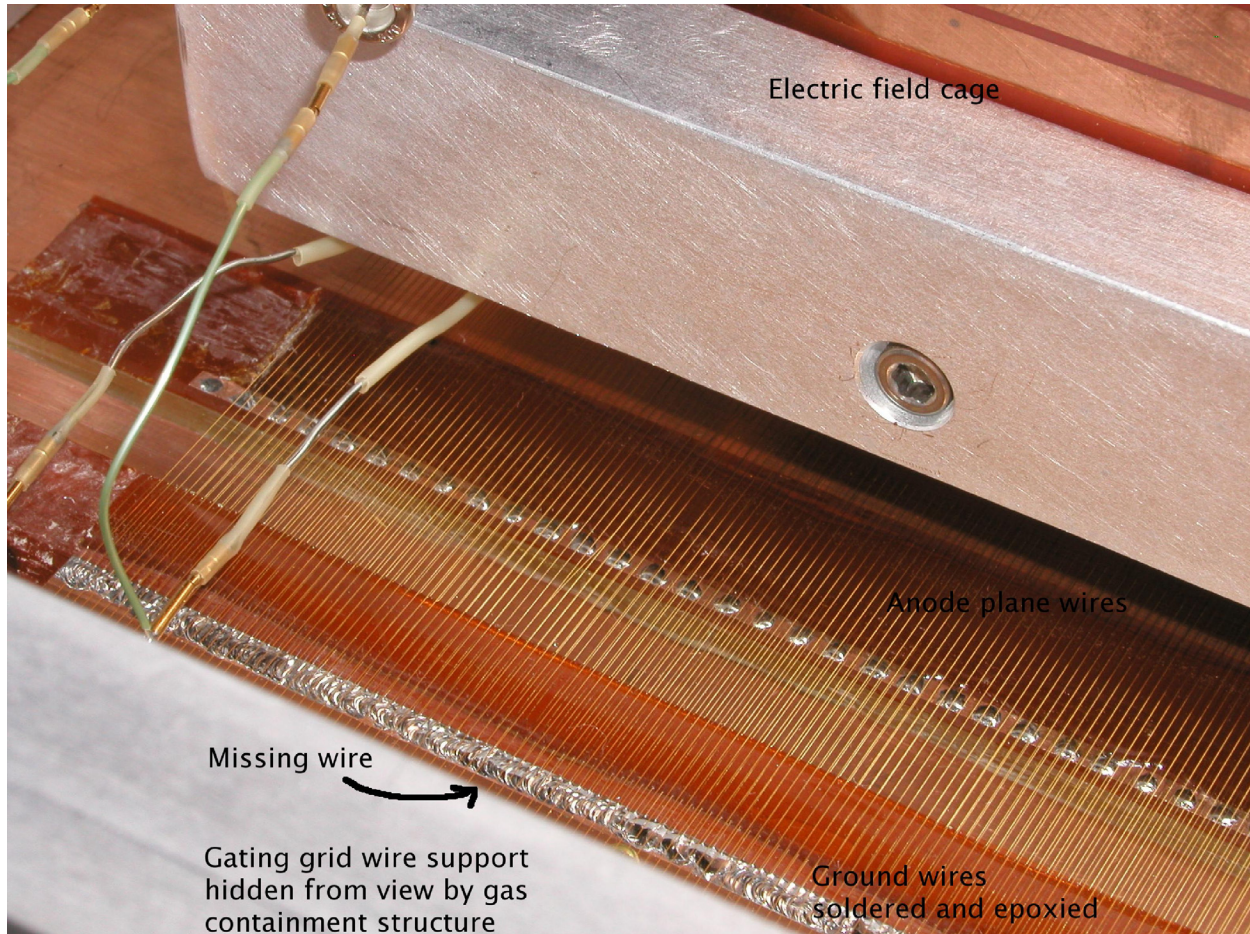


FIG. 67: One section of TPC wires during repair.

We propose to replace the wires in all planes. Lab 6 at Fermilab has a facility that can be used to wind wire onto construction frames and then transfer the wires onto the TPC wire support structures. The TPC wires are mounted in sections onto supports. These supports are not designed to hold the wire tension unless they are mounted in the TPC or on transfer frames. Frames and transfer hardware handling of the TPC wire planes need to be designed and built. The TPC wires need to be removed and the frames cleaned. Then new wires can be placed on the existing mounting supports.

This work is similar to projects previously performed at lab 6. The only less familiar aspect involves placement of two different kinds of wires onto the anode frame to get alter-

nating anode and field shaping wires with the correct spacing. The expertise for this job exists at Fermilab.

The cost for this project is approximately \$16k in material and labor.

#### **Q. Wire Chamber repairs**

MIPP uses six large wire chambers and three smaller beam chambers. The high voltage on one of the drift chambers (DC4) started to trip frequently during the last weeks of the first MIPP physics run. One of the MWPCs has a defect that causes two of the four planes to be inoperational.

A spare MWPC is now in lab6. We refurbished it during the last run. We propose to exchange the broken MWPC with the spare and repair it. We also propose to diagnose the reason for the DC4 HV trips and repair this chamber. Both types of chamber have been repaired by MIPP physicists before. All necessary hardware exists. The cost for this project is approximately \$5k.

## **VI. COST AND SCHEDULE**

### **A. Cost estimate of the MIPP Upgrade**

The MIPP upgrade project cost is shown in detail in table VI. The total cost for all tasks including non-Fermilab contributions and labor is \$1.45 million. In addition, we estimate a Guests and Visitors budget (G&V) to accommodate Indian and Russian collaborators of \$0.5 Million per year for a period of 3 years.

The most essential tasks for a successful run are the JGG repair, detector readout upgrades, and DAQ upgrades. These add to M&S costs of approximately \$715,000. Also important for the success of the project are the improvements to the detector hardware, especially the cryogenic target, the trigger system, and the enhanced beam veto wall and recoil detector.

WBS	Task Name	Fermilab M&S Cost	Fermilab Labor Cost	Total Project Cost	Remaining Cost
0	MIPP	\$2,788,830	\$615,568	\$3,477,158	\$2,950,777
1	Project Management	\$55,000	\$0	\$55,000	\$55,000
2	Jolly Green Giant Repair	\$288,500	\$132,384	\$438,644	\$110,036
2.1	Jolly Green Giant disassembly/assembly	\$80,000	\$94,380	\$192,140	\$105,236
2.2	JGG coil design and fabrication	\$199,000	\$25,524	\$224,524	\$0
2.3	Ziptrack JGG magnet	\$9,500	\$12,480	\$21,980	\$4,800
3	Improvements on detector hardware	\$290,600	\$114,554	\$405,154	\$404,767
3.1	Gas System and Slow Controls Upgrade	\$51,500	\$35,308	\$86,808	\$86,421
3.1.1	RICH vessel fill automation	\$2,500	\$5,610	\$8,110	\$7,981
3.1.2	Methylal bath fill automation	\$5,000	\$7,228	\$12,228	\$12,056
3.1.3	P10 supply upgrade	\$5,000	\$6,664	\$11,664	\$11,578
3.1.4	TOF wall thermal instrumentation	\$2,000	\$4,232	\$6,232	\$6,232
3.1.5	Replacement of CKOV pressure sensors	\$2,000	\$412	\$2,412	\$2,412
3.1.6	Ckov gas purification system	\$11,000	\$5,440	\$16,440	\$16,440
3.1.7	Beam Ckov vacuum system	\$3,000	\$1,340	\$4,340	\$4,340
3.1.8	Calibration and maintenance	\$0	\$2,952	\$2,952	\$2,952
3.1.9	Slow Controls infrastructure upgrade	\$21,000	\$1,430	\$22,430	\$22,430
3.2	Cryogenic System Upgrade	\$68,000	\$75,598	\$143,598	\$143,598
3.2.1	Hydrogen Target transfer line	\$13,000	\$38,120	\$51,120	\$51,120
3.2.2	Nitrogen Target	\$10,000	\$23,260	\$33,260	\$33,260
3.2.3	Spare Cryocooler	\$45,000	\$14,218	\$59,218	\$59,218
3.3	TPC rewind	\$10,000	\$0	\$10,000	\$10,000
3.4	Chamber wire repairs	\$1,100	\$3,648	\$4,748	\$4,748
3.5	Ckov Photomultiplier tubes	\$10,000	\$0	\$10,000	\$10,000
3.6	RICH Photomultiplier tubes	\$150,000	\$0	\$150,000	\$150,000
4	Detector Readout Upgrades	\$399,920	\$240,918	\$648,513	\$520,002
4.1	TPC Electronics	\$225,920	\$150,847	\$384,442	\$273,028
4.2	Drift Chamber/Wire Chamber electronics	\$121,250	\$28,718	\$149,968	\$136,219
4.3	ToF + CKOV electronics board design	\$15,750	\$18,352	\$34,102	\$34,102
4.4	Calorimeter electronics	\$17,000	\$1,720	\$18,720	\$15,372
4.5	large pixel array upstream of TPC	\$20,000	\$41,280	\$61,280	\$61,280
5	Trigger System Upgrade	\$145,900	\$51,400	\$208,300	\$197,300
5.1	Interaction Trigger Fpix	\$137,100	\$38,800	\$186,900	\$175,900
5.2	Interaction Trigger Board	\$8,800	\$12,600	\$21,400	\$21,400
5.3	Other Trigger Upgrades	\$0	\$0	\$0	\$0
6	DAQ Software and Hardware Upgrade	\$32,800	\$38,952	\$71,752	\$71,752
7	Offline farm Upgrade	\$0	\$0	\$0	\$0
8	Beam Line Upgrade	\$56,000	\$0	\$56,000	\$56,000
9	Enhanced Veto Wall	\$20,110	\$1,440	\$21,550	\$0
10	Recoil Detector	\$0	\$35,920	\$90,920	\$35,920
11	Visitor Support for collaborators	\$1,500,000	\$0	\$1,500,000	\$1,500,000

TABLE VI: Cost estimate for the MIPP upgrade project.

## B. Schedule

The schedule for all upgrade tasks is shown in the Gantt chart in figure 68. The critical tasks in the timeline are the development, fabrication, and testing of TPC readout electronics and the integration into the upgraded DAQ system. The new TPC electronics will be operational at the end of September 2011. All other tasks can be finished on or before this date.

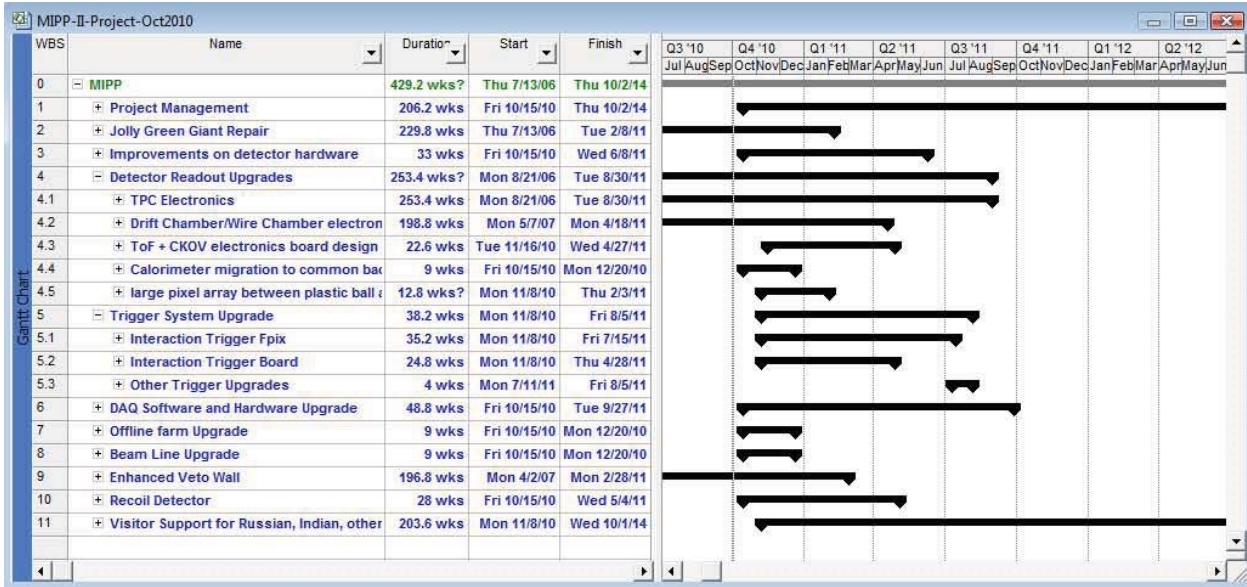


FIG. 68: Schedule for the MIPP upgrade project.

The project contains more than 450 tasks. The WBS is shown at summary level in the figure in this document. The full Gantt chart and cost and resource usage plots are available in a separate document.

## VII. PROPOSED RUN PLAN

We feel we will need a commissioning run lasting  $\approx 6$  months to debug and integrate the various components in the experiment. With the detector running at 3 kHz, we can generate a large quantity of data very quickly. After the commissioning, we propose a three stage run plan designed to use the data obtained in an optimal fashion. During the first phase we plan to acquire 110 million events as detailed in table VII. We propose to include 12 nuclei that are most commonly encountered in calorimetry in this list. This data sample

is a factor of 6 larger than what we have acquired so far in MIPP and would require  $\approx$  11 Terabyte of storage space to hold the raw data and approximately 3-5 times that to store the reconstructed data, with tracks and particle ID. If one were to keep the offline turn-around time to be similar to what we have currently in MIPP, we would like a farm size of  $\approx$  600 nodes of today's node speed. In 2 years time, the node speeds will have become faster.

Target	Number of Events (Millions)	Running Time (Days)	Physics Need Group
NuMI Low Energy target	10	2	MINOS, MINER $\nu$ A
NuMI Medium Energy Target	10	2	MINER $\nu$ A, NO $\nu$ A
Liquid Hydrogen	20	4	QCD, PANDA, DUBNA
Liquid Nitrogen	10	2	ICE CUBE
12 Nuclei $D_2, Be, C, Al, Si, Hg, Fe, Ni, Cu, Zn, W, Pb$	60	12	Nuclear Physics & Hadronic Showers
Total Events	110	22	
Raw Storage	11 TBytes		
Processed Storage	55 TBytes		

TABLE VII: Phase 1 Run Plan.

Target	Number of Events (Millions)	Running Time (Days)	Physics Need Group
18 Nuclei Li, B, O <sub>2</sub> , Mg, P, S, Ar, K, Ca			Nuclear Physics
Ni, Nb, Ag, Sn, Pt, Au, Pb, Bi, U	90	18	Nuclear Physics & Hadronic Showers
10 Nuclei B-list Na, Ti, V, Cr, Mn, Mo, I, Cd, Cs, Ba	50	10	Nuclear Physics & Hadronic Showers
Total Events	140	28	
Raw Storage	14 TBytes		
Processed Storage	70 TBytes		

TABLE VIII: Phase 2 Run Plan.

During phase 2, we plan to complete the remaining 18 nuclei of the A-List, as detailed in the section on hadronic shower simulation and then proceed with the B-list if there is need. The second phase of running is detailed in table VIII.

Before we go to phase 3, it is possible that additional running time is requested for the missing baryons search depending on the outcome of the analyses performed on the hydrogen data taken in phase 1.

During phase 3, we plan to go into the tagged neutral mode, where we run the liquid hydrogen target and allow the ILC calorimetry to run simultaneously in place of the MIPP calorimeter. This mode is shown in table IX. The running times for this will be dictated by the schedule of the ILC calorimetry test modules available then. It should be pointed out

Target	Number of Events (Millions)	Running Time (Days)	Physics Need Group
Liquid $H_2$	5 million events/day	As needed	ILC Tagged neutral beams

TABLE IX: Phase 3 Run Plan.

that the running times in Tables VII and VIII are the actual amount of beam on live times. They do not include the time taken to setup the various target conditions, target cool-down times (in case of cryo-targets) or calibration runs (such as magnetic field off runs, target empty runs). These end effects could become quite significant when computing the actual duration of a particular phase.

The upgrade factor of 100 in DAQ speed can be thought of as permitting the acquisition of 10 times the data we acquired so far in 10 times less time. This results in considerable savings in machine time and manpower to keep the experiment operational. The quality of data acquired will be considerably improved over what we had in the first run, due to improvements in triggering, recoil detector and Jolly Green Giant field quality.

## VIII. CONCLUSIONS

We have proposed a cost-effective upgrade solution to the MIPP DAQ that will make MIPP a powerful spectrometer with hitherto unprecedented particle identification and acceptance. Such a spectrometer will be capable of improving our understanding of hadronic shower simulations significantly and will help a large number of experiments which have

non-perturbative QCD processes as a signal or a background understand their systematics better. Particularly helped will be NuMI experiments (NO $\nu$ A, MINER $\nu$ A, LBNE experiments as well as the cosmic ray experiments such as ICE CUBE. MIPP will also acquire much wanted  $\bar{p}p$  data to help the PANDA collaboration and also test various hypotheses in non-perturbative QCD (Inclusive scaling relations, missing baryon resonances and multiplicity enhancements at high multiplicity). In addition, it can also serve as a source of tagged neutral beams to help benchmark the particle flow algorithm.

- 
- [1] The main MIPP web page is at <http://ppd.fnal.gov/experiments/e907/>. Information on the MIPP collaboration may be found using links there.
  - [2] The MIPP proposal and Addendum to the proposal may be found at [http://ppd.fnal.gov/experiments/e907/Proposal/E907\\\_Proposal.html](http://ppd.fnal.gov/experiments/e907/Proposal/E907\_Proposal.html)
  - [3] The Time of Flight detector was fabricated by MIPP and consists of an array of 10 cm $\times$ 10 cm scintillators and 5 cm $\times$ 5 cm scintillators. See <http://ppd.fnal.gov/experiments/e907/TOF/TOF.html> for a detailed description of the detector.
  - [4] The multi-cell Čerenkov detector was initially built for Brookhaven Experiment E766 and later in Fermilab experiment E690 and then used in several other Brookhaven experiments. In MIPP, we fill the detector with the gas  $C_4F_{10}$  which has the appropriate refractive index at atmospheric pressure.
  - [5] The details of the SELEX RICH construction and performance may be found at J. Engelfried *et al.*, *Nucl. Instr. and Meth.* **A43**,53(1999). We have replaced the front end electronics, and done extensive work on the safety systems. MIPP uses CO<sub>2</sub> gas as the radiator for the RICH.
  - [6] NuMI stands for Neutrinos at the Main Injector and refers to the Fermilab Main Injector neutrino beam. MINOS is the first experiment to utilize this beam MINOS proposal may be found at “P-875: A long baseline neutrino oscillation experiment at Fermilab”, E. Ables *et al.*; FERMILAB-PROPOSAL-P875,(1995). See also their website at <http://www-numi.fnal.gov/>
  - [7] The TPC was built by the BEVALAC group at Berkeley in the 1990’s and used effectively at several Brookhaven experiments (e.g. E910) and then donated to Fermilab by LBNL for use in MIPP. See, G. Rai *et al.*, *IEEE Trans.Nucl.Sci.***37**,56(1990); LBL-28141.

- [8] “Beamline design for particle production Experiment, E907 at FNAL”, C. Johnstone *et al.*, Proceedings of the PAC03 conference. So successful has the performance of this beamline been that the design has been adopted for use in the M-Test beamline upgrade for providing testbeams at Fermilab.
- [9] For more details on the beam Čerenkov system, see <http://ppd.fnal.gov/experiments/e907/Beam/BeamCerenkov/BeamCerenkov.html>
- [10] During the engineering run in 2004, we lost 20% of the phototubes in the RICH due to a fire in one of the phototube bases. This does not impact adversely on our pattern recognition, since the Čerenkov angle is large and there is plenty of light over most of our momentum range.
- [11] The electromagnetic calorimeter was fabricated by MIPP and uses lead as the radiator and an array of proportional tubes with 2.54 cm wire spacing as the readout. It has 10 radiation lengths and has 10 longitudinal segments.
- [12] The hadron calorimeter is recycled from the HyperCP collaboration and uses scintillator fibers embedded in iron as readout. It has 9.7 interaction lengths and has four longitudinal segmentations each of which is segmented in two transversely.
- [13] We have reused beam and drift chambers from the E690 collaboration. D.C.Christian *et al.*, *Nucl. Instr. and Meth.* **A345,62** (1994).
- [14] The large proportional chambers straddling the RICH find their use again after having been used by numerous previous experiments. M. De Palma *et al.*, *Nucl. Instr. and Meth.* **216** (1983) 393-397.
- [15] A. Malensek, Fermilab Technical Memo FN-341, 1981. (unpublished).
- [16] “Electromagnetic and hadron calorimeters in the MIPP experiment” T.S. Nigmanov *et al.*, *Nucl.Instrum.Meth.*A598:394-399,2009.
- [17] “Charged Kaon Mass Measurement using the Cherenkov Effect”, N. Graf *et al.*, *Nucl.Instrum.Meth.*A615:27-32,2010.
- [18] “Measurement of particle production on the NuMI target with a 120 GeV/c proton beam in the MIPP experiment”, MIPP Collaboration, Paper in preparation.
- [19] G. Rai *et al.*, *IEEE Trans. Nucl. Sci.* 37, 56 (1990).
- [20] L. Musa *et al.*, *IEEE NSS* Oct 2003.
- [21] H. Atherton *et al.*, **CERN 80-07**, (1980).  
D. Barton *et al.*, *Phy.Rev.* **27** (1983) 2580.

- G. Ambrosini *et al.*(SPY collaboration), Phys. Lett. **B420** (1998)225;Phys. Lett. **B425** 208;, Eur. Phys. J. **C10**(1999) 605.
- [22] R. Brun, F. Bruyant, A. C. McPherson and P. Zancarini, CERN Data handling Division, (Geant3), DD/EE/84-1, 1987; CERN Program Library, W5103(1994).  
M. Bonesini, A. Marchionni, F. Pietropaolo and T. Tabarelli de Fatis,(BMPT) Eur.J.Phys C, DOI 10.1007/S100520100656 (hep-ph/0101163).  
N. V. Mokhov and S. I. Striganov, “Model for Pion Production in Proton-Nucleus Interaction” AIP Conf. proc. **435** 91997) 543. N.V.Mokhov, The MARS Code System User’s Guide, version 13(95), Report Fermilab-FN-628(1995); <http://www-ap.fnal.gov/MARS>. A. J. Malensek, Fermilab-FN 341 (1981).
- [23] “Observation of Muon neutrino disappearance with the MINOS detectors and the NuMI neutrino beam“, hep-ex/0607088, submitted to Phys. Rev. Lett.
- [24] Sacha Kopp, “Neutrino Flux Uncertainties for the NuMI beam”, talk given at NUFACT06.
- [25] R. Tayloe, Fermilab Wine & Cheese talk, Jul 23, 2010, [http://theory.fnal.gov/jetp/talks/RT\\\_FNAL\\\_WandC\\\_0710.pdf](http://theory.fnal.gov/jetp/talks/RT\_FNAL\_WandC\_0710.pdf)
- [26] Information on the Hadronic Shower Simulation Workshop can be found at <http://conferences.fnal.gov/hss06/> See talk by S. Striganov on “Grand Validation” and references therein.
- [27] “Muon production in extensive air showers and its relation to hadronic interactions”, C. Meurer *et. al.*, to appear in the proceedings of the International Conference on Interconnection between High Energy Physics and Astroparticle Physics: From Colliders to Cosmic Rays, Prague, Czech Republic, 7-13 Sep 2005. astro-ph/0512536.
- [28] See Calorimeter-Energy Measurement in Particle Physics. R Wigmans, Oxford Science Publications, Page 71.
- [29] R. Raja, “Possibilities of new data in hadroproduction”, talk given at the workshop on Hadronic Shower Simulation [26].
- [30] The members of the Geant4 group attending the hadronic Shower Simulation Workshop consisted of J. Apostolakis, T. Koi, A. Ribon and D. Wright.
- [31] “Tagged Neutron, Anti-neutron and  $K_L^0$  beams in an Upgraded MIPP Spectrometer”, R. Raja, MIPP Note 130, <http://ppd.fnal.gov/experiments/e907/notes/MIPPnotes/public/pdf/MIPP0130/MIPP0130.pdf>

- [32] R. Raja, *Phys. Rev. D* **18**, 204 (1978).
- [33] “The PANDA detector at the GSI-FAIR project”, J. Ritman, *et.al.*, *Int. J. Mod. Phys. A* **20**, PP567-569, 2005. See also <http://www-panda.gsi.de/>
- [34] Information on FAIR, the Facility for Antiproton and Ion Research may be found at <http://www.gsi.de/fair>
- [35] B.Baldin, *Nuclear Instruments and Methods in Physics Research A* **610** (2009) 307-310, October 21, 2009
- [36] Holger Meyer, Specifications for MIPP readout electronics back end communication, MIPP-doc-186, April 2007, MIPP internal document
- [37] B.Baldin, et al. ”D0 Muon Readout Electronics Design,” *IEEE Trans. on Nuclear Science*, Vol.44, No.3, pp 363-369, June 1997
- [38] Y.Arai, TMC304(TEG3) User s manual, KEK, v1.4, November 1996, Unpublished
- [39] B.Baldin, S.Hansen, MIPP Data Cable Protocol, MIPP-doc-764, April 2008, MIPP internal document
- [40] J. Manjavidze and A. Sissakian, *Phys. Rep.* **346**, 1(2001). see also <http://sunse.jinr.ru/~nikitin> (file: thermaliz\_en.zip).
- [41] *Review of Particle Physics*, S. Eidelman *et al.*, (Particle Data Group), *Phys. Lett. B* **592** 1, (2004).
- [42] “JGG field Uniformity with extended coils”, H. Meyer, MIPP Note 134, <http://ppd.fnal.gov/experiments/e907/notes/MIPPnotes/public/pdf/MIPP0134/MIPP0134.pdf>
- [43] “Specifications for the new coils”, H. Meyer, W. Jaskierny, J. Kilmer, A. Lee, and R. Wands, MIPP Note 137, <http://ppd.fnal.gov/experiments/e907/notes/MIPPnotes/public/pdf/MIPP0137/MIPP0137.pdf>
- [44] B. Mota, L.Musa , R. Esteve and A. Jimenez de Parga, in *Proc. of the 6th Workshop on Electronics for LHC Experiments* (2000).
- [45] D. Subiela, S. Engels and L. Dugoujou, in *Proceedings of the ESSCIRC, 28th European Solid State Circuits Conference*, (2002).
- [46] L. Musa et al., in *Proc. of the IEEE Nuclear Science Symposium* (2003).
- [47] R. Bosch, A. Parga, B. Mota, and L. Musa, *IEEE Trans. Nucl. Sci.* **50** (2003).
- [48] R. Campagnolo *et.al.*, in *Proceedings of the 9th workshop on Electronics for LHC Experiments* (2003).

- [49] R. Albrecht *et. al.*, CERN Report CERN/SPSC/85-39 (august 1985), GSI Report GSI-85-32 (August 1985).
- [50] O. Ullaland, NIM A **553** (2005) 107-113.